FUNCTIONAL CHARACTERIZATION OF GENES THAT REGULATE INTESTINAL TUMOR PROGRESSION

Inaugural-Dissertation
to Obtain the Academic Degree
Doctor rerum naturalium (Dr. rer. nat.)

Submitted to the Department of Biology, Chemistry and Pharmacy
of Freie Universität Berlin

by

Marc Leushacke

from Aachen

2010

The present work was carried out at the Max Planck Institute for Molecular Genetics, Department of Developmental Genetics, Berlin, Germany from November 2005 to December 2010 and supervised by Dr. Markus Morkel.

1st Reviewer: **Prof. Dr. Stephan Sigrist**
Institut für Biologie / Genetik
Takustraβe 6
14195 Berlin

2nd Reviewer: **Prof. Dr. Bernhard G. Herrmann**
Max Planck Institute for Molecular Genetics
Ihnestr. 73
14195 Berlin

Date of Defense: 23rd February 2011

Acknowledgements

Zunächst möchte ich mich bei Prof. Bernhard Herrmann bedanken, der mir die Möglichkeit gegeben hat, meine Doktorarbeit in seiner Abteilung anzufertigen. Mein ganz besonderer Dank gilt Dr. Markus Morkel. Sowohl für seine intensive wissenschaftlich Betreuung, als auch für seine technische Unterstützung während dieser Arbeit. Herrn Prof. Stephan Sigrist danke ich für die Bereitschaft zur Übernahme des Erstgutachtens.

Mein Dank gilt auch allen Mitarbeiter der wunderbaren Abteilung Herrmann, die mir zu jeder Zeit hilfsbereit zur Seite standen und damit einen wichtigen Beitrag zum Gelingen meiner Doktorarbeit geleistet haben. Besonders möchte ich Dr. Ralf Spörle dafür danken, dass er mir die Liste mit den kaudal exprimierenden Genen zur Verfügung gestellt hat. In addition, special thanks to Alix, Bene, Pamela and Tracie for proofreading this thesis. Darüber hinaus danke ich Phillip für seine Unterstützung bei meinen FACS Experimenten. Antje und Uschi danke ich sehr für die technische Unterstützung, insbesondere bei den histologischen Arbeiten. Natürlich danke ich auch allen anderen aus Labor 0.15 für die tolle Zusammenarbeit. Es war wirklich eine schöne Zeit!

Desweiteren möchte ich mich sehr herzlich bei meinen Kooperationspartnern bedanken. Sowohl bei Prof. Frank Buchholz und seiner Arbeitsgruppe, für die Herstellung der esiRNAs, als auch bei Dr. Ulrike Korf und Ihrer Arbeitsgruppe, für die Umsetzung des IPAQ Experiments. Dr. Johannes Fritzmann danke ich für die Unterstützung bei der Auswertung der Tumor-Expressionsprofile.

Ein großer Dank geht auch an meine Freunde, die mir die Zeit in Berlin unvergesslich gemacht haben! Ich danke Simone und Steffen fürs Tatort gucken und dafür, dass es niemals langweilig gewesen ist! Thanks a lot to the “Best Pizza Place” people for having a really great time here in Berlin! Bene danke ich für die vielen Tüten Crokys und Kickerspiele in den Inkubationszeiten. Der Schwandorfer Schmaußerbande danke ich dafür, dass auch in der Heimat immer etwas los gewesen ist.

Zuletzt möchte ich mich sehr herzlich bei meiner Familie bedanken, die mir in allen Lebenslagen verständnisvoll und motivierend zur Seite stand. Vielen Dank vor allem an Jasmin und Roland sowie Stephi und Frank für Eure großartige Unterstützung.

Table of Contents

1 Summary / Zusammenfassung

1.1 Summary

The inner surface of the intestine is covered by a single epithelial cell layer that is subdivided into crypt and villus domains. The mammalian intestinal epithelium constantly renews every 4 to 6 days via stem cells that reside at the bottom of intestinal crypts, while organ size and cellular composition remain steady throughout adulthood. Multiple signaling pathways interact to control intestinal stem cell renewal and tissue homeostasis, and their deregulation can cause tumor formation and progression.

To identify novel genes and signaling pathways involved in intestinal tumor progression, I assessed the function of a shortlist of 364 metastasis candidate genes in intestinal cells. To this end, these genes were analyzed in a loss-of-function phenotypic screen in mesenchymal SW480 human colon cancer cells. I screened for genes whose inactivation promoted both an epithelial cell morphology and localization of the epithelial cell adhesion molecule E-cadherin to cell-cell contacts. Among 18 positively tested candidate genes, I identified *FGF9* and subsequently established novel roles for FGF signals in transformed and untransformed intestinal cells. In colon cancer cells, silencing of *FGF9* or inhibition of FGF receptors induced an epithelial cell morphology and blocked cell motility. These effects were transduced via the MAP kinase pathway, regardless of the existence of an activating *KRAS* mutation in these colon cancer cells. In line with a proposed function of FGF9 in intestinal tumor cells, I found generalized expression of *FGF9* in the tumor epithelium of a subgroup of colon carcinomas. In addition, I identified *Fgf9* specifically expressed in Paneth cells of the untransformed mouse small intestine. I therefore also investigated functions of FGF9 in the normal intestine. Using organotypic culture of primary intestine, I found FGF9 to promote intestinal stem cell proliferation leading to an increased number of intestinal stem cells and crypt domains. On the other hand, interference with *Fgf9* or general inhibition of FGF receptors resulted in loss of stem cell proliferation, crypt degeneration, and biased specification of intestinal progenitors towards the absorptive cell lineage. These results implicate FGF9 as a growth factor that regulates intestinal stem cell maintenance. The finding of specific

expression in Paneth cells that intermingle with stem cells suggests that FGF9 is among the growth factors that constitute the epithelial stem cell niche.

Taken together, my studies revealed different functions for FGF signals in the normal and transformed intestinal cells. Interestingly, I found increased *FGF9* expression in a subgroup of colon cancer patients, which negatively correlated with patient's survival. FGF9 could thus have functional roles in colon cancer by regulating tumor cell morphology and/or by regulating the tumor stem cell pool.

1.2 Zusammenfassung

Die Innenseite des Darms ist mit einer einzelligen Epithelschicht ausgekleidet, die in Krypten und Villus-Domänen unterteilt ist. Das intestinale Epithel eines Säugetiers erneuert sich kontinuierlich innerhalb von 4 bis 6 Tagen. Die Erneuerung geht von Stammzellen aus, die sich im unteren Teil der Krypten-Domäne befinden. Die Organgröße, sowie die zelluläre Zusammensetzung, bleiben während des gesamten Erwachsendaseins konstant. Eine Vielzahl von Signalwegen interagiert miteinander, um Stammzellerhalt und Gewebehomöostase zu gewährleisten. Eine fehlerhafte Regulierung dieser Signalkaskaden hingegen kann Darmkrebsentstehung bzw. -progression verursachen.

Zur Identifizierung neuartiger Gene und Signalwege, die an der Darmkrebsprogression beteiligt sind, habe ich die Funktion von 364 potentiellen Metastasierungsgenen untersucht. Hierzu habe ich eine Funktionsverlust-Phänotyp-Analyse dieser Gene in mesenchymalen SW480 humanen Kolonkarzinom-Zellen durchgeführt. Ich habe die Gene selektiert, deren Inaktivierung eine epitheliale Zellmorphologie bzw. eine membranständige Lokalisierung des Zelladhäsionmolekül E-cadherin in SW480 Zellen hervorgerufen hat. Eines von 18 positiv getesteten Genen war das *FGF9*-Gen. Im weiteren Verlauf meiner Arbeit habe ich bisher unbekannte Funktionen der FGF-Signale in transformierten und nicht-transformierten intestinalen Zellen aufgedeckt. In Kolonkarzinom-Zellen führte die Hemmung von *FGF9* bzw. die Inhibition der FGF-Rezeptoren zu einer epithelialen Zellmorphologie und zur Behinderung von Zellmotilität. Diese Effekte werden durch den MAP-Kinase Signalweg übermittelt, unabhängig von der in dieser Kolonkarzinom Zelllinie vorhandenen aktivierenden KRAS Mutation. Übereinstimmend mit einer vermuteten Funktion von FGF9 in Darmtumoren konnte ich eine erhöhte *FGF9*-Expression in einigen Kolonkarzinomen

nachweisen. Desweiteren habe ich eine spezifische *FGF9*-Expression in den Paneth-Zellen des Dünndarms von Mäusen detektiert. Da dieses Expressionsmuster auf eine FGF9 Signalaktivität im Normalgewebe schließen lässt, habe ich potentielle Funktionen von FGF9 im Normaldarmepithel untersucht. Mithilfe der organotypischen Primärkultivierung von intestinalem Gewebe konnte ich zeigen, dass FGF9 die intestinale Stammzell-Proliferation anregt, wodurch die Anzahl der Stammzellen bzw. Krypten-Domänen ansteigt. Andererseits führte die Hemmung von *Fgf9* oder die Inhibition der FGF-Rezeptoren zur Abnahme der Stammzell-Proliferation bzw. zum Kryptenabbau sowie zu einer Verschiebung der intestinalen Zelltyp-Spezifizierung zu Gunsten der absorbierenden Darmzellen. Diese Ergebnisse identifizieren FGF9 als Wachstumsfaktor, der den Erhalt von intestinalen Stammzellen mitbestimmt. Aufgrund der spezifischen Expression in Paneth-Zellen ist anzunehmen, dass FGF9 zu den Faktoren gehört, die die epitheliale Stammzell-Nische bilden.

Zusammengefasst haben meine Untersuchungen verschiedene Funktionen der FGF-Signale in normalen und transformierten Darmzellen aufgedeckt. Interessanterweise zeigte sich bei einer Darmkrebs-Patientengruppe mit erhöhter FGF9 Expression eine im Durchschnitt geringere Lebenserwartung. Dieses Ergebnis legt die Vermutung nahe, dass FGF9 Darmkrebs sowohl durch die Regulierung der Tumor-Zellmorphologie als auch durch Einflussnahme auf die Anzahl der Tumor-Stammzellen funktional beeinflussen kann.

2 Introduction

2.1 Intestinal Tissue

The major function of the intestine is to absorb nutrients to ensure nourishment of the entire organism. The mammalian intestinal tract can be divided into two major segments: the small and the large intestine. The small intestine has the form of a convoluted tube, located in the central and lower part of the abdominal cavity. In humans, it is on average 6 to 7 meters long. By comparison, the large intestinal canal is greater in its caliber but substantially shorter, measuring approximately 1.5 meters in length in humans (Gray 1918). The two joined segments of intestinal tract represent a tube, extending from the stomach to the anus (as reviewed by Sancho et al., 2004).

2.1.1 Tissue Composition of the Intestine

The intestinal tract is constituted of three tissue layers: the muscularis externa, submucosa and mucosa from the outside towards the intestinal lumen (Fig. 1). The outer located muscularis externa is a muscular wall of the intestinal tract that consists of several layers of innervated smooth muscles, conducting the rhythmic peristaltic movements of the intestine. The intermediate layer, termed the submucosa, is composed of loose connective tissue containing blood and lymphatic vessels, nerve fibers and immune cells. In addition to the supportive and transport function of this tissue, it allows the innermost surface layer, the mucosa, to move flexibly during peristalsis. A thin layer of smooth muscles, named muscularis mucosa, separates the intestinal submucosa and mucosa from each other. The mucosa itself consists of a single layer epithelium of cuboideal cells and the directly adjacent loose connective tissue, termed lamina propria. The mucosal epithelium primarily processes and absorbs nutrients and compacts stool. In addition, it forms a functional barrier to protect against ingested pathogens. Morphologically, the single cell layered mucosal epithelium of the small intestinal tract can be subdivided into evaginations termed villi, which project into the intestinal lumen, and epithelial invaginations known as crypts of Lieberkühn, pointing to the submucosa. The small intestinal tract can be further divided into three domains: Duodenum, Jejunum, and Ileum in their order from the stomach to the cecum. Those regions can only be distinguished by minor histological differences, such as

longer finger-like villi in the jejunum, or the presence of Peyer's patches in the ileum. In contrast, the epithelial layer of the large intestine is organized only in crypt domains, where instead of villi a flat surface epithelium is present. The mucosa is the most highly organized tissue of the intestinal tract, containing several differentiated cell types. Tissue specialization and surface shape are correlated with functional differentiation along the intestinal tract. Throughout adulthood, the mammalian mucosal epithelium is constantly renewed every 4-5 days (as reviewed by Sancho et al., 2004; van der Flier and Clevers, 2009).

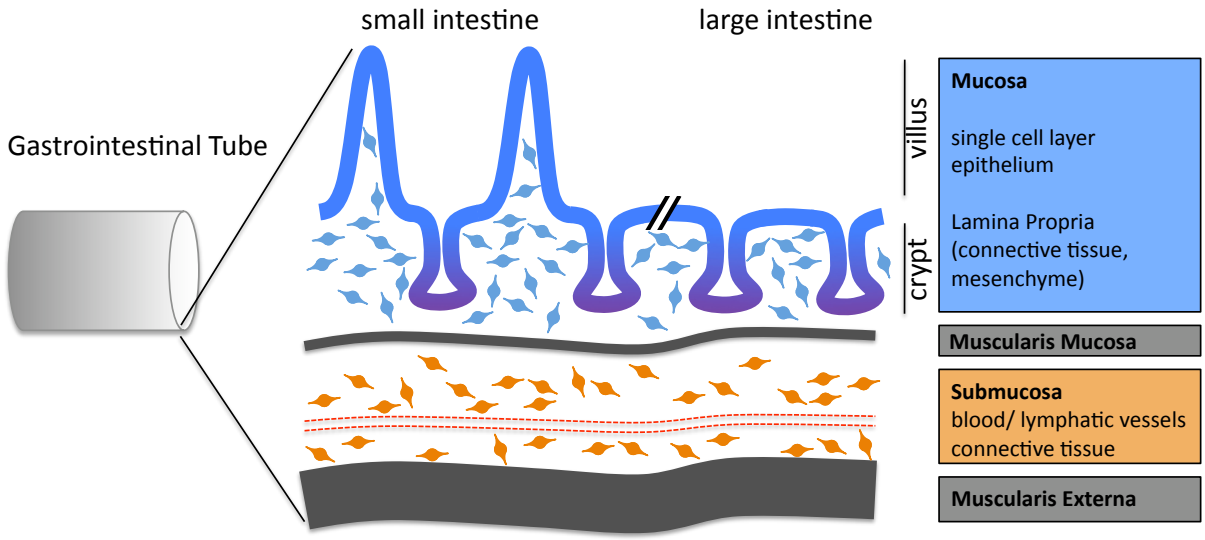

Fig. 1: Schematic representation of the intestinal tissue. The intestinal tract consists of three tissue layers: the muscularis externa, submucosa and mucosa in order from the outside towards the intestinal lumen.

2.1.2 Morphology and Cellular Composition of the Adult Intestinal Epithelium

In the small intestine four major differentiated cell types constitute the intestinal mucosal epithelium: absorptive enterocytes, mucous secreting goblet, hormone secreting enteroendocrine and serous secreting Paneth cells (Fig. 2).

Enterocytes, alternatively termed columnar cells, make up more than 80% of all intestinal epithelial cells and are consequently the most abundant differentiated cells of the intestinal epithelium. These cells are specialized for the absorption of nutrients and the secretion of hydrolytic enzymes. Nutrients are incorporated by endocytosis or diffusion at the apical surface, transported through the cell, and exported at the opposing cellular side across the basal membrane. Upon release, nutrient molecules diffuse through the loose connective tissue of the lamina propia and submucosa and are finally absorbed by surrounding capillaries of blood and lymphatic vessels.

Goblet cells are scattered among the absorptive cells in the intestinal epithelium. The proportion of goblet cells increases from the proximal part of the small intestine (around 4%) to the distal part of the large intestine (around 16%) (Karam, 1999). These cells generate a mucous lining, covering the epithelial sheet, which facilitates passage of digestive material through the bowel. In addition, the mucous layer protects against shear stress, chemical damage and infectious agents (van der Flier and Clevers, 2009). Enteroendocrine or neuroendocrine cells are likewise scattered among the absorptive cells of the intestinal epithelium. Although this cell type makes up less than one percent of the intestinal epithelium, enteroendocrine cells fundamentally control gut physiology by secreting a variety of hormones including serotonin, substance P, and secretin (Barker et al., 2008).

Paneth cells reside at the bottom-most position of the small intestinal crypt domain. By secreting antiseptic agents, such as cryptidins and lysozyme, Paneth cells play an important role in regulating the microbial environment of the intestine.

In addition to the four main differentiated cell lineages, the mucosal intestinal epithelium harbors a couple of rare differentiated cell types. These include M cells that cover intestinal lymph nodules, the so called Peyer's patches, brush/tuft/caveolated cells and cup cells (Barker et al., 2008).

Taken together, the villus domain harbors enterocytes, goblet and enteroendocrine cells, while Paneth cells reside at base position of the small intestinal crypts, where they intermingle with stem cells (Barker et al., 2007).

The large intestine consists of the colon and rectum. The colon's major function is the retrieval of ions and water from the gut contents. The rectum stores the fecal matter until it is excreted through the anus. The single cell layered mucosal epithelium of the large intestine is generally comparable to the small intestinal epithelium (Fig. 2). Both epithelial sheets show a modular fanfold organization, constituting individual crypt domains. However, the large intestine carries no villi but instead a flat surface epithelium harboring the differentiated cell types. Moreover, the large intestinal mucosal epithelium does not contain Paneth cells, while the proportion of goblet cells is strongly increased as compared to the proximal small intestinal epithelium.

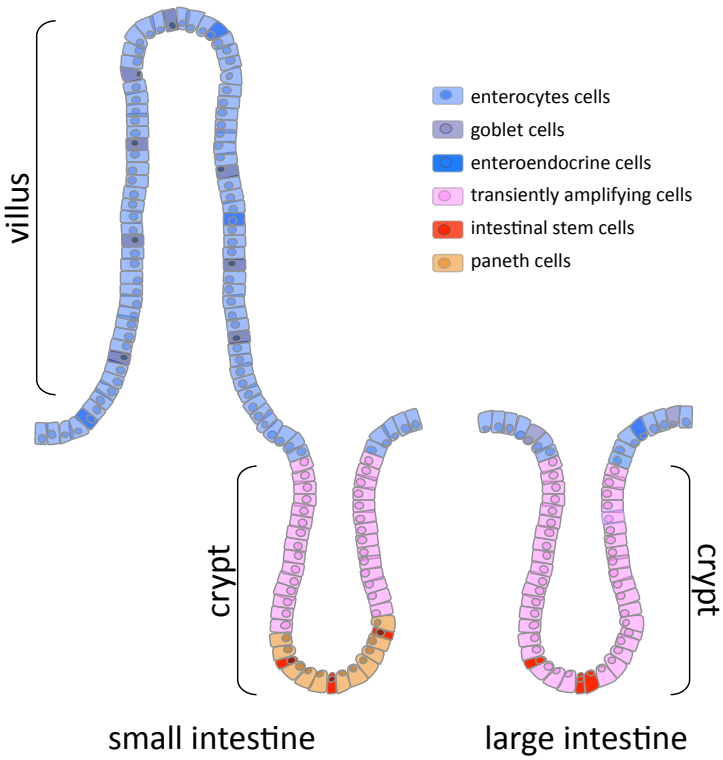

Fig. 2: Schematic representation of the intestinal epithelium. (A) The adult small intestinal epithelium is subdivided in crypts and villi domains. Putative stem cells reside in the crypt bottom and constantly give rise to transiently amplifying progenitor cells. Progenitors terminate proliferation at the crypt-villus junction and differentiate into the intestinal cell lineages. Enterocytes, Enteroendocrine and goblet cells constitute the villus epithelium. Paneth cells reside at the crypt bottom. (B) The large intestine forms a flat surface epithelium. Stem cells are located at the crypt base. Progenitors proliferate along the bottom two third of the crypts. Differentiation initiates when progenitors reach the top third of the crypt. Paneth cells are absent.

2.1.3 Embryonic Development of the Intestine

During embryogenesis, the intestinal epithelium derives from a uniformly proliferating, pseudostratified, endodermal tissue layer that converts into a single cell layered epithelium, starting between embryonic day 13.5 (= E13.5) and E14.5 in mice. During the morphogenetic process of the small intestinal epithelium, evaginations are formed, representing nascent villi. Cell division becomes restricted to intervillus regions. These correspond to the point of origin of intestinal invaginations, representing emerging crypt domains. Similarly, proliferation in the developing large intestine is confined to nascent epithelial pockets corresponding to forming crypts. Surrounding mesoderm constitutes the outer muscularis and the intermediate located submucosal connective tissue. The embryonic cytodifferentiation of the intestinal mucosal epithelium occurs as a proximal-to-distal wave (from E15.5 to E18.5 in mice). During this developmental stage the rate of intestinal elongation strongly exceeds that of the body, becoming exponential and decreases to a linear ratio as postnatal development commences (Geske et al., 2008). In the first weeks

after birth epithelial invaginations of the mucosa convert to mature crypts, by a process in which the intervillus pockets invade the wall of the small intestine. Likewise, crypts of the large intestine become progressively deeper during early postnatal development. Nascent crypts are initially polyclonal, but rapidly become monoclonal as they mature. To compensate for further growth of the organ until adulthood the number of crypt domains constantly increases by crypt fission, a process in which new crypts form by branching off from already existing crypts (as reviewed by Sancho et al., 2004; Barker et al., 2008).

2.2 Intestinal Tissue Homeostasis and Renewal

By definition, adult stem cells exhibit two major characteristics: the ability to generate more undifferentiated stem cells (self-renewal) and concomitantly the ability to generate differentiated cell lineages (tissue-renewal). Once activated, epithelial stem cells generally give rise to a vigorously proliferating progeny, often referred to as transiently amplifying (TA) cells. In their natural environment TA cells proliferate for a given period of time, thereby expanding the cellular pool, before these cells terminally differentiate into the individual cell lineages of the respective tissue. Tissue specific adult stem cells, which constantly fuel the process of tissue renewal during adulthood, have been identified in a variety of tissues, including the adult epidermis, muscle, blood, nervous system and the intestine (Wagers and Weissman, 2004). The turnover of tissue differs substantially among the various epithelia. For instance, the epithelium of the lung can take as long as 6 months to be replaced, whereas the epidermis completely self renews within around 4 weeks (Blanpain et al., 2007). By comparison, the mucosal epithelium of the intestinal tract is the most rapidly self-renewing tissue in adult mammals. In mice, the epithelial layer renews on average every three to five days (Barker et al., 2007). Due to the high cell turnover, the intestine is one of the most attractive adult organ system for studying stemness, proliferation and differentiation.

2.2.1 Stem Cells and Transiently Amplifying Cells

The renewal of the intestinal mucosal epithelium is sustained by a functional stem cell compartment that resides within crypt bases of the small and large intestinal epithelium. Analysis of chimeric mice showed that nascent crypts are initially polyclonal, but rapidly become monoclonal as they mature (Schmidt et al., 1988). In contrast, the villi are

considered to be polyclonal as they obtain epithelial cells from multiple crypts throughout their lifespan. Although it was generally assumed that each individual crypt domain contains an independent stem cell compartment, the lack of specific molecular markers prevented the definitive and direct proof of intestinal stem cells. Two opposing models predominantly discussed in the literature – the classic +4 position model and the stem cell zone model – define the exact identity of intestinal stem cells.

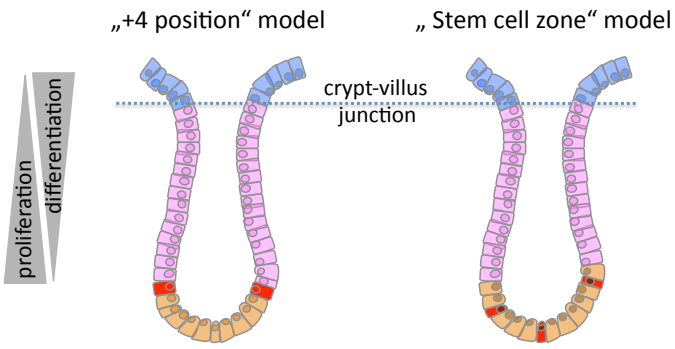

Fig. 3: Two models, which define the exact identity of the intestinal stem cells coexist. In "+4 position" model the intestinal stems are assumed to be located just above the Paneth cells at the +4 position. The "Stem cell zone" model proposes that slander, undifferentiated, cycling cells (termed crypt base columnar cells), which intermingle with Paneth cells, to represent the intestinal stem cells.

2.2.1.1 Intestinal Stem Cells

Since the early 20th century the small intestinal crypt has been regarded as an epithelial tube containing proliferating cells, which are restricted from below by Paneth cells (Barker et al., 2008). One classical model therefore considered stem cells to reside at the +4 position relative to the crypt bottom, directly above terminally differentiated Paneth cells, which occupy the first three crypt base positions. In the 1970's Potten and colleagues supported the "+4 position" intestinal stem cell model as they identified label retaining cells residing specifically at this position (Potten et al., 1974) (Fig. 3). As +4 cells were shown to actively cycle, label retention is considered to result from asymmetric segregation of old and new DNA strands based on the "immortal strand hypothesis" postulated by John Cairns in 1975 (Potten et al., 1974; Cairns, 1975). In addition, it was demonstrated that the potential +4 stem cells are extremely sensitive to irradiation resulting in apoptosis, which in effect would protect the putative stem cell compartment from genetic disorders (Potten, 1977). In this model, damaged stem cells are substituted by early TA progenitor cells, which would drop back to the +4 position and re-acquire stem cell properties. In 2008, Capecchi and colleagues found expression of *Bmi1* in a discrete cell population located near the crypt bottom of the small intestinal epithelium, predominantly residing at the +4 position. Bmi1 lineage tracing

analysis identified these cells to be undifferentiated, proliferating, giving rise to differentiated cells and self-renewing, indicating that *Bmi1* expressing cells represent a stem cell population of the small intestine (Sangiorgi and Capecchi, 2008). The question arises whether the Bmi1 labeled cells correspond to the +4 position cells described by Potten and colleagues. If that is the case, *Bmi1* positive cells should be DNA label-retaining and highly sensitive to irradiation, neither of which has been assessed to date. Crypts containing *Bmi1* positive cells were found to be present in a proximal to distal descending gradient along the small intestinal tract. Accordingly, many crypts were positively tested for Bmi1 expressing cells in the duodenum and proximal domain of the jejunum, to progressively fewer in distal regions, to none present in the ileum and large intestine. Due to this non-uniform distribution of Bmi1 expressing stem cells in the small intestinal epithelium, the authors claim that more than one adult stem cell population might contribute to tissue homeostasis and renewal of the small intestinal epithelium (Sangiorgi and Capecchi, 2008).

The alternative model of a “stem cell zone” has been based on the identification of Crypt Base Columnar (CBC) cells more than 30 years ago (Fig. 3). In 1974, Cheng and Leblond were the first to indentify this distinct cell population and described these as small, undifferentiated and cycling cells, which intermingle with Paneth cells. Based on morphological considerations, the authors suggested that CBC cells might constitute crypt stem cells (Cheng and Leblond, 1974a, b). More recently, Cheng and colleagues reinforced the “stem cell zone” model based on genetically labeling studies of intestinal epithelial cells by chemical mutagenesis of the *Dbl-1* locus (Winton et al., 1988; Bjerknes and Cheng, 1999). This analysis identified the existence of short-lived progenitors, generating one or two cell types as well as long-lived cell progenitors, which are capable of giving rise to all epithelial cell types. This approach revealed essential characteristics of the self-renewing process in the intestinal epithelium. However, it is not clear which cell generates the first clonal mutation, since mutagenesis occurs randomly in this method. The actual nature of the intestinal stem cell therefore remained to be defined. In an alternative strategy to study stem cell function, the putative stem cell population would be genetically marked *in situ*. This would allow for visualization of the labeled potential stem cell and tracing of its clonal progeny over time. However, this strategy can only be employed if a distinct gene marker would have been identified that particularly distinguishes the putative stem cell population from all other cell types.

Wnt signaling has a unique and central role in intestinal biology, as it has been shown by a large number of recent studies that this signaling pathway is a basic requirement for crypt proliferation and essential for homeostasis of the intestinal epithelium (Pinto et al., 2003; Sancho et al., 2004; Barker et al., 2008). In 2007, Hans Clevers and colleagues reasoned that some Wnt target genes might be specifically expressed in intestinal stem cells. As a promising candidate the Wnt target gene Lgr5 has been identified, which is exclusively expressed in cycling CBC cells that are interspersed between Paneth cells (Van der Flier et al., 2007a; Barker et al., 2007). To test this hypothesis transgenic mice expressing a tamoxifen-inducible version of the Cre-recombinase, under the control of the endogenous *Lgr5* promoter, were crossed to a Rosa26-lacZ reporter strain (Barker et al., 2007). In this genetic model, tamoxifen induction genetically marks CBC cells and CBC cell derived progeny, due to irreversible Cre-induced recombination activating the genetic reporter Rosa26-lacZ by excision of a roadblock DNA sequence (Soriano, 1999). This approach therefore allows lineage-tracing studies of Lgr5 expressing CBC cells in adult mice over time. One day after tamoxifen induction individual CBC cells in the crypts of small intestine and colon expressed the *LacZ* reporter gene. At later time points, ribbons of blue cells, emerged from genetically labeled CBC cells to form domains that encompassed entire crypt-villus units, comprising all differentiated cell types of the intestinal epithelium. Blue clones generating all epithelial intestinal lineages were shown to persist over a time period of at least 14 months. Thus the authors conclude that Lgr5-expressing CBC cells in the small intestine and colon fully meet the definition of intestinal stem cells in that these cells self propagate and have the ability of generating all cell types of the respective epithelium (Barker et al., 2007; Barker et al., 2008; van der Flier and Clevers, 2009). At present, these studies indicate that the intestine contains a quiescent stem cell population at the +4 position and an actively cycling Lgr5 expressing stem cell interspersed between Paneth cells. Future studies are necessary to identify the relationship of these cell populations to each other.

2.2.1.2 The Stem Cell Niche

Adult tissue-specific stem cells from various systems are functionally regulated by extracellular cues, derived from the so called stem cell niche, and by intrinsic genetic programs within the stem cell (Li and Xie, 2005). It is generally accepted that intestinal stem

cell integrity relies on such a directing niche (Li and Xie, 2005; van der Flier and Clevers, 2009). Possibly, this niche consists of, and is influenced by, neighboring proliferating and differentiating epithelial cells as well as by surrounding tissues (Yen and Wright, 2006). In the intestine, epithelial and mesenchymal cells, such as subepithelial myofibroblasts are believed to create a specialized cellular niche at the crypt bottom by secreting various growth factors and cytokines promoting epithelial to mesenchymal interactions sustaining the intestinal stem cell niche (Mills and Gordon, 2001). Multiple signaling molecules, such as Wnt, Notch and receptor tyrosine kinase (RKT) ligands, are probably important for niche and stem cell maintenance (Sancho et al., 2004). Bone morphogenetic protein (BMP) signals, expressed in the mesenchyme of the villi, appear to negatively regulate intestinal crypt properties. Consequently, inhibition of BMP signaling in the villus by overexpression of the BMP inhibitor Noggin results in ectopic crypt formation (Haramis et al., 2004). Importantly in 2009, Clevers and colleagues showed that a self-renewing intestinal epithelium can be established *in vitro* from single $Lgr5^+$ intestinal stem cells by uniform administration of a limited set of growth factors, including R-spondin, EGF and Noggin (Sato et al., 2009). Consequently, the authors conclude that individual $Lgr5^+$ intestinal stem cells can operate independently of positional cues from the surrounding microenvironment. Finally, it has been demonstrated that multiple essential factors for intestinal stem cell maintenance in vitro, are generated by Paneth cells (Sato et al., 2010). In agreement, it has been shown that co-culturing of individual intestinal stem cell with Paneth cells significantly enhanced stem cell maintenance and organotypic outgrowth in vitro (Sato et al., 2010). Paneth cells are therefore considered to provide important niche signals for intestinal stem cells.

2.2.1.3 Transiently Amplifying Cells

In the intestine, renewal of the epithelium is accomplished by a relatively small population of intestinal stem cells, which constantly give rise to a much larger pool of fast proliferating transiently amplifying (TA) progenitor cells. Lineage commitment of early TA progenitors remains largely undefined. Clonal analysis of mouse intestinal epithelium identified however several intermediate progenitors with the ability to generate one or several intestinal differentiated cell types (Bjerknes and Cheng, 1999). The Wnt target gene c-Myc is expressed by all cycling cells of the intestinal epithelium and conditional knock out of *c-Myc* in the intestinal epithelium results in a rapid loss of c-Myc deficient crypts. Within weeks,

such c-*Myc*$^{-/-}$ crypts are replaced through crypt fission by crypts that retained *c-Myc*. Myc therefore triggers cell cycle progression of crypt progenitor cells. In general, the morphologically distinguishable TA cells undergo 4-6 rounds of cell division before they irreversibly differentiate into the individual intestinal cell lineages and replenish the intestinal epithelium (Barker et al., 2008; van der Flier and Clevers, 2009). TA progenitor cells divide every 12-16 hours, thereby generating around 200-300 cells per crypt each day, which migrate continuously upwards towards the adjacent villi (small intestine) or the surface epithelium (colorectum) in a coherent cellular column. Each villus of the small intestine is replenished by around six surrounding autonomous crypt domains (Barker et al., 2008). Once committed TA cells reach the crypt-villus junction they readily differentiate into the respective cell types of the villus. Moving further upwards, differentiated cells reach the top of the villus within three to five days. Finally, cells undergo apoptosis and are shed into the intestinal lumen, leading to a balanced tissue homeostasis of the intestine (Heath, 1996; Marshman et al., 2002). In contrast, long-lived Paneth cells, which have a lifespan of around three to six weeks, and the immortal stem cells remain within the crypt base escaping the epithelial conveyor belt of the intestine (Barker et al., 2008).

2.2.2 Cell Lineage Specification

As described above, TA cells irreversibly differentiate into the individual intestinal cell lineages of the small and large intestinal epithelium. Terminally differentiated intestinal cells are basically classified into two main cell lineages: the secretory and the absorptive lineages. Goblet, enteroendocrine and Paneth cells belong to the secretory lineage, whereas enterocytes constitute the absorptive cell lineage. Multiple molecular pathways interact keeping a delicate balance of proliferation and terminal differentiation into the individual cell lineages of the intestinal epithelium. Similar to Wnt signaling, the Notch pathway is required to maintain the crypt compartment in its undifferentiated, proliferative status (van der Flier and Clevers, 2009). Specifically, Notch signaling inhibition or genetic inactivation of the pathway result in a rapid loss of proliferating crypt progenitors associated with a complete conversion of all epithelial cells into goblet cells (Milano et al., 2004; Wong et al., 2004). Conversely, Notch signaling hyperactivation leads to the opposite effect, i.e. a depletion of goblet cells and a partial decrease in enteroendocrine and Paneth cell differentiation resulting in villi populated by an increased percentage of enterocytes (Fre et

al., 2005; Stanger et al., 2005). The Notch pathway consequently regulates absorptive versus secretory fate decisions in the intestinal epithelium. Wnt signaling was shown to antagonistically influence the cell lineage determination in the intestine. Accordingly, the intestinal epithelium of transgenic mice with impaired Wnt signaling, features an elevated rate of absorptive cells, while the secretory lineages are depleted (Korinek et al., 1998; Pinto et al., 2003; Ireland et al., 2004).

2.3 Intestinal Cancer

The majority of malignant cancer cells, derived from various tissues, harbor six alterations in cell physiology collectively leading to the cancer phenotype: 1) self-sufficiency in growth signals, 2) insensitivity to growth-inhibitory (antigrowth) signals, 3) evasion of programmed cell death (apoptosis), 4) limitless replicative potential, 5) sustained angiogenesis, and 6) tissue invasion (Hanahan and Weinberg, 2000). The latter trait, leading to metastatic progression of carcinomas, accounts for more than 80% of cancer deaths (Waerner et al., 2006). The capability for invasion and metastasis enables cancer cells to escape the primary tumor mass and colonize new terrain of the body. Several protein classes involved in the adhesion of cells to their surroundings within the respective tissue are altered in cells possessing invasive or metastatic characteristics. The most commonly identified alteration in cell-to-environment interactions in cancers involves E-cadherin, a homotypic epithelial cell-to-cell adhesion molecule. Epithelial cells ubiquitously express E-cadherin, tightly connecting adjacent cells within an epithelial tissue to each other (Hanahan and Weinberg, 2000). E-cadherin function is impaired in the majority of epithelial cancers, by various mechanisms such as mutational inactivation of the E-cadherin gene, transcriptional or translational repression, as well as proteolytic cleavage of the extracellular E-cadherin domain. Overexpression of E-cadherin in cultured cancer cells and in transgenic mouse models of carcinogenesis counteracts invasive and metastatic properties, whereas blocking the E-cadherin function enhances both features (Christofori and Semb, 1999). Consequently, E-cadherin acts as a common suppressor of invasion and metastasis of epithelial cancers, while its functional inactivation represents a key step in the acquisition of such capabilities.

2.3.1 Human Intestinal Cancer as a Multistep Process

Colorectal cancer (CRC) is one of the most common types of cancer with around one million new cases diagnosed per year worldwide. The disease-specific mortality rate is nearly 33% in the developed world. In the United States and Europe CRC represents the third most diagnosed cancer type (Lynch and de la Chapelle, 2003; Ferlay et al., 2007; Jemal et al., 2008; Cunningham et al., 2010). The prognosis for patients with CRC strongly depends on the stage of diagnosis: 5-year survival rate decreases from over 90% in locally confined non-metastatic cancer to 5% in metastatic cases (de la Chapelle, 2004). The genetic background also has a key role in predisposition to CRC influencing both, tumor initiation and progression (de la Chapelle, 2004). The classic model of CRC describes a well-defined sequence of histological stages– from aberrant crypt proliferation or hyperplasia to benign adenomas, to locally circumscribed carcinoma and finally to metastatic carcinoma – corresponding to the stepwise progression of this disease, which often may take years to decades (Fig. 4). The multiple stages of tumorigenesis are characterized by the occurrence of distinct somatic mutations in oncogenes and tumor suppressor genes (Fearon and Vogelstein, 1990). In the early phases, these mutations occur – at least to some extent – in a predictable manner: CRC is very frequently triggered by loss-of-function mutations in the adenomatous polyposis coli (APC) tumor suppressor gene, leading to aberrant activation of the WNT pathway. In a minority of cases, mutations of β-catenin or Axin2 could lead to a similar effect (Lustig and Behrens, 2003). Wnt hyperactivation is often followed by activating mutations in *KRAS*. *TP53* mutations tend to occur later in the progression of the malignancy (as reviewed by Fearon and Vogelstein, 1990). This makes colorectal tumorigenesis an excellent system to identify and link novel genetic alterations to the various developmental stages of human neoplasms. However, although genetic mutations leading to CRC frequently occur according to a preferential sequence, the total accumulation of alterations, rather than their order with respect to one another, is eventually responsible for the cancer's biology (Fearon and Vogelstein, 1990).

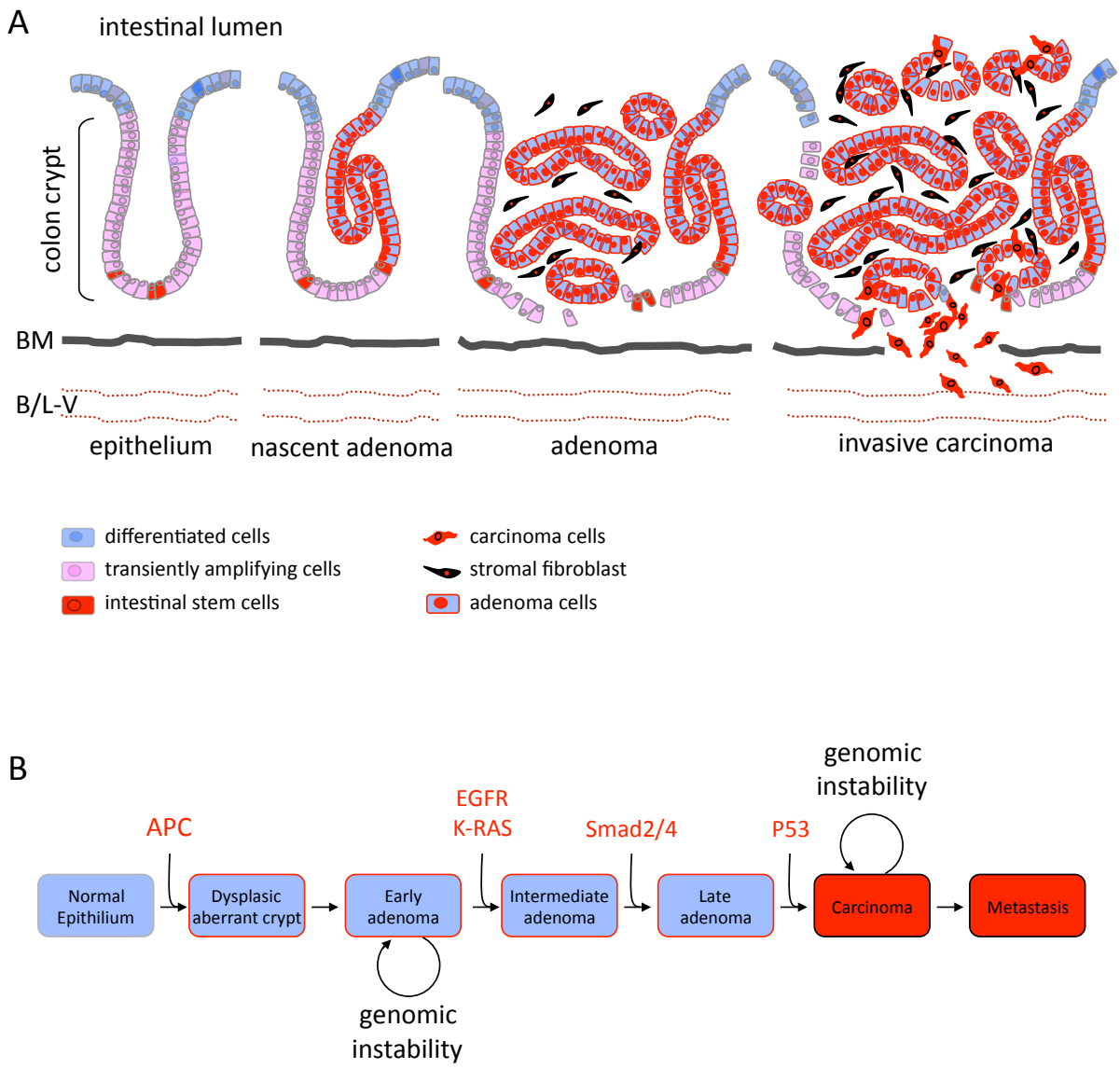

Fig. 4: Schematic representation of histological and molecular steps in intestinal tumor initiation and progression. (A) Colon cancer is multi-step process at which different stages of the malignancy coexist. The stages of the malignancy represent tumors of increasing size and dysplasia. Early-stage adenomas were defined as adenomas that are 1.0 cm in size or less. Late-stage adenomas are greater than 1.0 cm in size and contain foci of malignant carcinoma. (BM: basal membrane; B/L-V: blood/lymphatic vessel) (B) Tumorigenesis proceeds through a series of genetic alterations involving oncogenes (ras) and tumor suppressor genes (Apc, Smad2/4 and p53).

2.3.1.1 Sporadic Versus Familial CRC

CRC is traditionally divided into sporadic and familial (hereditary) cases. Patients with a family risk – those who have two or more first- or second-degree relatives (or both) with colorectal cancer – constitute around 20% of all patients with CRC, while only around 5% or

less of CRC cases account for hereditary syndromes, that are inherited in an autosomal-dominant manner (Lynch and de la Chapelle, 2003; de la Chapelle, 2004; Cunningham et al., 2010). The two most frequently autosomal-dominant inherited CRC syndromes, the familial adenomatous polyposis (FAP) and the hereditary non-polyposis colorectal cancer (HNPCC), will be briefly described first, followed by sporadic CRC and the general course of the disease.

FAP patients inherit a heterozygous mutation in the tumor suppressor gene *APC* and develop numerous colon tumors after spontaneous somatic inactivation of the second allele. Consequently, the causative mutation affects the Wnt pathway, controlling intestinal physiology. FAP patients typically carry numerous (around 100-2500) florid colonic adenomas, unless operated frequently. In most cases, such adenomas are precursors of CRC. Due to the high number of polyps, FAP patients develop CRC in 100% of cases at a mean age of 40 years. FAP-induced CRC tumors characteristically display chromosomal instability (CIN), an aneuploid karyotype and exhibit mutational alteration of important tumor suppressor genes and oncogenes, including first and foremost *APC*, *K-RAS* and *TP53*. In general, these tumors are aggressively invasive and metastatic. The only treatment is prophylactic colectomy at a certain age to prevent progression to malignant stages.

HNPCC is diagnosed by the presence of multiple primary cancers lacking intestinal polyposis. Tumors, presenting distinguishable pathological features, are predominantly located in the proximal colorectum. On average, the age of onset of the disease is between 40 and 45 years. HPNCC patients generally harbor mutations in up to five ubiquitous DNA mismatch repair genes, leading to impaired DNA replication. As a consequence, mutations in tumor suppressor genes and oncogenes, including the *APC* gene, can arise.

Most cases of CRC evolve sporadically. Risk factors include increasing age, being of male sex, previous colonic polyps (adenomas), or previous CRC and lifestyle factors, including intake of fat or red meat, smoking and high consumption of alcohol (Cunningham et al., 2010). By the age of 70 around 50% of the western population generates an adenoma, while the average lifetime CRC risk is approximately 5%. Abundant clinical and histopathological data suggest that most likely all malignant CRC tumors evolve from preexisting benign adenomas (Fearon and Vogelstein, 1990). Sporadic as well as familial CRC occur by the same spectrum of mutations, such as APC inactivation as initiating mutation. However, the manifestation in

sporadic forms occurs later in life, since for most of the tumor suppressor genes, including APC, both alleles have to be inactivated to induce the malignancy (Knudson, 1996).

In the adenoma to carcinoma progression of the disease, the earliest detectable lesion is an aberrant crypt focus (ACF). Histological analysis revealed different ACF subtypes ranging from hyperplasia to dysplasia. Two types can be distinguished (Nucci et al., 1997): the most frequent type constitutes a hyperplastic crypt that only rarely develops into malignant carcinoma. In contrast, the second type generates a dysplastic ACF or unicryptal adenoma, which commonly evolves into invasive CRC. Cells within such dysplastic lesions are generally $APC^{-/-}$. Therefore, loss of APC is considered the gatekeeper mutation, leading to hyperactivated intestinal Wnt signaling. As tumor progression occurs, dysplastic ACFs convert stepwise into benign adenoma to finally form invasive and metastatic carcinoma. Vogelstein and colleagues proposed a “top-down” morphogenetic cascade, which describes colorectal adenomas to arise and grow across the large intestinal mucosal surface epithelium and subsequently invade downwards into the intestinal crypts. In contrast, in an alternative model adenomas are proposed to grow conversely, namely “bottom-up” (Preston et al., 2003). In any case, expansion of ACFs generates larger adenoma, which eventually accumulate further mutations. Consequently, a high proportion of intestinal adenoma that reach a size larger than 1 cm in diameter, harbor additional activating mutations in the protooncogene *KRAS* or complementary mutations in the downstream signaling component *B-RAF* (Fearon and Vogelstein, 1990; Cunningham et al., 2010). Genomic instability as well as further mutations, for instance in the Tgf-β pathway lead to progression of adenomas (Sancho et al., 2004). Still benign, those adenomas are histologically characterized by regularity of the tumor epithelium as well as integrity of the basal membrane. Invasive growth is initiated by inactivating mutations of the tumor suppresser gene *TP53* in around 50% of tumors (Iacopetta, 2003). The interference of the cell cycle regulator *TP53* triggers additional genetic alterations as a consequence of DNA damage and further genetic instability. At this stage, tumor cells are classified as malignant since these cells lose cell adhesion, dissociate from each other and start to aggressively invade the basal membrane of the intestinal epithelium. Following submucosal invasion, malignant tumor cells eventually infiltrate the vascular system to finally disseminate to distant organs, where they possibly succeed in founding new colonies, referred to as metastases.

Of all processes involved in intestinal tumorigenesis, local invasion and formation of metastases are clinically the most relevant (Brabletz et al., 2005). It is therefore of interest to better understand these processes on a molecular level. The perturbation of epithelial cell homeostasis resulting in malignant cancer progression is correlated with loss of epithelial cell adhesion and the acquisition of cell motility (Brabletz et al., 2005). Tumor-related cellular motility can resemble cell migration and tissue rearrangements that occur during various developmental stages, referred to as epithelial to mesenchymal transition (EMT). During embryogenesis, developmental EMT triggers a variety of tissue remodeling events, for instance the formation of mesoderm from primitive ectoderm during gastrulation, which is the earliest developmental EMT (Yang and Weinberg, 2008). Later in embryonic development, EMT affects well-differentiated epithelial cells that are destined to be converted into distinct mesenchymal cell types (Yang and Weinberg, 2008). Consequently, it is easily conceivable that the EMT process may also be induced under certain physiological or pathological conditions in adult tissues, leading to dissemination of single carcinoma cells from primary epithelial tumors (Thiery, 2002). Indeed, key molecules are conserved between development and tumor-associated EMT (Yang and Weinberg, 2008; Thiery and Sleeman, 2006). However, the important features that enable invasive tumor growth and single cell dissemination are reversible, as a redifferentiation towards an epithelial phenotype, resembling a mesenchymal to epithelial transition (MET), is essential during recolonization and metastasis outgrowth. This demonstrates that malignant progression cannot be explained solely by irreversible genetic alterations, indicating the existence of a dynamic component that influences CRC progression. In fact, compelling evidence identified a regulatory role for the tumor environment in many experimental systems (Fodde and Brabletz, 2007; Vermeulen et al., 2010). Tumors do not represent autonomous proliferative clusters of cells, but are heterogeneous, both in their morphology and their function. In particular, individual tumors constitute distinct sub-domains of proliferation and cell cycle arrest, epithelial differentiation and EMT, cell adhesion and dissemination. The identification of novel molecular pathways and signaling networks, orchestrating all these different traits, is necessary to improve and generate new types of cancer therapeutics.

2.3.2 Mouse Models

The mouse provides an excellent *in vivo* system to model human diseases and to test therapies. To establish models for intestinal cancer, mice are genetically manipulated by random mutagenesis or site-specific knockout techniques. These mouse models develop malignancies in the intestinal tract in a predictable manner and allow the analysis of onset and progression of the disease. Consequently, they help to understand in depth the molecular events that contribute to the development and spread of CRC. In addition, such mutant mouse models provide a valuable biological system, suitable for testing therapeutics that CRC patients potentially benefit from.

2.3.2.1 *Apc* Mutant Mouse Model

In 1990, Dove and colleagues established the current most commonly used mouse model for intestinal cancer. This mutant mouse form, which was generated by random mutagenesis with ethylnitrosourea, develops multiple intestinal neoplasias (Min) (Moser et al., 1990). It was subsequently established that Min mice harbor a truncation mutation at codon 850 of the *Apc* tumor suppressor gene (hence termed Apc^{Min}), which corresponds to the human homolog that is generally perturbed in FAP and sporadic CRC patients (Su et al., 1992). In the C57BL/6 background, heterozygous mice develop on average 30 adenomas, most frequently in the small intestine (Taketo et al., 2006). Employing the gene knockout technology, different distinct *Apc* mutations have been generated. Like Apc^{Min} mice, the knockout variants develop adenomas predominantly in the small intestine. Histologically, all *Apc* mutants generate adenomas, which are indistinguishable from each other. Interestingly, the absolute numbers of adenomas differs dramatically in between the mutant variants, even in the same C57BL/6 background. As the histopathology of Apc^{Min} mice adenoma is very similar to human polyps of FAP and sporadic CRC patients, this mouse mutant serves as an excellent animal model to study tumor initiation. Molecularly, APC is best-characterized for its function as a negative regulator of the canonical Wnt pathway via its interaction with β-catenin (Lustig and Behrens, 2003).

2.3.2.1 Stabilizing β-catenin Mutant Mouse Model

β-catenin is the central player in the canonical Wnt signaling cascade and consequently involved in gut physiology (Logan and Nusse, 2004). Importantly, stabilizing mutations of β-

catenin have been identified in a subpopulation of colon cancer that does not harbor *APC* mutations (Taketo et al., 2006). It is therefore reasonable to ask whether stabilizing mutations of β-catenin generate intestinal neoplasia in mice. For this purpose, Taketo and colleagues specifically expressed a stabilized β-catenin variant in the mouse intestinal epithelium. Compared to Apc deficient mutants, transgenic mice carrying a stabilized β-catenin variant develop significantly more (around 3000 by three weeks after birth) intestinal adenomas. Polyps were found at highest densities in the duodenum and proximal jejunum, and at lower densities in the ileum, in contrast to APC mutant mice (Harada et al., 1999). Together, these results confirm the role of Wnt signaling activation in the formation of intestinal adenomas.

2.3.2.2 *Apc* Compound Mutant Mouse Models

Apart from the wealth of information that Apc mutant mouse models have provided, there are critical drawbacks in relating these models to human intestinal neoplasia. For instance, all Apc mutant mice develop adenomas in the small intestine and do not progress to invasive and metastatic carcinomas at a significant frequency, whereas in humans the colon and rectum are favored and adenomas regularly convert over time to invasive carcinomas. These discrepancies are likely to result from a combination of factors, such as differences in intestinal biology, environmental influences, underlying genetics and life-span (McCart et al., 2008). The timescale for the disease development in humans generally takes years to decade. Most *Apc* mutant mice however die after approximately 5 months, due to anemia and cachexia as well as by intestinal obstruction (Taketo et al., 2006). The short life span might be the reason that *Apc* mutant derived adenomas generally do not progress to invasive and metastatic carcinomas, as time is required to acquire further mutations, driving the disease's progression (McCart et al., 2008). Achievements in speeding up intestinal neoplasia in the mouse were made by combining the *Apc* mutation with additional gene defects, leading in some cases to markedly malignant cancer phenotypes. In the following paragraphs relevant *Apc* compound mutant mouse models, discussed in the literature, will be briefly presented.

Oncogenic mutation of the *KRAS* gene is detectable in around 50% of human CRC (Fearon and Vogelstein, 1990). In agreement, Apc deficient mice carrying an additional oncogenic K-ras^{V12} show accelerated intestinal tumorigenesis. Essentially, K-ras^{V12} expression confers an

invasive behavior after APC loss over the long term, as double mutant mice show morphological evidence of invasion into the muscularis in around 17% of tumor incidences (Sansom et al., 2006). The compound mice of mutant *Apc* combined with perturbed Smad2 or Smad4 demonstrated that these key players of the TGFβ signaling pathway play a significant role in malignant progression of CRC. Interestingly, neither KRAS nor SMAD2/4 initiate tumorigenesis by themselves but both factors accelerate malignant progression of tumors to invasive cancers only after loss of *Apc* (Takaku et al., 1998; Hamamoto et al., 2002). In addition, it has been shown that P53 deficiency increases multiplicity and invasiveness of intestinal adenomas of Min mice (Halberg et al., 2000).

The analysis of tumor multiplicity, morphology and behavior in compound mutant offspring led to the identification of several CRC associated genes and their function in tumor initiation and progression. Nevertheless, whereas some of the *Apc* compound mice show increased intestinal tumor invasion properties, no mouse model of intestinal neoplasia consistently generates metastasis. Such metastatic mouse models would however be of top priority, especially given the fact that metastatic progression is the major cause of cancer death.

2.4 Signaling Pathways Involved in Intestinal Development and Cancer

Embryonic development and adult tissue homeostasis require a tight regulation of cell-cell communication, often mediated by secreted ligands and their interaction with corresponding receptors. Receptor stimulation in turn, intracellularly initiates distinct signaling cascades, which generally trigger the gene expression program of targeted cells. Cancer cells engage and perturb such signaling pathways for their benefits. As a consequence, the balance between stemness, proliferation, differentiation and apoptosis is lost in the developing tumor. The most relevant pathways involved in intestinal development, homeostasis and tumorigenesis that are discussed in the literature will be described below.

2.4.1 WNT Signaling Pathway

Secreted WNT factors are highly conserved throughout the animal kingdom. The signaling proteins were shown to trigger and regulate several fundamental processes, including cell growth, motility and differentiation during embryonic development and adult tissue homeostasis (Lustig and Behrens, 2003). Wnt proteins are extracellular ligands that act on target cells in a paracrine manner, leading to the stimulation of the transmembrane receptor Frizzled. Intracellularly, the pathway branches into three major signaling cascades: 1) the canonical Wnt/β-catenin pathway, 2) the planar cell polarity pathway and 3) the Wnt/Ca^{2+} pathway (Huelsken and Behrens, 2002).

2.4.1.1 Canonical Wnt/β-catenin Pathway

The key factor of the canonical Wnt signaling cascade is β-catenin, which has a dual function. On the one hand, membrane-bound β-catenin is involved in the control of cell-cell adhesion as it physically links the cadherin family of cell adhesion molecules to the actin cytoskeleton. On the other hand nuclear β-catenin serves as a transcriptional activator. For this purpose, β-catenin has to associate with DNA binding proteins, as it cannot intrinsically bind to DNA. The T cell factor/lymphoid-enhancing factor (TCF/LEF) family represents the best characterized nuclear β-catenin interaction partner, involved in the transcriptional activation of Wnt target genes (Lustig and Behrens, 2003). Intracellularly, Wnt signaling stabilizes β-catenin on a protein level. The secreted Wnt glycoproteins specifically bind to receptor complexes consisting of the Frizzled seven transmembrane receptor and homologues of the LDL receptors termed LRP5/6, which act as essential co-receptors. Wnt signaling is inhibited by several secreted factors, such as WIF, Cerberus, and FrzB, which antagonize Wnt binding to the Frizzled receptor. Alternatively, Wnt signaling is antagonized by Dickkopf (Dkk), which blocks the Wnt/LRP interaction, while an additional membrane associated protein named Kremen binds to Dkk and induces endocytosis of LRP, likewise resulting in Wnt signal inhibition (Lustig and Behrens, 2003). In the absence of Wnt factors, cytosolic β-catenin is phosphorylated at a series of highly conserved serin/threonine residues close to its N-terminal site. Phosphorylation of β-catenin is carried out by the “degradation complex”. This multiprotein complex consists of the scaffold protein Axin, which forms a homodimer or a heterodimer with the related protein Axin2, the kinase Glycogen synthase kinase 3 β (Gsk3β), the tumor suppressor protein APC and Diversin, which links the kinase Casein

kinase 1 ε (CK1ε) to the complex. CK1ε serves as a priming kinase for Gsk3β, which in turn phosphorylates β-catenin at distinct serine/threonine residues. Phosphorylation promotes ubiquitination of β-catenin and consequential proteasomal degradation. In the presence of Wnts the cytoplasmatic protein Dishevelled (Dsh) interferes with the "degradation complex" and prevents β-catenin degradation. Stabilized cytosolic β-catenin accumulates and subsequently translocalizes into the nucleus where it associates with LEF/TCF DNA binding factors. The LEF/TCF-β-catenin complex represents a transcriptional activator that induces target gene expression, whereas in the absence of β-catenin, LEF/TCF proteins bind to transcriptional co-repressors such as groucho, thereby silencing their target genes. Consequently, the interaction with β-catenin transiently converts TCF proteins into transcriptional activators. Wnt signals therefore manifest in the transcription of TCF target genes such as the oncogene c-myc, Axin2, Cyclin D1 or the matrix metalloprotease MMP7.

2.4.1.2 Planar Cell Polarity Pathway

The planar cell polarity pathway modulates the organization of the cytoskeleton and coordinates the polarization of cells within the plane of an epithelial layer. In this pathway, Frizzled receptors trigger Dsh, which is connected via Dam1 to downstream effectors. These are e.g. the Rho-associated kinase (ROCK) as well as the small GTPase RhoA, which in turn regulates the jun-Kinase (JNK) (Huelsken and Behrens, 2002).

2.4.1.3 Wnt/Ca^{2+} Pathway

The Wnt/Ca^{2+} pathway involves the interaction of the Frizzled receptor with G-proteins, which induces the release of intracellular calcium. Key players of this signaling cascade are the phospholipase C (PLC) and the protein kinase C (PKC). Increased Ca^{2+} levels were shown to activate the phosphatase calcineurin, which results in dephosphorylation and nuclear translocation of the transcription factor NF-AT (Nuclear Factor of Activated T Cells) (Huelsken and Behrens, 2002).

2.4.1.1 Wnt Pathway in the Intestine

Expression analyses of Wnt signaling pathway components and Wnt target genes indicate active Wnt signaling in the intestine, which forms a gradient, showing the strongest activity in the lower crypt domain (Sancho et al., 2004; Gregorieff et al., 2005). In addition, nuclear β-catenin has been demonstrated to accumulate in dividing cells at the crypt bottom.

Several functional studies confirmed a fundamental role of canonical Wnt signals in the intestine. For instance, proliferation of epithelial progenitors in intestinal crypts was shown to depend on active Wnt signaling. This was evidenced by several intestinal specific Wnt signaling interference studies, including mutational inactivation of the intestinal specific LEF/TCF family member *TCF7L2* or the ectopic expression of the secreted Wnt inhibitor *DKK-1* in the intestine (Korinek et al., 1998; Pinto et al., 2003). In all of these genetic modifications a dramatic reduction of intestinal epithelial cell proliferation and loss of crypts was observed. Conditional depletion of β-catenin from the intestinal epithelium showed a similar effect. On the other hand, Wnt signaling pathway activation, as for example by transgenic expression of the Wnt agonist R-spondin induced a rapid onset of crypt cell proliferation (Kim et al., 2005). Similarly, other activating mutations in the WNT pathway are clearly associated with intestinal hyperproliferation, leading to CRC in humans as well as to the formation of adenoma in the murine intestine. Moreover, several Wnt target genes are specifically expressed in intestinal stem cells (Van der Flier et al., 2007a). Consequently, the pathway has emerged as a critical regulator of crypt stem cells (Reya and Clevers, 2005; van der Flier and Clevers, 2009). A functional study confirmed this relationship, showing that intestinal stem cell maintenance depends on the Wnt target gene *Ascl2* (van der Flier et al., 2009b). Finally, Wnt signals do not only control undifferentiated intestinal progenitor cells, but also influence terminal maturation of post mitotic Paneth cells (van Es et al., 2005a).

2.4.1.2 WNT Pathway in CRC

Mutations of the Wnt pathway are generally found in human colorectal tumors, and are required for tumor initiation. It has also been proposed that the presence of other oncogenes does not transform the intestinal epithelium in the absence of mutations in the Wnt pathway. Mutations in the Wnt pathway are thus considered as "Gatekeeper" mutations for oncogenic transformation of the intestine (Kinzler and Vogelstein, 1996). Loss-of-function mutations in APC are found in around 85% of CRC patients leading to inappropriate Wnt signaling (Fearon and Vogelstein, 1990). APC is a classical tumor suppressor gene that follows Knudsen's "two-hit hypothesis", implying that both alleles must be affected before an effect is manifested. Loss of the first allele is either inherited (as in the case of FAP patients) or spontaneously acquired (as in the bulk of sporadic CRC patients). The following "loss-of-heterozygosity" (LOH) triggers early steps of CRC.

Furthermore, mutations in other components of the Wnt pathway, including Axin2 and β-catenin were associated to CRC. As a common result, these genetic alterations ultimately cause nuclear accumulation of β-catenin and consequential transcriptional activation of LEF/TCF target genes. As *TCF7L2* is ubiquitously expressed in epithelial cells of the intestine, pathologically increased levels of nuclear β-catenin result in transcriptional activation of TCF7L2 target genes, which was shown to drive CRC (van de Wetering et al., 2002). Moreover several mouse models for intestinal cancer (see above) underscore that mutational activation of the Wnt pathway is the principal driver of intestinal carcinogenesis. However, Wnt pathway-activating mutations have to specifically occur in crypt stem cells to trigger tumorigenesis as has been recently demonstrated by two mouse studies (Barker et al., 2009; Zhu et al., 2009). Importantly, in addition to its function in tumor initiation Wnt signaling was shown to promote intestinal tumor progression and EMT (Brabletz et al., 2005; Phelps et al., 2009). As a consequence intestinal tumor cells that harbor high levels of nuclear β-catenin appear to undergo transient cell cycle arrest and to progressively lose the expression of epithelial markers such as E-cadherin, while acquiring mesenchymal markers including fibronectin, matrix metalloproteinases, the transcription factors Slug, Cdx1, and Fra-1 and others (Fodde and Brabletz, 2007).

2.4.2 Notch Signaling Pathway

Notch signals influence several developmental processes such as spatial patterning and cell differentiation in metazoans by regulating communication between adjacent cells. The Notch gene family comprises four members (NOTCH1-4) in mammals, which encode large single-span transmembrane receptors. There are five Notch-stimulating ligands including Delta-like 1, 3 and 4 as well as Jagged 1 and 2, which likewise represent transmembrane proteins. The Notch-ligand interaction, which is typically generated by two neighboring cells, leads to proteolytic cleavage of the Notch receptor. Subsequently, the released Notch intracellular domain (NICD) translocates into the nucleus. Here, it binds to the transcription factor CSL, leading to the transcriptional activation of target genes including the hairy/enhancer of split (HES) gene family. These genes encode for basic helix-loop-helix (bHLH) proteins, which represent well-characterized transcriptional repressors.

2.4.2.1 Notch Pathway in the Intestine

Multiple studies suggested an involvement of Notch signals in intestinal development. For instance, notch signaling was shown to be essential for the maintenance of proliferating crypt cells in the intestinal epithelium (Fre et al., 2005). In addition, Notch1 stimulation is present in crypt stem cells as demonstrated by Cre-mediated lineage tracing studies of Notch1 activity (Vooijs et al., 2007). Finally, notch signaling also critically influences intestinal cell fate decisions as demonstrated by notch intestinal specific loss and gain-of-function experiments (Fre et al., 2005; Stanger et al., 2005). These studies established a regulatory function of the Notch pathway in the control of absorptive versus secretory cell fate decisions in the intestinal epithelium (see above).

As discussed above, inactivation of Notch signaling completely converts proliferating intestinal cells into postmitotic goblet cells. A direct Notch target in the intestine is *Hes1*, which was shown to repress the bHLH transcription factor *Math1* (Jensen et al., 2000). Intestinal Math1 in turn is essential for cell differentiation into the secretory lineage (including goblet cells), as the intestinal epithelium of *Math1* mutant mice only harbors enterocytes (Yang et al., 2001). In agreement, it has been recently demonstrated that *Math1* is essential for the conversion of intestinal stem cells into goblet cells, induced by inhibition of the Notch signaling pathway (van Es et al., 2010).

2.4.3 TGF-β Superfamily Signaling (TGF-β/BMP)

The Transforming Growth Factor (TGF)-β superfamily of growth factors participates in multiple biological processes including cell proliferation, differentiation, apoptosis, and specification of developmental fate during embryogenesis as well as in mature tissues. The TGF-β family of cytokine ligands diversifies into two subfamilies, the TGF-β/Activin/Nodal subfamily and the Bone Morphogenetic Protein (BMP) subfamily, classified by sequence similarity and the specific signaling pathways that they activate. The corresponding receptor family consists of two subclasses the type I and the type II classes of transmembrane receptor proteins. Signaling initiates with the interaction of the TGF-β superfamily ligand to a type II receptor dimer, which recruits a type I receptor dimer forming a hetero-tetrameric complex with the ligand. This interaction results in phosphorylation of the type I receptor by the type II receptor. Intracellularly, the signal is transduced by SMAD proteins, which are subdivided into three classes: 1) receptor-regulated SMADs (R-SMADs), 2) a common SMAD

(co-SMAD) and 3) inhibitory SMADs (I-SMADs). After receptor stimulation and association with the co-SMAD, R-SMADs proteins become phosphorylated and translocate to the nucleus. There, the R-SMAD proteins associate with transcriptional co-activators or repressors to control target gene expression. The class of R-SMADs contains five members (SMAD-1, -2, -3, -5 and -8). TGF-β signaling is mediated predominantly through SMAD-2 and -3, while the BMP pathway signals through SMAD-1, -5 and -8 (Shi and Massagué, 2003).

2.4.3.1 TGF-β Signaling in CRC

Multiple inactivation mutations of TGF-β signaling factors have been characterized at the conversion of intestinal benign adenoma to invasive carcinoma (Fearon and Vogelstein, 1990). For instance, TGF-β receptor type II as well as SMAD2 and -4 are frequently perturbed in CRC (Sancho et al., 2004). In line, overexpression of the TGF-β feedback inhibitor BAMBI is associated with a poor prognosis in colon cancer (Fritzmann et al., 2009). As discussed above, compound mouse models of mutant Apc combined with perturbed Smad2 or Smad4 functionally confirmed that these core elements of the TGFβ signaling pathway play a significant role in the malignant progression of CRC (Takaku et al., 1998; Hamamoto et al., 2002). Collectively, these data provide evidence that lack of TGF-β signaling in the intestine contributes to the progression of early pre-existing intestinal neoplasms.

2.4.3.2 BMP Signaling in CRC

Bone morphogenetic protein (BMP) ligands are found to be expressed predominantly in the mesenchyme of the villus, whereas phosphorylated SMAD-1, -5 and -8 are present in the villus epithelium, suggesting paracrine BMP signaling in this region. Inhibition of BMP signaling by transgenic expression of the BMP inhibitor noggin induces the formation of numerous ectopic crypt units along the crypt-villus axis. Morphologically, these transgenic mice are reminiscent of patients carrying the Juvenile Polyposis Syndrome (JPS), which is frequently associated mutational inactivation of BMP signaling in the intestine. Consequently, these data indicate that intestinal BMP signaling represses *de novo* crypt formation and polyp growth (Haramis et al., 2004).

2.4.4 Hedgehog Signaling

Hedgehog (Hh) signaling tightly controls the development of many tissues and deregulation can lead to birth defects and cancer in several organs such as skin, cerebellum, muscle, pancreas, prostate or digestive tract (Hooper and Scott, 2005). Secreted Hh proteins are typically distributed in form of a gradient and cells respond to a distinct Hh ligand concentration. Hh responsive cells express three different transmembrane proteins, which are involved Hh signaling: 1) Smoothened (SMO), 2) Patched (PTCH) and 3) Hedgehog interacting protein. In the absence of Hh ligands, the PTCH receptor inhibits SMO. This inhibition however, is released after Hh ligand binding to the PTCH receptor. Hh signaling pathway activation results in the translocation of Cubitus Interruptus (CI) family members of Zn-finger transcription factors into the nucleus, driving the expression of target genes (Sancho et al., 2004). In mammals, three Hh genes (Shh, Ihh and Dhh); two PTCH genes (PTCH1 and PTCH2); and three CI homologues (Gli1, Gli2 and Gli3) have been identified (Hooper and Scott, 2005).

2.4.4.1 Hedgehog Signaling in the Intestine

Proliferative epithelial progenitors in the intervillus domain of developing mouse small intestinal epithelium were shown to express Ihh and Shh. Interestingly, $Ihh^{-/-}$ mutant mice have shorter villi and reduced numbers of epithelial precursors, in agreement with a function for Ihh in promoting small intestinal cell renewal (Sancho et al., 2004).

2.4.5 Receptor Tyrosine Kinases Signaling

Receptor tyrosine kinases (RTK) tightly regulate a plethora of cellular processes such as growth, differentiation, migration and apoptosis during embryonic development and adult tissue homeostasis. As a consequence, deregulation of RKT signaling was shown to promote tumor development and progression in several human cancers (Zwick et al., 2001). The family of RTKs is divided into 20 subfamilies based on their structural characteristics. All RTKs are single-span transmembrane receptor proteins and share a homologous intracellular tyrosine kinase domain (Zwick et al., 2001). Ligand binding to the extracellular domain results in receptor dimerization and auto-phosphorylation of intrinsic tyrosine residues. Phosphorylation of these tyrosine residues creates binding sites for adaptor molecules that link RTK activation to several downstream pathways including the Ras signaling cascade.

Three *Ras* genes (*HRAS*, *KRAS* and *NRAS*) work as G-proteins, which are active when bound to GTP and inactive when bound to GDP. RAS activation (triggered for instance by RTK ligand binding) stimulates RAF, which phosphorylates kinases of the MEK family. This kinase in turn phosphorylates members of the Mitogen-Activated-Protein Kinase (MAPK) family that subsequently translocate to the nucleus to phosphorylate various transcription factors (Sancho et al., 2004). The RAS-RAF-MAPK signaling cascade regulates cell growth, differentiation and survival and can, when deregulated, promote tumor progression and metastasis (Hancock, 2003). As a result, one third of all human cancers carry *RAS* activating mutations, while the frequency of KRAS mutations in CRC is between 38% and 50%. Moreover, 20% of CRC with wild-type *K-RAS* carry activating mutations in *B-RAF*, mimicking thereby a *K-RAS* activating mutation (Sancho et al., 2004). Several mouse models were generated to delineate the role of *K-RAS* in intestinal carcinogenesis. As discussed above, Apc deficient mice carrying an additional oncogenic K-ras^{V12} show accelerated intestinal tumorigenesis insofar as adenomas convert more efficiently to invasive carcinomas (Sansom et al., 2006). However, expression of constitutively active K-RAS alone generates no or very few intestinal tumors in mice. Consequently, RAS signaling is assumed to promote malignant progression rather than to initiate intestinal cancer. In agreement, activating mutations in K-RAS and B-RAF are typically first detectable in large adenomas and carcinomas (Sancho et al., 2004).

2.4.5.1 RTKs in the Intestine and CRC

Multiple RTK transmit signals that control aspects of intestinal biology and are deregulated in CRC. For instance, overexpression of Met, which represents the RTK for the hepatocyte growth factor HGF, cooperates with activating mutations of K-RAS to accelerate tumor growth by enhanced MAPK activation and decreased apoptosis in human CRC cells (Birchmeier et al., 2003). In line it was shown that down regulation of MET efficiently inhibits an invasive and metastatic behavior of CRC (Herynk et al., 2003). In addition, the RTK EphB2 and EphB3 are essential to restrict cell intermingling and assign distinct cell populations to specific regions within the intestinal epithelium (Batlle et al., 2002b). Loss of EphB activity in turn promotes intestinal tumor progression (Batlle et al., 2005). Finally, the epidermal growth factor receptor (EGFR) and the vascular endothelial growth factor receptor (VEGFR), both belonging to the RTK family, were shown to mediate CRC progression. Importantly,

monoclonal antibodies and small molecule inhibitors targeting the EGFR and VEGFR have been developed, which now serve as relevant additions to the treatment options of advanced CRC patients (Winder and Lenz, 2010).

2.4.5.2 FGF Signaling

Fibroblast growth factor (FGF) signaling regulates multiple biological functions including cellular proliferation, survival, migration and differentiation while deregulation can promote tumor development of diverse cancer types. The mammalian FGF family of secreted ligands consists of 18 members, which interact with 4 highly conserved RTK (FGFR1-4). FGFRs consist of three extracellular immunoglobulin (Ig) domains, a single-span transmembrane helix and an intracellular tyrosine kinase domain (Eswarakumar et al., 2005; Turner and Grose, 2010). All four FGFRs have several isoforms. The receptor-ligand binding specificity is constituted by the second and third Ig domains, which form a distinct ligand-binding pocket. FGF ligand binding induces FGFR dimerization, which results in intermolecular transphosphorylation of the cytosolic tyrosine kinase domain. A central mediator of FGF signaling is the fibroblast-growth-factor-receptor-substrate 2 (FRS2), which binds to the phosphorylated cytosolic FGFR domain after FGF stimulation. The activated FGFR phosphorylates FRS2 at distinct tyrosine residues. Phosphorylated FRS2 in turn acts as core unit of a signaling complex, which consists of the tyrosine phosphatase Shp2, the adaptor Grb2, and the docking protein GAB1. Depending on the cellular context, FGF signals are linked to distinct downstream signaling cascades including the RAS-RAF-MAPK and the PI3-kinase/AKT pathways (Turner and Grose, 2010).

FGF signals are known to play crucial roles in intestinal development: in the mouse, loss of *Fgf9* disrupts the formation of the intestinal tract in the embryo, and loss of *Fgfr3* affects stem cell and Paneth cell lineages (Geske et al., 2008; Vidrich et al., 2009). Deregulation of FGF signaling has been observed in various tumors, and promotes malignant progression in skin, ovarian and prostate cancer (Turner and Grose, 2010). Importantly, overexpression of a specific FGFR3 protein isoform was recently shown to promote CRC growth and migration (Sonvilla et al., 2010).

2.5 Aim and Scope of the Work

The aim of this thesis work was to identify novel genes involved in intestinal tumor progression. We reasoned that genes whose products play roles in tumor progression may be enriched among those expressed in the caudal end of the mid-gestation mouse embryo, a place where epithelial cells undergo a phenotypic switch to a mesenchymal state of low cell adhesion and high cell motility, as is observed during the formation of invasive tumor cells. We therefore targeted human homologues of genes expressed in the embryonic caudal end in a loss-of-function phenotypic screen of human colon cancer cells, which feature a mesenchymal morphology, motility, and little cell adhesion. Genes whose inactivation promoted a conversion of such tumor cells to an epithelial cell morphology along with localization of the epithelial cell adhesion molecule E-cadherin to cell-cell contacts, were considered as positively tested candidates, as these genes would potentially direct tumor progression. The expression of positively tested candidate genes was then characterized in human intestinal tumors to determine the significance of such genes with respect to human colon cancer. In addition, we assessed the impact of these genes on intestinal “stemness” and tissue homeostasis. To this end, we employed the recently published organotypic culture of primary intestine (Sato et al., 2009) that retains a controlled hierarchy of stemness, proliferation, and differentiation, which is generally lost in 2-dimentional cultures of intestinal cancer cells.

3 Results

3.1 Identification of Novel Genes Involved in Intestinal Tumor Progression

3.1.1 Outline of the Loss of Function RNAi Phenotypic Screen in SW480 Cells

The inner surface of the intestinal tract is lined by a simple layer of epithelial cells. These cells are closely connected to each other by specialized membrane structures such as tight junctions, adherens junctions, desmosomes, and gap junctions. In addition, these epithelial cells display an apical–basolateral cell polarity, harboring polarized organization of the actin cytoskeleton, and a basal lamina at the basal surface (Thiery and Sleeman, 2006). Under normal conditions, cells within the epithelial layer do not detach and move away from each other. However, invasive growth and metastasis of colon carcinoma involves loss of epithelial cell adhesion and gain of cell motility. We therefore reasoned that genes whose products play roles in loss of cell adhesion and gain of cell motility during tumor progression might be enriched in the mouse embryo at sites, where cells undergo a similar loss of cell adhesion and gain of cell motility, i.e. in the embryonic primitive streak. This embryonic structure is formed early in mammalian development, marking the onset of gastrulation (Arnold and Robertson, 2009). Within the primitive streak, a complex network of signaling pathways including Wnt, TGF-β, Fgf and others affect the epithelial cells of the epiblast, which subsequently undergo an Epithelial to Mesenchymal Transition (EMT) leading to a phenotypic switch to a mesenchymal state of low cell adhesion and high cell motility (Thiery and Sleeman, 2006; Yang and Weinberg, 2008). Similar processes have been proposed to take place in tumors. Tumor associated EMT has been suggested to promote the dissemination of single carcinoma cells from primary epithelial tumors leading to the formation of metastases. Consequently, several signaling pathways and key molecules that direct EMT in the developing embryo have been associated with tumor progression (Thiery, 2002). Ralf Spörle (Max Planck Institute for Molecular Genetics, Berlin) has, before the start of this PhD project, analyzed the molecular anatomy of the mouse embryo database (MAMEP; http://mamep.molgen.mpg.de/) and identified approximately 350 genes that display restricted areas of expression in the caudal end of the mouse embryo at E9.5, a place

and time where cells undergo EMT in the primitive streak. A list of ensemble IDs of those genes restrictively expressed in the caudal end of a mid-gestation mouse embryo is given in Appendix 1.

The aim of this PhD work was to identify novel genes involved in intestinal tumor progression. Therefore, I intended to target the human homologues of these previously isolated genes in an RNA interference phenotypic screen (Fig. 5). For this, the Buchholz group from Max Planck Institute of Molecular Cell Biology and Genetics (Dresden) generated and provided corresponding esiRNAs (Buchholz et al., 2006), which I employed to knockdown the selected candidate genes individually in SW480 human colon cancer cells (Leibovitz et al., 1976). SW480 cells are derived from an invasive primary CRC, carry a loss of function APC mutation, and an activating mutation of the *KRAS* GTPase, and typically display a mesenchymal (“spindle-form”) morphology, characterized by low epithelial cell adhesion and high cell motility. I screened for genes whose inactivation promoted an epithelial ("cobblestone") morphology and localization of the epithelial cell adhesion molecule E-cadherin to cell-cell contacts. As a positive control, SW480 cells were transfected with an siRNA targeting the *BCL9L* gene, which codes for a transcriptional co-activator of β-catenin (Birchmeier, 2005). Importantly, it has been shown before that BCL9L siRNA-treated SW480 cells translocated β-catenin from the nucleus to the cell membrane and gained an epithelial-like morphology (Brembeck et al., 2004).

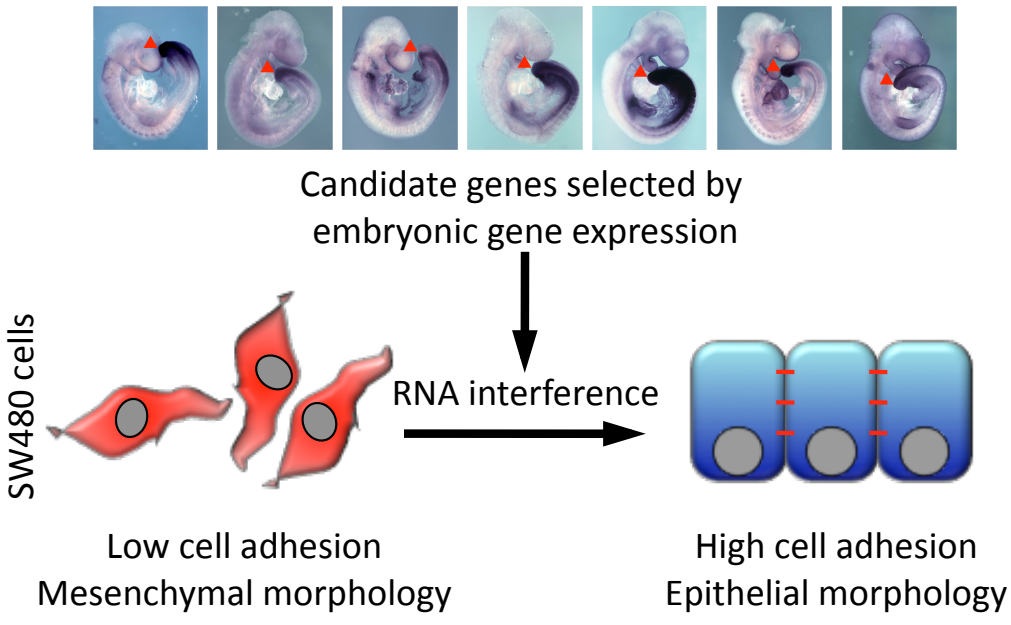

Fig. 5: Schematic overview of the loss-of-function phenotypic screen for genes that modulate intestinal tumor progression. Genes were selected from the MAMEP database and literature searches for their caudal expression pattern (indicated by red arrowheads) in the mid-gestation mouse embryo (E9.5). Human orthologues of candidates were inactivated by esiRNA transfection in human colon cancer SW480 cells, and positive genes were selected for their ability to promote epithelial morphology and cell adhesion when inactivated.

Initially, the average knockdown efficiency was evaluated for several randomly chosen esiRNAs. For this purpose, SW480 cells were transiently transfected with esiRNAs targeting their related genes or with a negative control esiRNA (directed against the firefly luciferase mRNA). mRNA levels were assessed 48h after transfection, using quantitative real-time PCR (qRT-PCR) analysis. All tested esiRNAs downregulated their particular target gene expression by more than 70%, relative to control transfections (Fig. 6). After affirming the functionality of the provided esiRNAs, the impact of the selected set of 364 genes on the phenotype of SW480 cells was assessed.

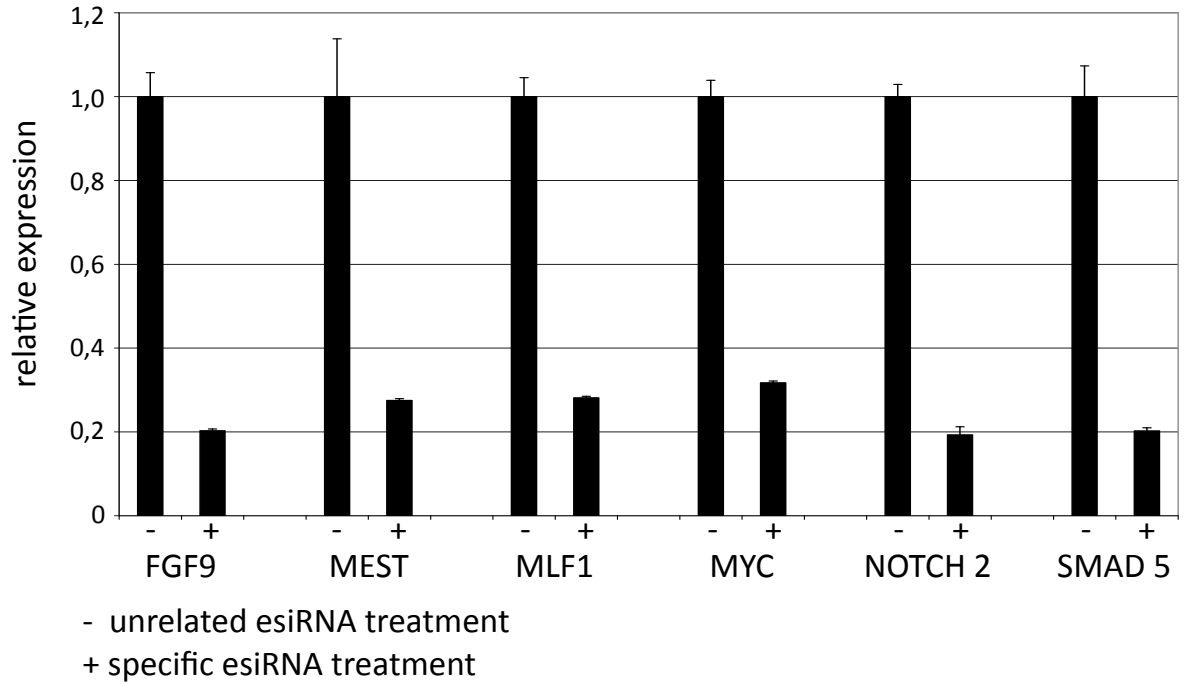

Fig. 6: esiRNA treatment induces effective mRNA interference in SW480 cells. SW480 cells were transfected with esiRNAs directed against selected genes (as indicated) or with control esiRNA and mRNA levels were assessed 48h after transfection, using qRT-PCR. Expression of experimental genes was normalized against GAPDH. Residual gene expression after specific esiRNA treatment is given relative to control transfections. Bars indicate mean of 3 technical replicates, ± SE.

3.1.2 Identification and Evaluation of Candidate Genes for Tumor-associated EMT

To identify novel genes involved in tumor associated EMT, mesenchymal SW480 human colon cancer cells were individually transfected with each of the 364 esiRNAs directed against those genes restrictively expressed in the caudal end of E9.5 mouse embryos. For this, SW480 cells were plated at a low density onto coverslips and transiently transfected 24h after seeding using Oligofectamine. The cell morphology was evaluated in comparison to control transfected cells 72h after esiRNA transfection. At this time point, I additionally visualized and evaluated the sub-cellular distribution of the epithelial marker E-cadherin by immunofluorescence. Cell morphology and immunofluorescence images were judged independently and without knowledge of gene names of the individual transfections. I considered these genes as candidate genes for tumor-associated EMT, which scored positive, independently in both assays, i.e. led to formation of epithelial ("cobblestone") patches, and re-localization of E-cadherin to cell-cell junctions.

This loss of function phenotypic screen led to the identification of 18 genes. Among the positively tested genes, I found *PTCH*, *GLI2*, and *GLI3*, which are components of the Hedgehog signaling pathway (Yang et al., 2010). Furthermore, *SIX1* was identified, which is a homeobox transcription factor implicated in cell differentiation and tumor progression (Christensen et al., 2008; Micalizzi et al., 2009). Finally, the screen identified FGF9, which encodes a high affinity ligand for the FGF receptors 2 and 3 (Hecht et al., 1995). As expected, the positive control *BCL9L* also led to formation of cell clusters with an epithelial phenotype.

The screen also revealed three genes whose inactivation promoted a more spindle-form cell morphology: *BICC1* and *MAGI1*, whose homologues have been found recently to stabilize E-cadherin-based cell adhesion (Mizuhara et al., 2005; Fu et al., 2010), and *EPHA4* (Bisson et al., 2007). In contrast, control-transfected cells did not display consistent morphological changes.

Gene Name	Protein Family	Function
TCF7L1	HMG-box	transcrptional regulation
PTCH	transmembranen receptor	signal transduction
GLI3	extracellular ligand	transcrptional regulation
GLI2	extracellular ligand	transcrptional regulation
FGF9	extracellular ligand	signal transduction
SIX1	Homeobox	transcrptional regulation
SOX8	Homeobox	transcrptional regulation
PELI2	n.d.	interaction with BCL
GAD1	n.d.	decarboxylase
TAX1BP3	PDZ domain protein	transcrptional regulation
PROX1	Homeobox	transcrptional regulation
ETS2	helix-turn-helix DNA-binding Protein	transcrptional regulation
BCAR3	putative src homology 2 SH2	signal transduction
CSNK2A1	serine/threonine protein kinase	signal transduction
HDAC7A	histone deacetylase	transcrptional regulation
LPHN2	G-protein coupled receptor	signal transduction
SFRP1	extracellular ligand	signal transduction
FAM120A	RNA binding protein	signal transduction

Tab. 1: Positively tested candidate genes. The loss-of-function phenotypic screen identified 18 genes whose inactivation in SW480 CRC cells induced an epithelial ("cobblestone") cell morphology and re-localization of the epithelial cell adhesion molecule E-cadherin to cell-cell junctions.

FGF9 represents a promising candidate gene for promoting intestinal tumor progression for several reasons: FGF signaling was shown to orchestrate the EMT program at the primitive streak during gastrulation in mice (Ciruna and Rossant, 2001), while genetic alterations of FGF family members have been implicated to trigger scattering of individual carcinoma cells from bladder carcinoma (Vallés et al., 1990). In addition, deregulation of FGF signaling has been observed in various other tumors, and promotes malignant progression in skin, ovarian and prostate cancers (Turner and Grose, 2010). Importantly, colon cancer cells show deregulation of several FGF receptor isoforms (Sonvilla et al., 2010) and other FGF pathway components that can transduce oncogenic signals (Tassi et al., 2006).

I therefore focused on the impact of FGF signals on intestinal tumor progression. I investigated the significance of FGF signals in the intestine using several approaches: (i) I employed small molecule inhibitors targeting the FGF receptors and evaluated the impact on the morphological and migratory behavior in SW480 and other human colon cancer cells. (ii)

I determined downstream events of FGF signaling and analyzed the expression pattern of the FGF9 ligand and corresponding receptors in tissue sections of untransformed intestinal epithelium and colon cancer tumors. (iii) Using the organotypic culture system of primary intestine, I investigated the effect of FGF signals on intestinal stem cell function and tissue homeostasis. These experiments established novel roles for FGF signals in the intestine and are presented in detail in the following chapters.

3.2 Functional Impact of FGF Signals on the Intestinal Tumor Cell Phenotype

3.2.1 FGF9 Regulates Cell Morphology and E-cadherin Distribution in SW480 Cells

As outlined above, *FGF9* was indentified as candidate gene for tumor-associated EMT in a loss-of-function phenotypic screen in SW480 human colon cancer cells. *FGF9* silencing induced an epithelial cell morphology and localization of the epithelial marker E-cadherin to cell-cell contacts in SW480 cells 72h after RNA interference, as judged by bright field microscopy and immunofluorescence (Fig. 7). This appearance resembles the phenotype induced by RNA interference of the positive control *BCL9L*. In contrast, control cells transfected with an esiRNA targeting Firefly luciferase remained mesenchymal and displayed low levels of membranous E-cadherin (Fig. 7). This result suggested that the extracellular ligand FGF9 is essential to maintain a mesenchymal phenotype in human SW480 colon cancer cells.

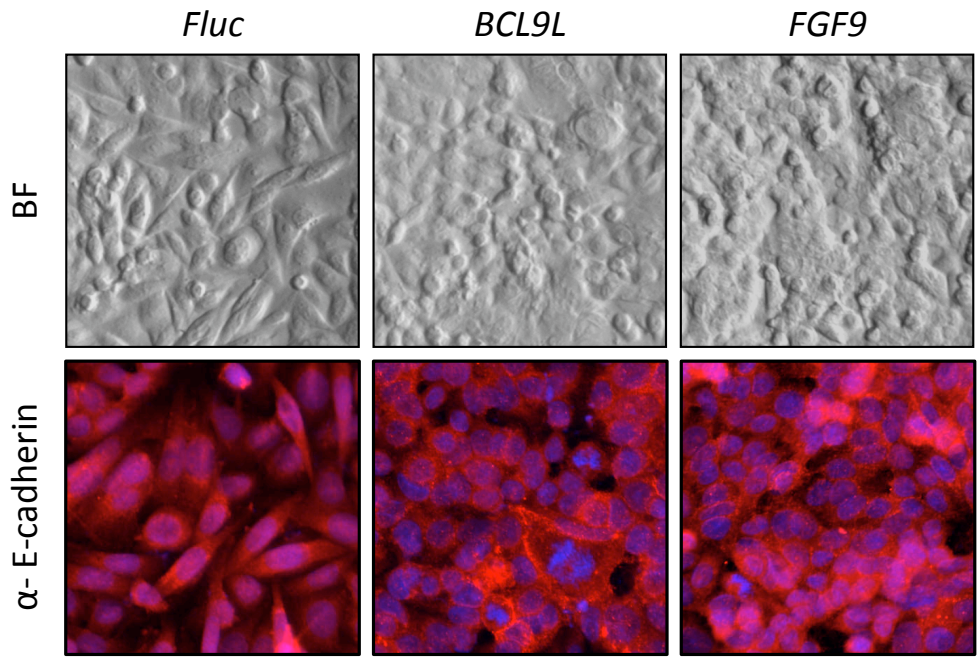

Fig. 7: FGF9 regulate cell morphology and E-cadherin distribution in SW480 cells. Morphology and E-cadherin distribution of SW480 cells transfected with esiRNA against firefly luciferase (*Fluc*, negative control), *BCL9L* (positive control) and *FGF9.* Images were taken 72h after transfection.

3.2.2 FGF Receptor Signals Regulate Cell Morphology of SW480 Cells

Receptor tyrosine kinase (RTK) signals are known to play important roles in colon cancer progression (Clevers and Batlle, 2006). To further study the impact of FGF signals on intestinal SW480 cells I targeted the FGF receptors using the small molecule inhibitor (SMI) SU5402. This chemical compound was shown to act as potent and specific inhibitor of the tyrosine kinase activity of all four FGF receptors, and, to a lesser extent, the VEGF receptor (Mohammadi et al., 1997). Initially, I verified that SW480 cells receive FGF signals, manifested by FGF receptor phosphorylation, as shown by phospho-specific western blot analysis. FGF receptor phosphorylation can be efficiently blocked by SU5402 administration (Fig. 8A). Next, I investigated the morphological and migratory behavior of SW480 cells 72h after start of FGF receptor inhibition. In agreement with the RNA interference data, treatment with the FGF receptor inhibitor leads to re-epithelialization of SW480 cells, as judged by morphological alterations of the cellular shape. In particular, FGF receptor inhibition promoted a dramatic morphological change to an epithelial cobblestone phenotype and recruited E-cadherin and β-catenin to cell-cell contacts, indicating *de novo* assembly of epithelial adherens junctions (Fig. 8B).

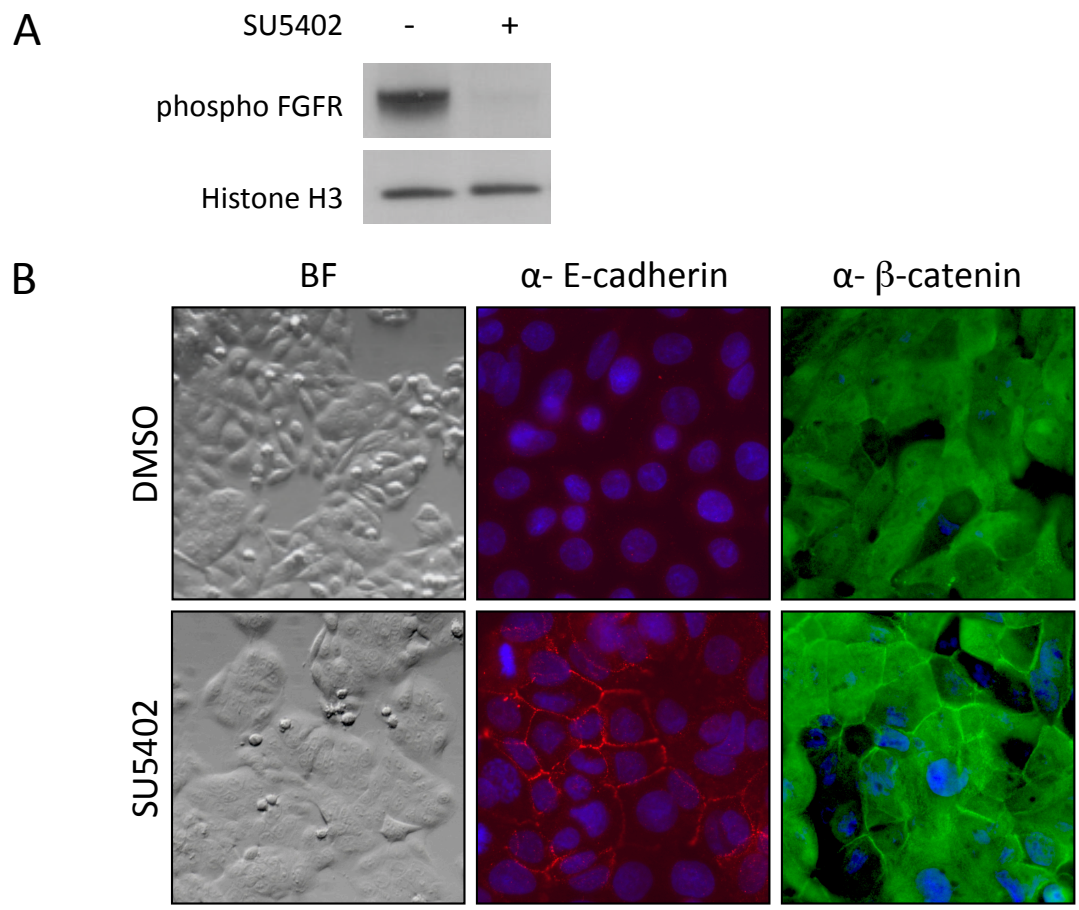

Fig. 8: FGFR inhibitor induces re-epithelialization of SW480 cells. (A) SW480 cells receive FGF signals, which can be blocked by SU5402. Western blot analysis of phospho-FGF receptor in SW480 cells after treatment with DMSO (solvent negative control) and SU5402 (inhibiting FGFR). Histone H3 is shown as loading control. Phosphorylation status was assessed 40 minutes after inhibitor treatment. (B) FGF receptor signals regulate cell morphology and distribution of E-cadherin and β-catenin in SW480 cells. Bright field images show the phenotypic switch of SW480 cells upon FGF receptor inhibition (SU5402). DMSO serves as control. Left to right: Cell morphology in Bright field, immunostaining of E-cadherin (red) and β-catenin (green). Cell nuclei were counterstained with DAPI (blue). Images were taken 72h after start of SU5402 treatment.

3.2.3 FGF Receptor Signals Regulate Cell Morphology of Various CRC Cell Lines

In order to exclude a cell line specific influence of FGF signals present restrictively in SW480 cells, the impact of FGF receptor inhibition on a panel of CRC cell lines was analyzed. Similar to the effect in SW480, morphological alterations were observed in SW620 cells, which are derived from a lymph node biopsy of the same patient used to establish SW480 cells (Kubens and Zänker, 1998). In addition, FGF receptor inhibition induced a pronounced epithelial cell morphology in HT29 and Caco-2 colon cancer cells, which are derived from primary colorectal carcinomas of different patients (Trainer et al., 1988), 72h after start of FGF receptor inhibition (Fig. 9). In all of these cell lines, FGF receptor inhibition increased the formation of cell clusters with an epithelial phenotype concealing their cellular boundaries (Fig. 9). These results indicate that the regulation of morphological characteristics by FGF signals is not confined to SW480 cells. However, other intestinal cell lines such as HCT116 and DLD1 showed no morphological alterations upon FGF receptor inhibition (data not shown). Of note, these cells already displayed an epithelial phenotype in the absence of FGF receptor inhibitor, making the identification of additional morphological alterations difficult.

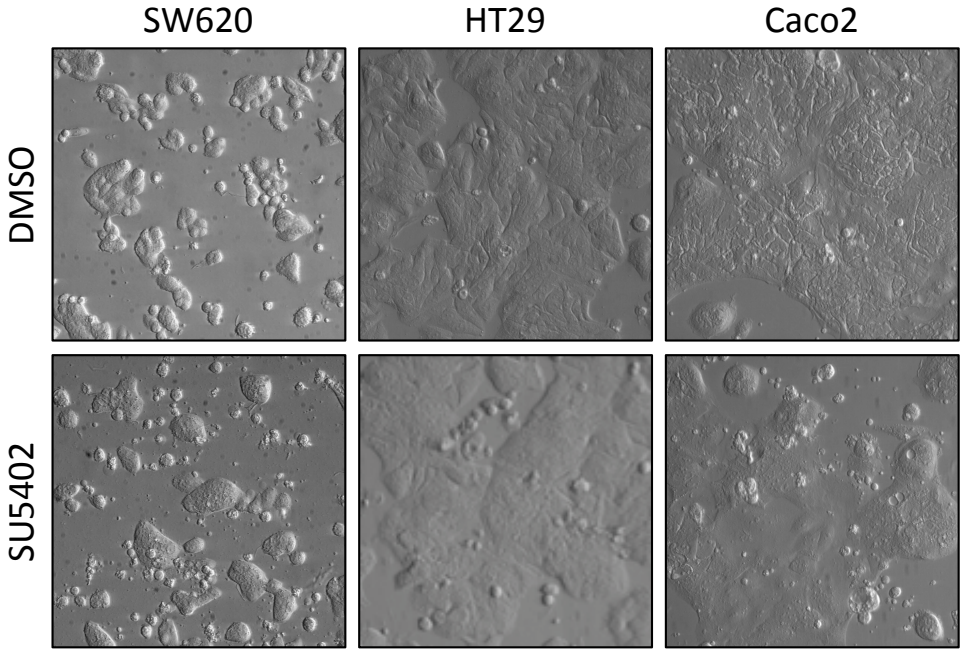

Fig. 9: FGF receptor signals regulate cell morphology in SW620, HT29 and Caco2 colon cancer cells. Phenotypic switch of SW620, HT29, and Caco2 cells upon FGF receptor inhibition (SU5402). DMSO serves as solvent control. Images were taken 72h after start of SU5402 treatment.

3.2.4 FGF Receptor Signals Regulate Cell Motility in SW480 Cells

Cancer cell migration, leading to tumor invasion and metastasis, is the main cause of death for cancer patients (Brabletz et al., 2005). Cell adhesion and cell motility are typically inversely correlated (Friedl and Wolf, 2003). To investigate the influence of FGF signals on cell motility in intestinal cells, I assessed the migratory properties of SW480 cells in a scratch wound healing assay. For this, SW480 cells were grown to a confluent monolayer, and subsequently scratch-wounded in the presence of the FGF receptor inhibitor SU5402. DMSO treatment served as solvent control. As demonstrated in Figure 10, control SW480 cells rapidly migrated into the wound leading to a complete closure of the wound after 72h. In contrast SU5402-treated cells could no longer invade into the scratch-wound. These data suggest that FGF receptor signals play essential roles in the switch from a stationary to a migratory phenotype, which is a hallmark of the late steps of intestinal tumor progression resulting in metastasis.

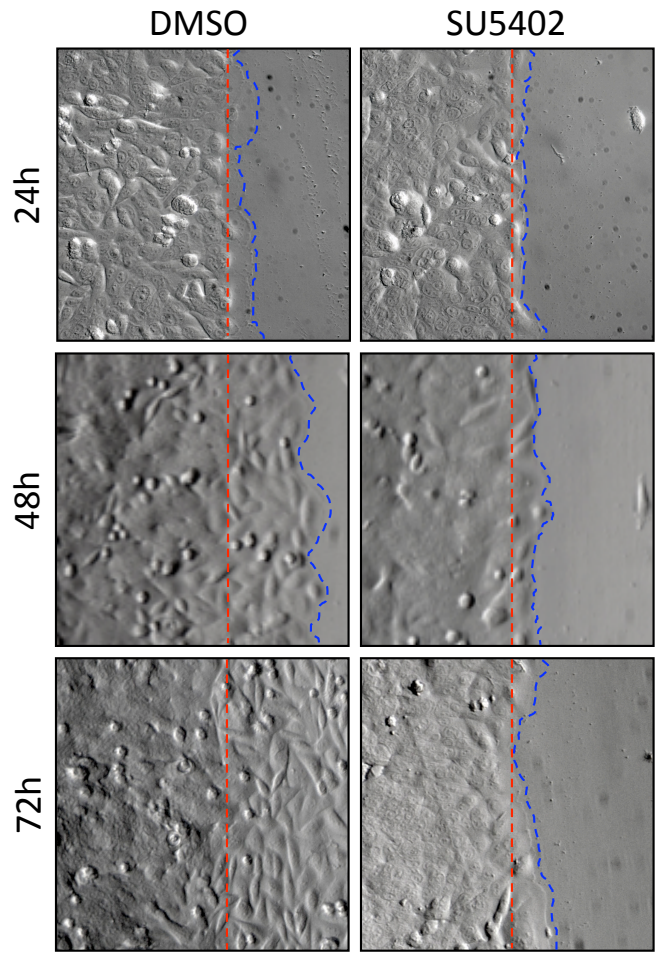

Fig. 10: FGF receptor signals regulate cell motility in SW480 cells. Scratch-wound motility assay upon FGF receptor inhibition (SU5402). DMSO serves as control. SW480 cells were grown to confluence, and scratches were performed 24h after start of inhibitor treatment. Bright field images of the scratch edge and were taken 24, 48 and 72 hours after wounding. Dashed red line indicates the scratch edge and dashed blue line represents the migratory cellular front.

Several studies have shown that actin dynamics correlate with cell morphology and motility (Jaffe and Hall, 2005; Olson and Nordheim, 2010). To investigate the effect of FGF signals on actin dynamics the actin cytoskeleton was analyzed in control and FGF receptor inhibitor treated SW480 cells. Hereto, I visualize the actin cytoskeleton using fluorochrome-labeled phalloidin, which specifically binds actin filaments. Importantly, fluorescence microscopy demonstrated that FGF receptor inhibited cells at a scratch wound edge displayed increased staining of cortical actin and reduced numbers of focal adhesion contacts, as compared to migratory control cells (Fig. 11). These results revealed altered actin dynamics upon FGF receptor inhibition. FGF signals may therefore impinge on migratory properties of SW480 cells by affecting the actin cytoskeleton.

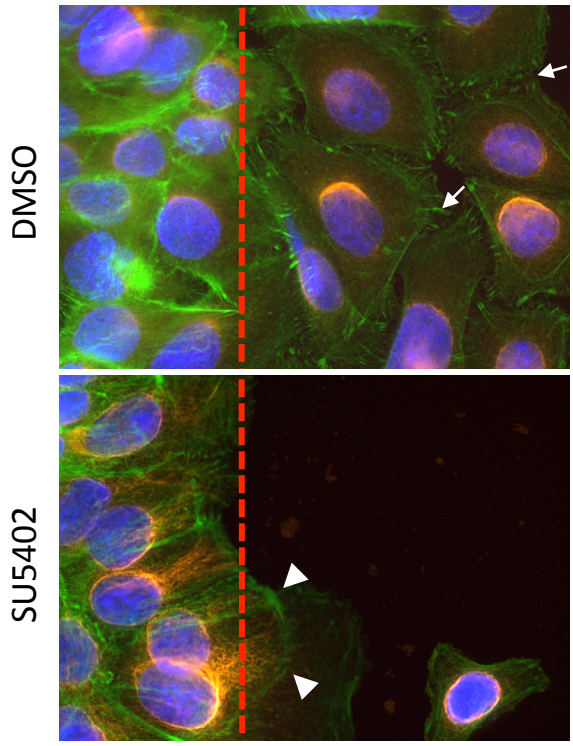

Fig. 11: Inhibition of FGF receptor signals leads to rearrangement of the actin cytoskeleton. Staining of the actin cytoskeleton in control (DMSO) and FGF receptor inhibited (SU5402) cells at a scratch wound edge (represented by the dashed red line). Green: actin (phalloidin staining); yellow: γ-tubulin; blue: nuclei (DAPI); white arrows: areas of dense focal adhesions in motile control cells; arrowheads: enhanced cortical actin staining in SU5402-treated cells.

3.2.5 FGF Signals do not Strongly Influence Cell Proliferation

Cancer cells are typically self-sufficient for growth signals (Hanahan and Weinberg, 2000), generating the growth advantage of neoplastic cells. Colorectal cancer, for instance, is generally initiated by hyperactive, ligand-independent WNT signaling in intestinal stem cells leading to increased cell proliferation (Barker et al., 2009). To determine the impact of FGF signals on cell proliferation several different approaches were employed. Using a cell-doubling assay, I demonstrate that SW480 cells inhibited for FGF signals proliferated at nearly equivalent levels as compared to controls (Fig 12A). In addition, the mitotic index of control and FGF receptor inhibited SW480 cells was determined by immunofluorescence for phospho Histone H3. H3 is specifically phosphorylated during chromosome condensation and thus, served as a mitotic marker. Fluorescence microscopy revealed that, independently of the treatment, around 2% of each cell population was mitotic (Fig. 12B, C). These results suggest that cell proliferation is only mildly affected by FGF receptor inhibition.

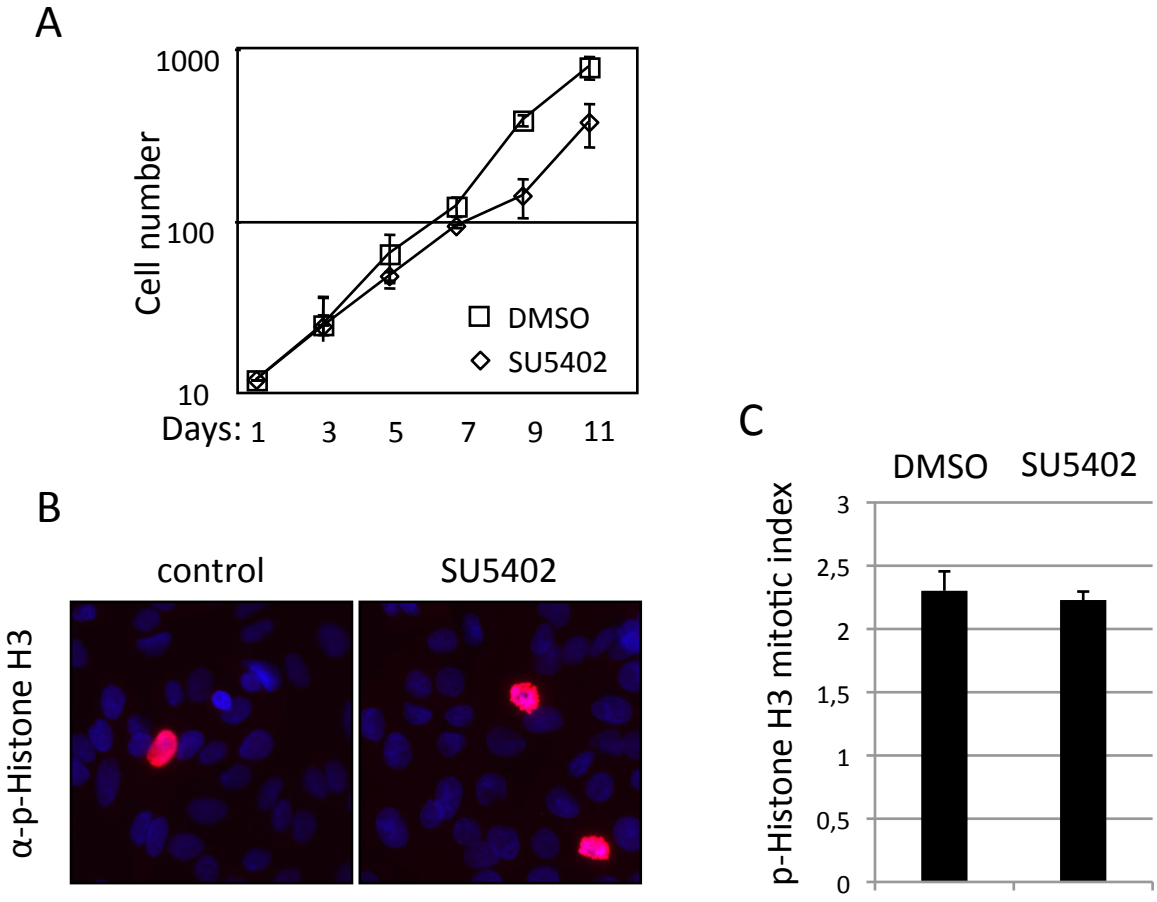

Fig. 12: Inhibition of FGF receptor signals does not significantly alter proliferation of SW480 cells. (A) Quantification of proliferation in control and SU5402-treated cells. For a time-course of proliferation, cells were plated in replicates, and duplicate samples were counted bi-daily using a Neubauer hematocytometer. (B)

Inhibition of FGF receptor signals does not alter the mitotic index of SW480 cells. Triplicates of control (DMSO) and FGF receptor inhibitor (SU5402) cell populations were treated for 72h and immunostained for p-Histone3 (red). Cell nuclei were counterstained with DAPI (blue). (C) p-HistoneH3 mitotic index represents the mean of 3 independent enumerations. Bars indicate mean of 3 biological replicates, ± SEM.

3.2.6 Alternative FGF Receptor Inhibitors Regulate Cell Morphology of SW480 Cells

Depending on the specificity, small molecule inhibitors may have side effects due to inhibition of additional molecular targets. I therefore applied a second small molecule inhibitor, PD173074 (Mohammadi et al., 1998), which also specifically targets the FGF receptors but is structurally unrelated to the SU5402 compound. Both FGF receptor inhibitors generated comparable effects on the morphology of SW480 cells. This observation implies that the induced re-epithelialized phenotype of intestinal cells is, in fact, directly related to the inhibition of FGF signals.

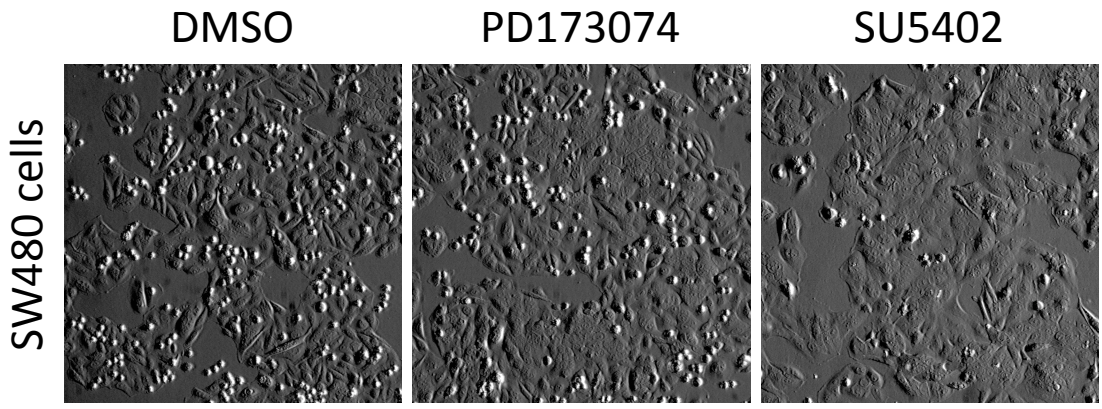

Fig. 13: Structurally unrelated FGF receptor inhibitors regulate cell morphology in SW480 cells. FGF receptor inhibition by either PD173074 or SU5402 induces a phenotypic switch to an epithelial morphology in SW480 cells. DMSO serves as solvent control. Images were taken 72h after the start of drug treatment.

3.3 Analysis of Signaling Events Downstream of FGF Receptors

3.3.1 FGF signals Regulating Morphology and Motility in SW480 Cells are Transduced via MAP kinase (Judged by Western Blot)

As outlined in the introduction, FGF receptor stimulation initiates multiple intracellular signaling pathways, including the mitogen-activated protein kinase (MAPK) and phosphinositid-3-kinase (PI3K)/AKT signaling cascades (Turner and Grose, 2010). Protein phosphorylation is essential for the regulation and transduction of a wide range of intracellular signals. To investigate signaling pathways downstream of FGF receptors in SW480 cells, the activity level of key cellular signal transducers was determined. For this, I used phospho-specific western blot analysis, which detects whether a protein is phosphorylated at a particular site. SW480 cells were treated for 40 minutes with the FGF receptor inhibitor before harvesting the cells for phosphorylation level analysis. As positive controls, individual SW480 cell populations were treated with inhibitors for FGF associated signaling pathways (MAP kinase pathway and PI3 kinase pathway), by using the small molecule inhibitors U0126 and LY294002, respectively (DeSilva et al., 1998; Conacci-Sorrell et al., 2003). These analyses identified a minor, but reproducible reduction in ERK1/2 phosphorylation (around 30%) after FGF receptor inhibition (Fig. 14A). Expectedly, ERK1/2 phosphorylation was completely abolished in SW480 cells inhibited for MAP kinase signaling. By contrast, the activity of the PI3K pathway component P85PI3 was not affected following FGF receptor inhibition (Fig.14B). Changes in AKT phosphorylation after FGF receptor inhibition, however, indicate that additional signal transduction networks are modulated. Taken together, these results indicate that the FGF receptors can transduce signals that regulate cell adhesion and motility via the MAP kinase cascade in colon cancer cells.

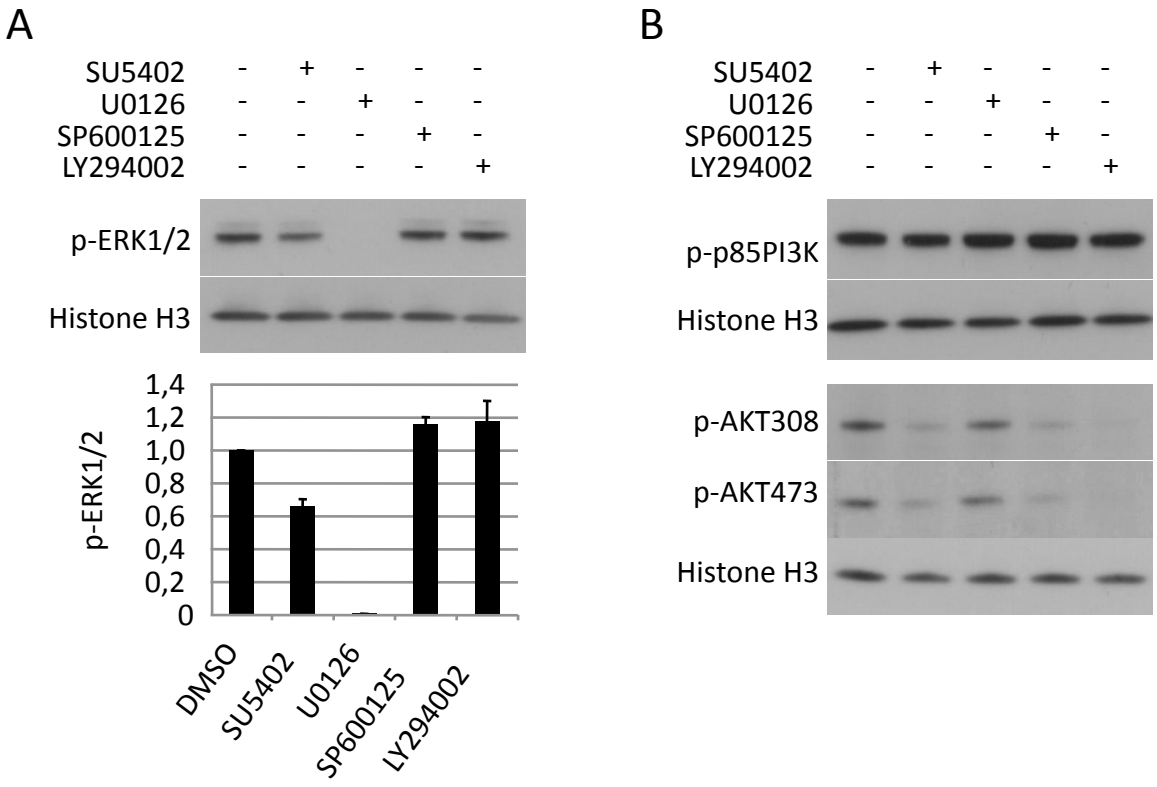

Fig. 14: FGF signals for epithelialization are transduced via MAP kinase (Western Blot). Western Blot Analysis of Phospho-ERK1/2 (A), Phospho-P85PI3K (B top) and Phospho-AKT (B bottom) in SW480 cells after treatment with DMSO (solvent control), SU5402 (inhibiting FGFR), U0126 (inhibiting MEK1/2 dependent ERK1/2 phosphorylation), SP600125 (inhibiting JNK), and Ly294002 (inhibiting PI3K-mediated AKT phosphorylation) are shown. Histone H3 is shown as loading control. Phosphorylation status was assessed 40 minutes after inhibitor treatment. Quantification (A bottom) of the immunoblot of ERK1/2 phosphorylation represents the mean of 3 experiments.

3.3.2 FGF Signals Regulating Morphology and Motility in SW480 Cells are Transduced via MAP kinase (Judged by IPAQ)

Quantitative western blot analyses have been reported to possess a technical standard error of up to 20-35% from potential uneven blotting conditions (Loebke et al., 2007). Therefore, I confirmed the phospho-specific Western Blot results using an alternative approach. To this end, I re-analyzed the level of ERK1/2 phosphorylation in control and SU5402-treated SW480 cells, using the Infrared-based Protein Arrays with Quantitative readout (IPAQ) approach in co-operation with the laboratory of Ulrike Korf (German Cancer Research Center, Heidelberg). In this approach, the protein samples are printed directly onto a nitrocellulose coated glass slide, which is subsequently incubated with a highly sensitive antibody for the detection of the protein of interest (Loebke et al., 2007). A 24 h time course experiment of

FGF receptor inhibition was performed in SW480 cells. As illustrated in Figure 15 SW480 cells were harvested for IPAQ analysis at 2min, 5min, 10min, 18min, 6h and 24h after the start of FGF receptor inhibition. In addition, individual SW480 cell populations were treated with the MAP kinase inhibitor (U0126) as a positive control. DMSO served as solvent control. In agreement with the result of the western blot quantification, the IPAQ approach revealed an approximate 50% reduction in ERK1/2 phosphorylation after 40 minutes of FGF receptor inhibition. These results confirm that FGF receptors have the potential to transduce signals controlling cell adhesion and motility via the MAP kinase signaling cascade in colon cancer cells.

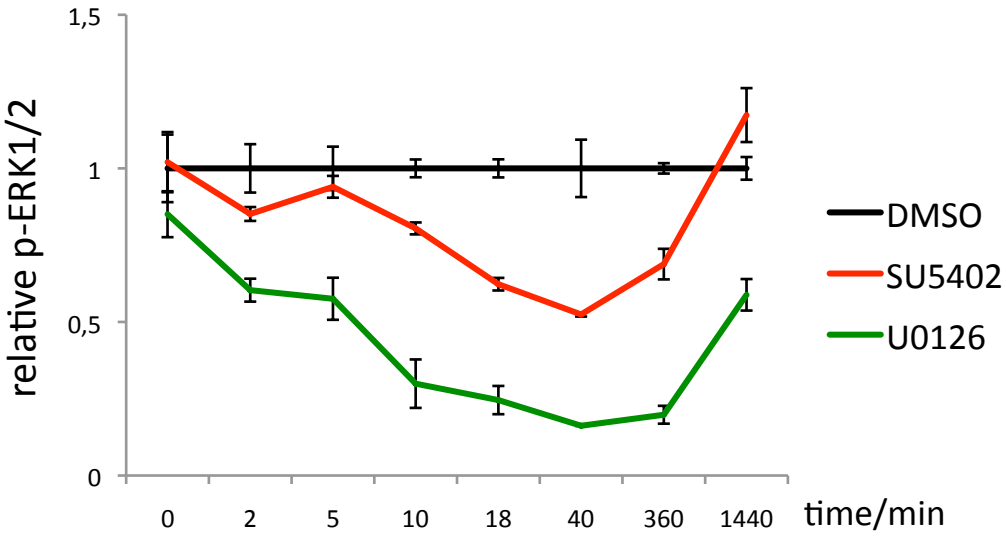

Fig. 15: FGF signals for epithelialization are transduced via MAP kinase (IPAQ). Time-resolved analysis of the proportion of phosphorylated ERK1/2 protein with respect to total ERK1/2 protein in SW480 cells blocked for FGF receptor signals (SU5402; red) or MAP kinase signals (U0126; green). Samples were normalized to non-inhibited control cells (DMSO; black). Highest reduction of ERK1/2 phosphorylation is present 40 minutes after inhibitor treatment (residual ERK1/2 phosphorylation after 40 minutes treatment: 52% in FGF receptor inhibited cells and 16% in MAPK inhibited cells).

3.3.3 FGF Receptor Signals Regulate Cell Morphology of SW480 Cells

The analysis of signaling events downstream of FGF receptors revealed an epistatic relationship between FGF signals and the MAP kinase pathway in colon cancer cells. To assess the impact of MAP kinase signals on cell morphology I analyzed the phenotypic characteristics of SW480 cells upon MAP kinase inhibition. For this, SW480 cells were

cultured for three days in the presence of the chemical compound U0126 or SP600125 inhibiting canonical MAP kinase or JNK kinase signaling respectively. SW480 cells were also treated with inhibitors targeting components of the PI3 kinase signaling cascade to evaluate the influence of this pathway on the morphology of intestinal cells. DMSO treatment served as solvent control. As demonstrated in Figure 16, small molecule inhibition of the MAP kinase or the alternative JNK kinase pathway similarly induced epithelial morphology in SW480 cells. This result confirms a central role for the MAP kinase signaling cascade in the transduction of FGF receptor signals that regulate cell adhesion and motility. In contrast, the inhibition of PI3Kinase or AKT kinase had no apparent morphological effect.

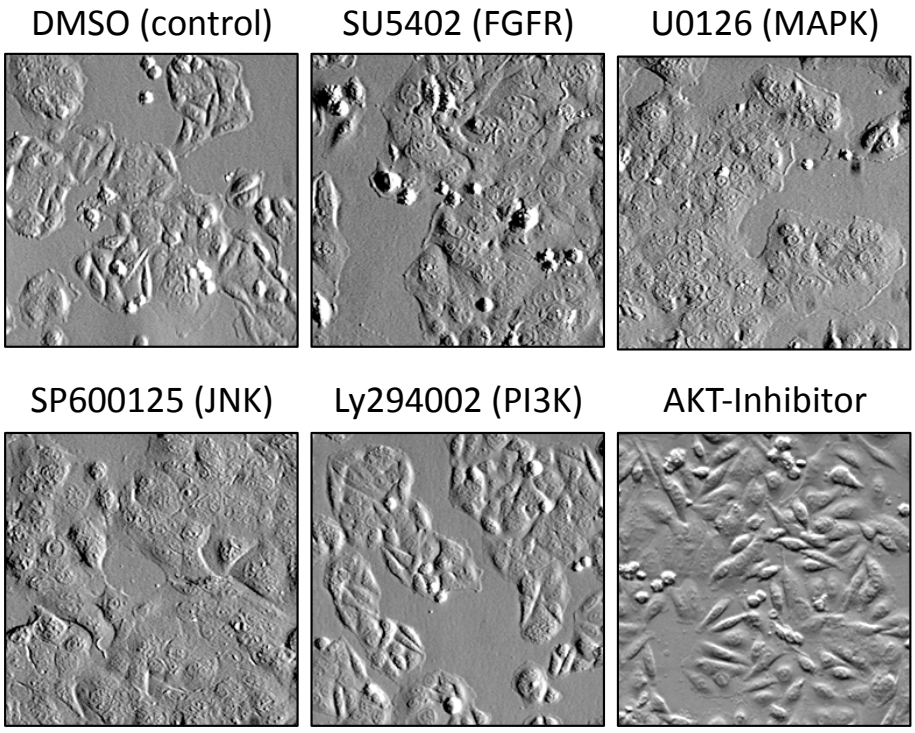

Fig. 16: FGF receptor and MAP kinase signaling regulate cell morphology in SW480 cells. Morphology of SW480 cells 72h after inhibitor treatment. Inhibition of FGF receptors, classical ERK1/2 MAP kinase or alternative JNK-MAP kinase pathways leads to re-epihelialization of SW480 cells, while inhibition of PI3K or AKT kinase had no effect.

To further elucidate the re-epithelialized morphology of MAP kinase-inhibited SW480 cells, the distribution of E-cadherin and β-catenin was then determined in these cells. Immunofluorescence microscopy revealed that MAP kinase inhibition recruited the E-cadherin and β-catenin to cell-cell contacts, indicating *de novo* assembly of epithelial adherens junctions (Fig. 17A), similar to the result after FGF receptor inhibition. In addition, I

assessed the migratory properties of SW480 cells in a scratch wound healing assay upon MAP kinase blockade. As demonstrated previously for FGF receptor signals (Fig. 10), MAP kinase signaling in SW480 cells was also found to be essential for cell motility (Fig. 17B). These results reinforce the proposed role of the MAP kinase pathway in transmitting FGF receptor signals that regulate cell morphology and motility.

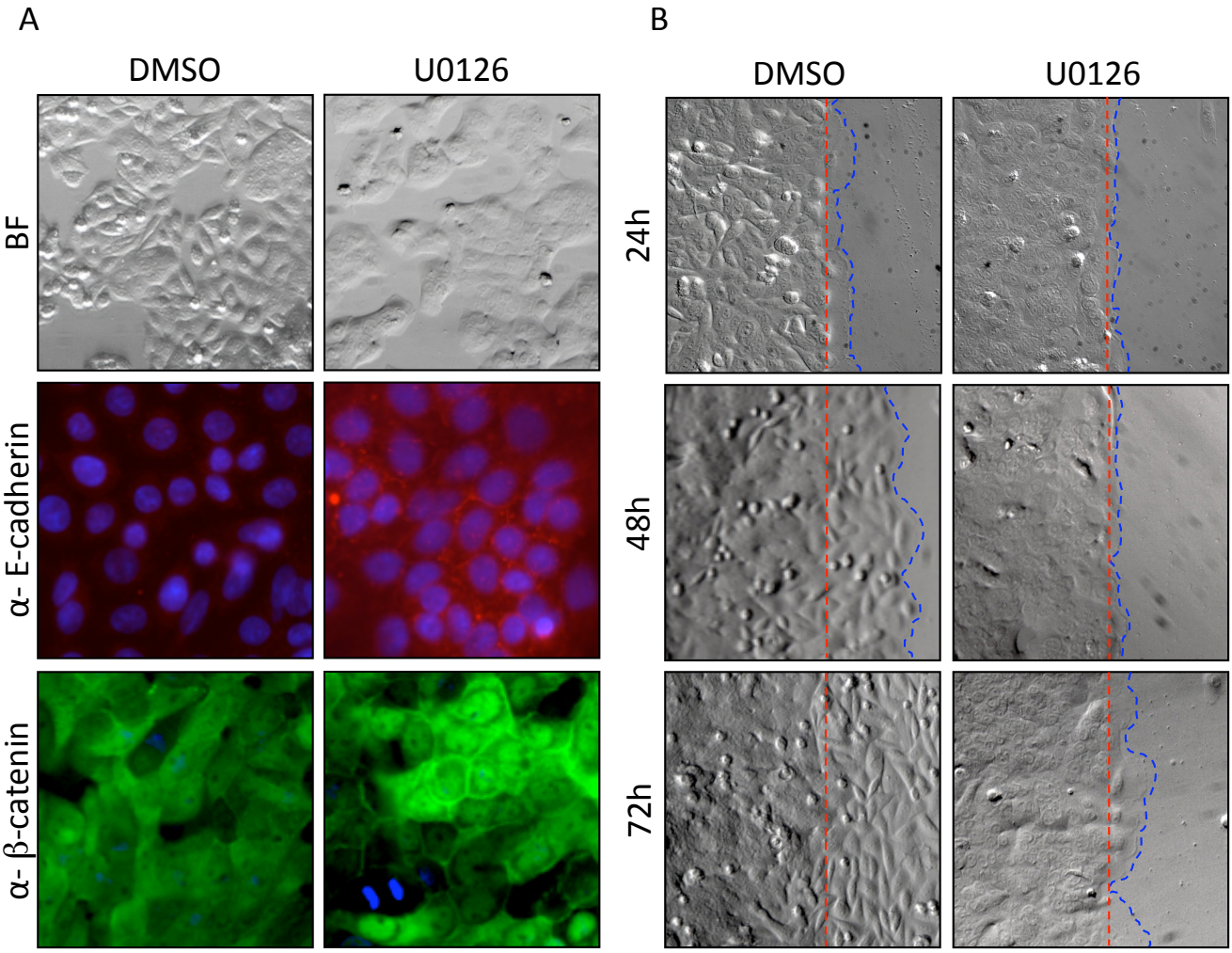

Fig. 17: MAP kinase inhibitor induces re-epithelialization and regulates cell motility in SW480 cells. (A) MAP kinase signals regulate cell morphology and distribution of E-cadherin and β-catenin in SW480 cells. Phenotypic switch of SW480 cells upon MAP kinase inhibition (U0126). DMSO serves as control. Top to bottom: Cell morphology in bright field, immunostaining of E-cadherin (red) and β-catenin (green). Cell nuclei were counterstained with DAPI (blue). Images were taken 72h after start of SU5402 treatment. (B) Scratch-wound motility assay upon MAP kinase inhibition (U0126). DMSO serves as control. SW480 cells were grown to confluence, and scratches were performed 24h after the start of inhibitor treatment. Bright field images of the scratch wound edge and were taken at 24, 48 and 72 hour after wounding. Dashed red line represents the scratch wound edge, and dashed blue line represents the migratory cellular front.

3.3.4 FGF and MAP Kinase Signals Regulate Common Target Genes in SW480 Cells

As discussed above, FGF signaling funnels into the MAP kinase pathway in SW480 cells. Pathway activation, in turn, triggers the differential expression of selected target genes. To further investigate FGF receptor associated signaling events in SW480 cells, I assessed gene expression profiles by microarray (Illumina). First, gene expression patterns of solvent control versus FGF receptor inhibited cells were compared. To verify the correlation between FGF receptor and MAP kinase signals in SW480 colon cancer cells differential gene expression patterns upon MAP kinase inhibition were additionally evaluated. For the gene expression analysis, SW480 cells were individually treated for 6h with the corresponding inhibitor before the total RNA was isolated for further analysis. The expression profile analysis was performed in collaboration with my supervisor Markus Morkel. We found that inhibition of FGF receptor signals induced a differential expression of 243 genes while inhibiting the MAP kinase signals altered the expression pattern of 616 genes (Fig. 18). Within these deregulated genes, an overlap of 93 genes is targeted by both signaling cascades. This significant intersection strengthens the proposed epistatic relationship of these pathways in SW480 cells.

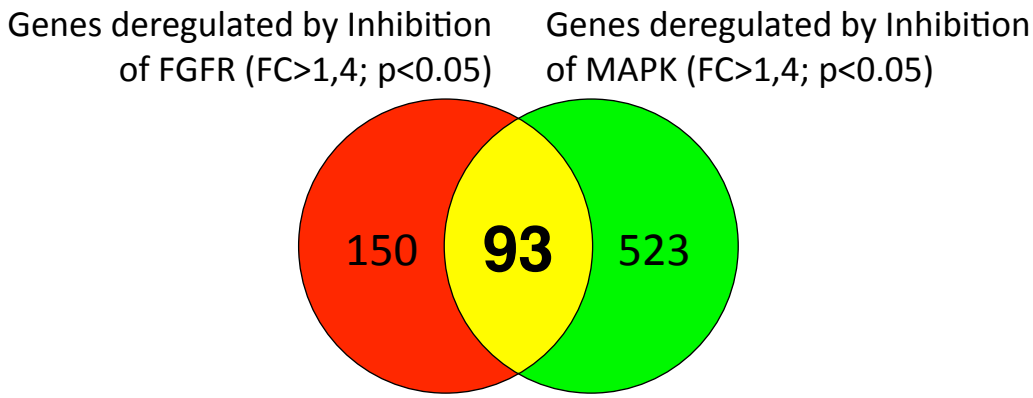

Fig. 18: Expression of a set of overlapping genes is regulated by FGF and MAP kinase signals. Expression profiles from biological triplicates after 6h of FGF receptor inhibited (red) or MAP kinase inhibited (green) SW480 cells. Red: 150 deregulated genes (>1.4-fold) upon FGF receptor inhibition. Green: 523 deregulated genes (>1.4-fold) upon MAP kinase inhibition. Yellow: 93 deregulated genes (>1.4-fold) upon FGF receptor and MAP kinase inhibition. Profiles were normalized in Illumina Bead Studio using quantile normalization. Absent and marginally expressed genes were removed before analysis.

The connection between FGF and MAP kinase signals was then validated using Ingenuity Pathway Analysis (www.ingenuity.com). Here, we compared the gene expression profiles of solvent control and SU5402-treated SW480 cells. By this approach, we identified a network of deregulated genes related to cell motility that centers around the ERK1/2-dependent MAP kinase pathway (Fig. 19). Green colored molecules within the network represent downregulated genes while red colored compounds correspond to upregulated genes after SU5402 treatment.

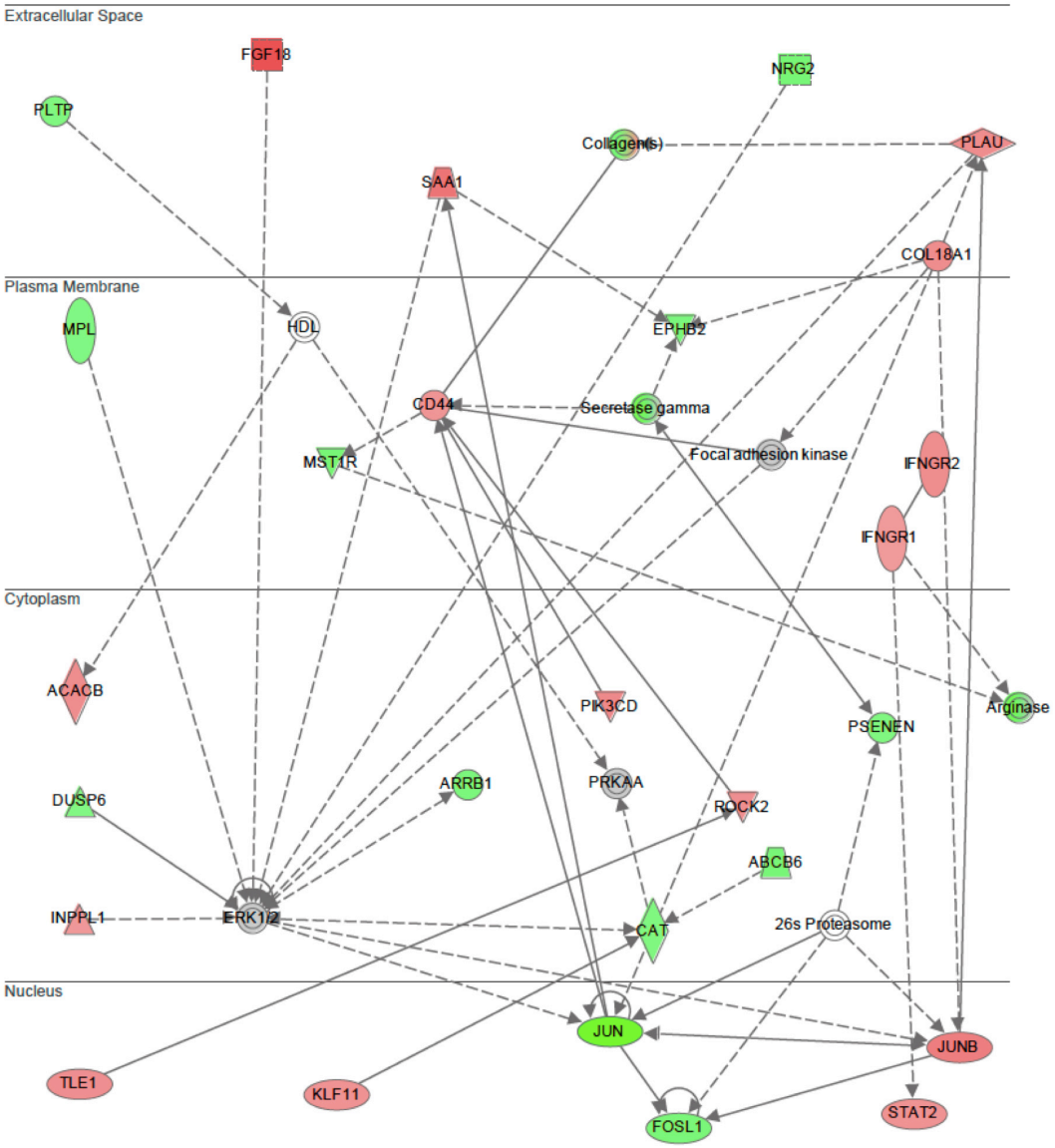

Fig. 19: Ingenuity Pathway Analysis identifies a network implicated in cell motility, which is enriched in FGF-regulated genes. Green: downregulated genes after SU5402 treatment Red: upregulated genes after SU5402 treatment. Grey: non-regulated genes within the Network. Network was derived from genes deregulated (>1.3-fold) in expression profiles from biological triplicates of SU5402-treated SW480 cells and solvent controls. Profiles were normalized in Illumina Bead Studio using quantile normalization. Absent and marginally expressed genes were removed before analysis.

3.3.5 Rho Activity is Modulated by FGF signaling

Rho GTPases operate as molecular switches. In response to extracellular signals, Rho proteins cycle between an active GTP-bound state and an inactive GDP-bound state (Jaffe and Hall, 2005). Rho GTPases are known to be key modulators of the actin cytoskeleton, thereby coordinating the balance between cell adhesion and motility (Hall, 1998). In order to assess their regulation in control and SU5402 treated SW480 cells I initially investigated the subcellular localization of the RhoA protein. By immunofluorescence, I detected RhoA protein to be organized in perinuclear speckles in motile control SW480 cells invading a scratch wound. In contrast, such punctuated staining of RhoA protein was mostly absent after 3 days of FGF receptor inhibition (Fig. 20A). To assess the influence of FGF signals on the Rho activity level in SW480 cells, I quantified the amount of GTP-bound Rho protein in the presence or absence of FGF receptor inhibition or MAP kinase inhibition by using a Rho-GTP bound pull-down assay. For this Rho loading activity assay, SW480 cells were serum-starved for 24h in the presence of the individual inhibitors or solvent-control (DMSO). The Rho-GTP pull-down was conducted 5 minutes after re-stimulation with 10% serum. As demonstrated in Figure 20B, Rho-GTP loading by serum was compromised either by FGF receptor or MAP kinase inhibition. Taken together, these results imply that the FGF receptors may transduce signals that regulate cell adhesion and motility via the MAPK cascade and Rho GTPases in colon cancer cells.

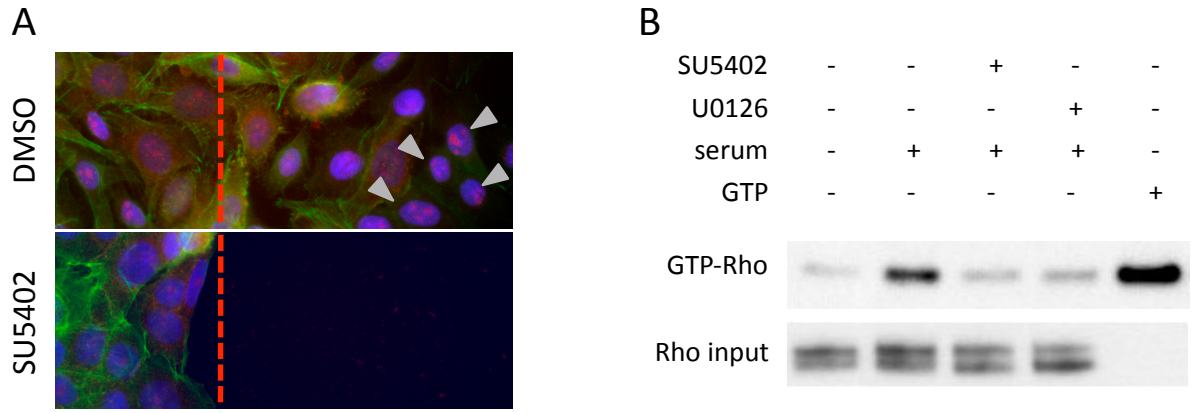

Fig. 20: Rho activity is modulated by FGF signals. (A) RhoA re-distribution in migrating cells at a scratch wound edge (represented by the dashed red line), which is reduced in inhibitor treated cells. Green: actin (phalloidin staining); magenta: RhoA; blue: nuclei (DAPI); grey arrowheads mark perinuclear RhoA protein. (B) Rho GTPase loading assays in starved SW480 cells after serum re-stimulation (5 minutes) in the presence or absence of FGF receptor inhibition (SU5402) or MAPK inhibition (U0126).

3.4 Impact of FGF Signals on Stem Cell Traits in Tumor Cells

Recent models of tumor progression imply that uncontrolled activation of developmental signaling pathways and embryonic gene expression programs not only result in a coordinated loss of cell adhesion and gain of cell motility, but also in the acquisition of stem cell traits in metastatic tumor cells (Mani et al., 2008). In order to reveal a potential impact of FGF signals on intestinal stemness, I determined the expression of the intestinal stem cell marker *LGR5* in colon cancer cells upon FGF signal inhibition. However, SW480 cells per se do not express known intestinal stem cells markers, including *LGR5*. This cell line is consequently inappropriate to study intestinal stem cell properties. In contrast, Caco2 human colon cancer cells show high levels of *LGR5* expression (Uchida et al., 2010). I therefore used Caco2 cells to assess a potential alteration in *LGR5* expression in the presence of the FGF receptor inhibitor SU5402. To this end, I blocked endogenous FGF signals in Caco-2 cells, and determined the expression level of the CBC stem cell marker *LGR5* one and three days after FGF receptor inhibition in comparison to solvent control samples. Using qRT-PCR, I found a strongly reduced expression of the intestinal stem cell marker in Caco2 cells treated for 1d with the FGF receptor inhibitor (Fig 21A). The decrease in *LGR5* expression was even more pronounced after 3d SU5402 treatment (Fig 21B). This result indicates a potential link between the expression of intestinal stem cell markers and FGF signaling.

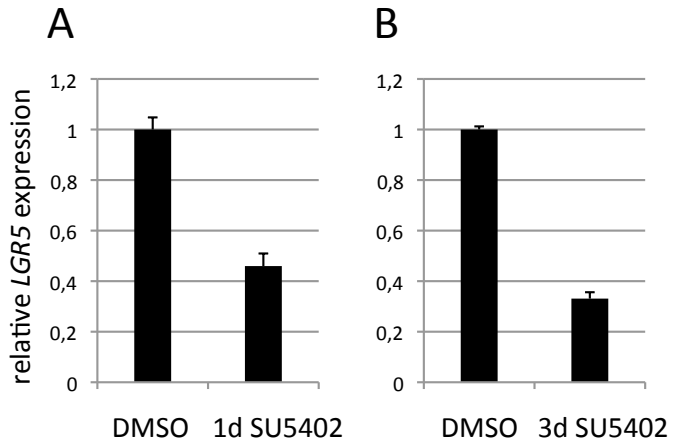

Fig. 21: FGF signals regulate LGR5 expression in Caco2 cells. LGR5 expression is reduced by FGF receptor inhibition after 1d (A) and 3d (B) treatment. Expression of LGR5 was normalized to GAPDH. Residual gene expression after inhibitor treatment is given relative to DMSO treatment. Mean of 3 biological replicates, ±SEM.

3.5 Expression of *FGF9* and *FGF Receptors* in the Intestine

The above results suggested a potential link between stem cell traits and FGF signals. To further establish the significance of endogenous FGF receptor signals in the intestinal epithelium, I assessed the expression of *Fgf9* and the FGF receptors in the normal intestine of the mouse. For this purpose I isolated villi and crypts preparations of the mouse small intestine, as well as colon crypts, and subsequently extracted RNA for qRT-PCR analysis. To control for purity of the isolated tissue I initially determined the expression of intestinal lineage marker genes, which are known to have restrictive expression domains within the intestinal epithelium. For instance, I assessed the expression of *Lgr5* (expressed in stem cells localized in the crypt), *Ifabp* (expressed enterocytes localized in the villus), and *Mmp7* (expressed in Paneth cells localized in the crypt of the small intestine, but absent in the colon) within the individual tissue samples (Fig. 22B). The marker gene analysis gave the expected expression pattern, indicating correct tissue preparation. Using these samples, I then determined the expression of *Fgf9* and the FGF receptors (*Fgfr1-4*). By qRT-PCR, it was ascertained that a higher level of expression of *Fgf9* was present in villi and crypts of the small intestine, as compared to the expression in the colon (Fig. 22A). Moreover, robust expression of multiple Fgf receptors was observed in both small intestinal and colon epithelium. Particularly, *Fgfr2* and *Fgfr3*, which are both high affinity receptors for FGF9 (Hecht et al., 1995), were highly expressed in small intestinal crypts and colon crypts. In contrast, *Fgfr1* expression was virtually absent from all samples (Fig 22A). The expression data again are in line with a possible role for FGF signals in homeostasis of the untransformed mouse intestinal epithelium.

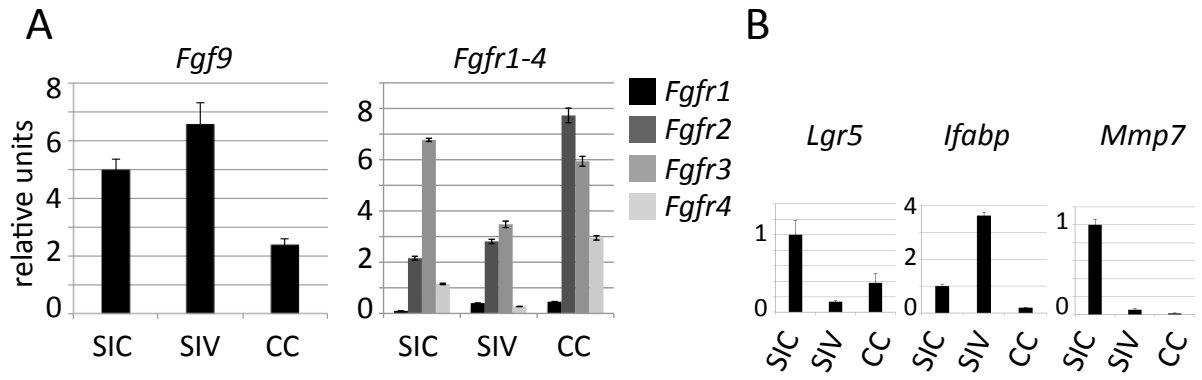

Fig. 22: *Fgf9* is expressed in the intestinal epithelium. Gene expression in the mouse intestine by qRT-PCR. (A) RNA preparations from small intestinal crypts (SIC), villi (SIV) or colon crypts (CC) were probed for *Fgf9*, *Fgfr1*, *Fgfr2*, *Fgfr3* or *Fgfr4*. Expression was normalized against *Pmm2*. (B) *Lgr5* (expressed in stem cells), *Ifabp* (expressed in villus enterocytes) and *Mmp7* (expressed in small intestinal Paneth cells) serve as controls for the cDNA samples. Bars (in A and B) indicate mean of 3 technical replicates, ± SE.

To verify the *Fgf9* expression pattern within the intestinal epithelium we performed an *in-situ* hybridization for *Fgf9* on cryosections of the mouse small intestinal epithelium. This approach was conducted together with Antje Brouwer-Lehmitz and Markus Morkel. Here we detected a signal in the small intestinal crypt, which is highest at a region overlapping with the expression of the crypt base columnar stem cell marker *Olfm4* (Fig. 23).

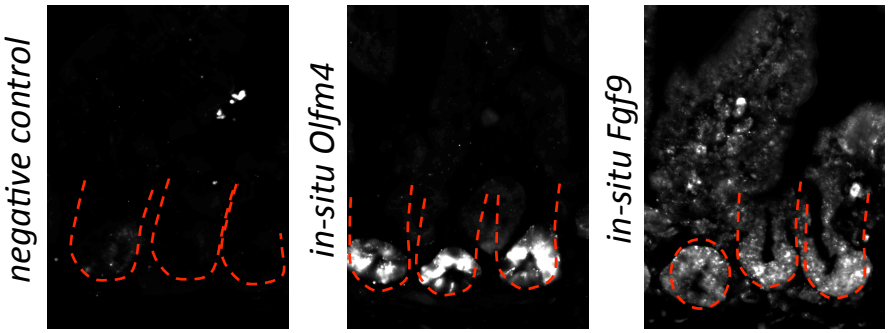

Fig. 23: *Fgf9* is expressed in the small intestinal crypt. *In situ* hybridization for *Fgf9* on sections of the mouse small intestine. Probes complementary to *reverse tet-dependent transcriptional activator* (*rtTA*) and *Olfm4* serve as negative and positive controls, respectively. Crypts are outlined by red dotted lines.

In order to analyze the presence of FGF9 positive cells in the intestinal epithelium on a protein level, an FGF9 immunostaining was conducted on paraffin sections of the mouse intestinal epithelium. The immunostaining was performed together with Antje Brouwer-

Lehmitz and Markus Morkel. This experiment revealed that FGF9 protein levels are highest in Paneth cells, which are adjacent to intestinal stem cells in the small intestinal crypt bases (Snippert et al., 2010) (Fig. 24A). In contrast, no strong signals were found at the base of colon crypts (Fig. 24A). In the colon and in the small intestinal villus, the FGF9 signal was more widespread, increasing towards the intestinal lumen. When we combined immunostaining for FGF9 and *in situ* hybridization for the stem cell marker *Olfm4*, we found that stem cells and FGF9-positive cells intermingle in a regular pattern in the small intestinal crypt (Fig. 24B). Taken together, our expression analyses of untransformed mouse intestinal tissue demonstrate that FGF9 signals are in close proximity to mouse small intestinal stem cells. It is currently believed that Paneth cells provide LGR5 positive stem cells with crucial factors, representing the niche for small intestinal stem cells (Snippert et al., 2010). Our results indicate that FGF9 could potentially contribute to this niche and thus play a role in the regulation of intestinal stem cells. Regulation of stemness and tissue homeostasis cannot be studied in cultured tumor cell lines, as these generally do not have a cellular hierarchy of stemness, proliferation, and differentiation. Therefore this hypothesis was tested using an i*n vitro* model of intestinal epithelial homeostasis, the so-called crypt organoid culture (Sato et al., 2009).

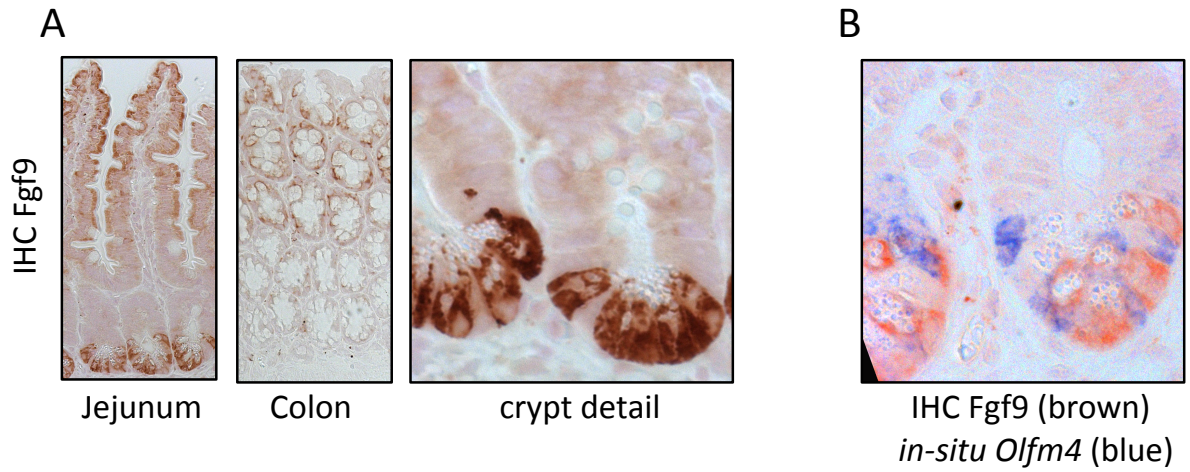

Fig. 24: *Fgf9* is confined to Paneth cells. (A) Immunohistochemistry for FGF9 on sections of small intestine and colon, as indicated. (B) Immunohistochemistry for FGF9 (brown) and *in situ* hybridization for *Olfm4* (marking crypt base columnar stem cells, blue).

3.6 Impact of FGF signals on Intestinal Stemness and Tissue Homeostasis

3.6.1 Intestinal Organoids Serve as a Long-term Culture of the Intestinal Epithelium

In 2009, Hans Clevers and colleagues presented a long-term *in vitro* culture system for the intestinal epithelium that maintains the basic crypt-villus physiology. For this, isolated mouse small intestinal crypts are re-suspended in laminin-rich Matrigel, which represents solubilized basement membrane matrix (BD Matrigel™). Embedded crypts are cultured in the presence of Epidermal Growth Factor (EGF), Noggin (a known BMP inhibitor, which induces ectopic crypt formation (Haramis et al., 2004)) and the Wnt agonist R-spondin. Cultured intestinal crypts behave in a stereotypical manner. Generally, freshly embedded crypts rapidly seal the upper opening to form a single-layered spherical structure, which is subsequently filled with apoptotic cells. Within days, single isolated crypts grow out into so-called crypt organoids, which contain several organized crypt and villus domains, similar to their natural counterpart (Fig. 25). Cultured crypts undergo multiple crypt fission events, while concomitantly giving rise to villus-like domains, which contain all major differentiated cell types of the small intestinal epithelium (Sato et al., 2009). For long-term cultivation, organoids have to be periodically (every 1-2 weeks) dissociated and split into approximately one-quarter of their preplating density. Intestinal organoids have been successfully cultured for more than 8 months without losing general crypt-villus characteristics (Sato et al., 2009).

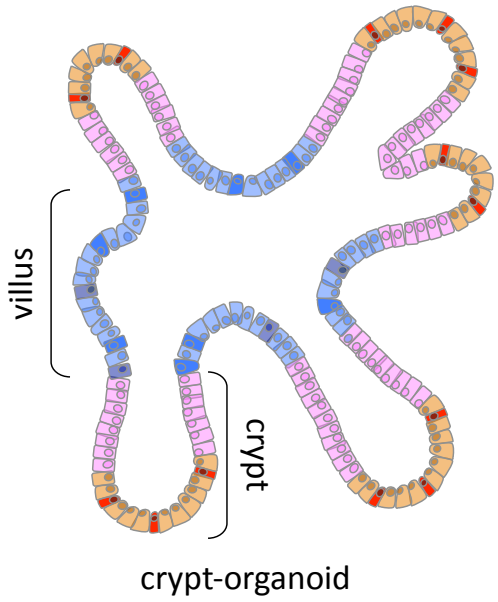

Fig. 25: Schematic representation of an intestinal crypt organoid. The single-layered organotypic structure consists of a central lumen lined by villus-like epithelium and several surrounding crypt-like domains.

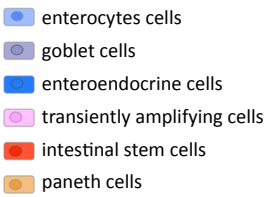

3.6.2 FGF9 Induces Growth of Intestinal Organoids and Stem Cell Proliferation

To investigate the impact of FGF signals on intestinal stemness and tissue homeostasis, intestinal organoids were cultured in the presence of exogenous FGF9. For this, I isolated mouse small intestinal crypts of the jejunum, which were supplemented with FGF9 recombinant protein and compared to control crypt cultures. Exogenous FGF9 stimulation of intestinal crypt organoids strongly increased the organoid size (Fig. 26A). This finding infers highly accelerated cell proliferation in FGF9-treated organoids. FGF9 stimulation also influenced the number of crypt domains per organoid, perhaps as a secondary consequence of increased organoid growth. Freshly isolated untreated crypts of the jejunum developed into organoids that contained an average of 6.3 crypts within six days, while FGF9-treated counterparts underwent rapid crypt fission, resulting in larger organoids that contained an average of 19.4 crypts (Fig. 26B).

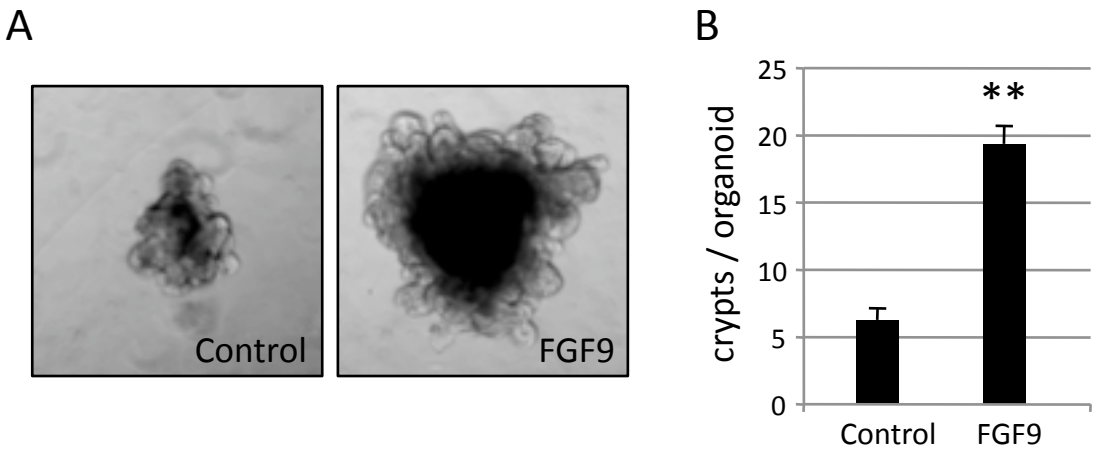

Fig. 26: FGF9 increases the number of crypt domains of intestinal organoids. (A) Bright field images of organoids 6 days after crypt isolation and 5 days after the start of FGF9 treatment. (B) Quantification of crypt domains in FGF9-treated and control organoids described in (A). Mean ±SEM, n>20 organoids; **=p<0.01, t-test.

To assess the impact of FGF9 stimulation on lineage specification in the intestinal epithelium, the cellular composition of organoids was quantified, using qRT-PCR for marker genes of the various intestinal cell lineages. For this, mouse small intestinal crypts of the jejunum were again isolated and cultured in the presence of exogenous FGF9. Crypt organoids were harvested for qRT-PCR analysis three days after the start of the treatment, when organoid size differences were already markedly pronounced between FGF9-treated

and control organoids. I found equivalent expression levels of the crypt cell lineage markers *Mmp7* (Van der Flier et al., 2007b)*, Ephb2* and *Ephb3* (Batlle et al., 2002a), and the villus marker *Ifabp* (Green et al., 1992) in FGF9-treated as compared to control organoids (Fig 27). These observations indicate that the crypt-to-villus ratio is not altered by exogenous FGF9 stimulation.

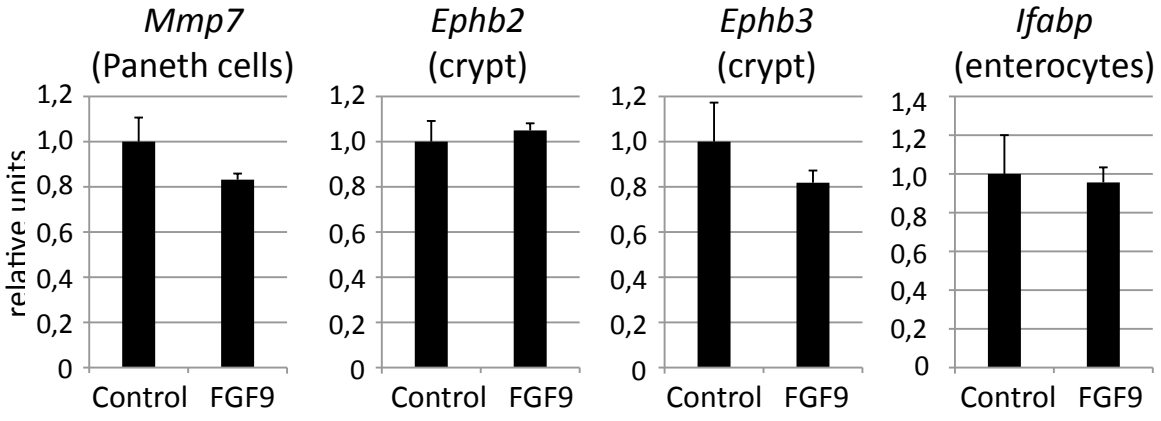

Fig. 27: FGF9 stimulation does not affect the crypt-to-villus ratio in the intestinal epithelium. Analysis of crypt (*Mmp7*, *Ephb2*, *Ephb3*) and villus (*Ifabp*) marker expression in organoids upon 3d FGF9 stimulation, using qRT-PCR (mean of 3 biological replicates, ±SEM). Expression was normalized against *Pmm2.* Asterisks indicate significance (**=p<0.01, t-test).

In addition the expression of the CBC intestinal stem cell marker *Lgr5* and *Olfm4* (van der Flier et al., 2009a) were assessed three days after the start of FGF9 treatment. Using qRT-PCR I detected that FGF9-supplemented organoids expressed lower amounts of both *Lgr5* and *Olfm4* (Fig.28A). However, stem cells and TA cells were present in sections of both FGF9-treated and control organoids, as visualized by *Olfm4* and Ki67, respectively (Fig. 28B). Importantly, subcultured FGF9-treated organoids proliferated for many generations (>30 days; data not shown) and maintained their growth advantage. These results confirm a preserved and functional stem cell pool in FGF9-treated organoids.

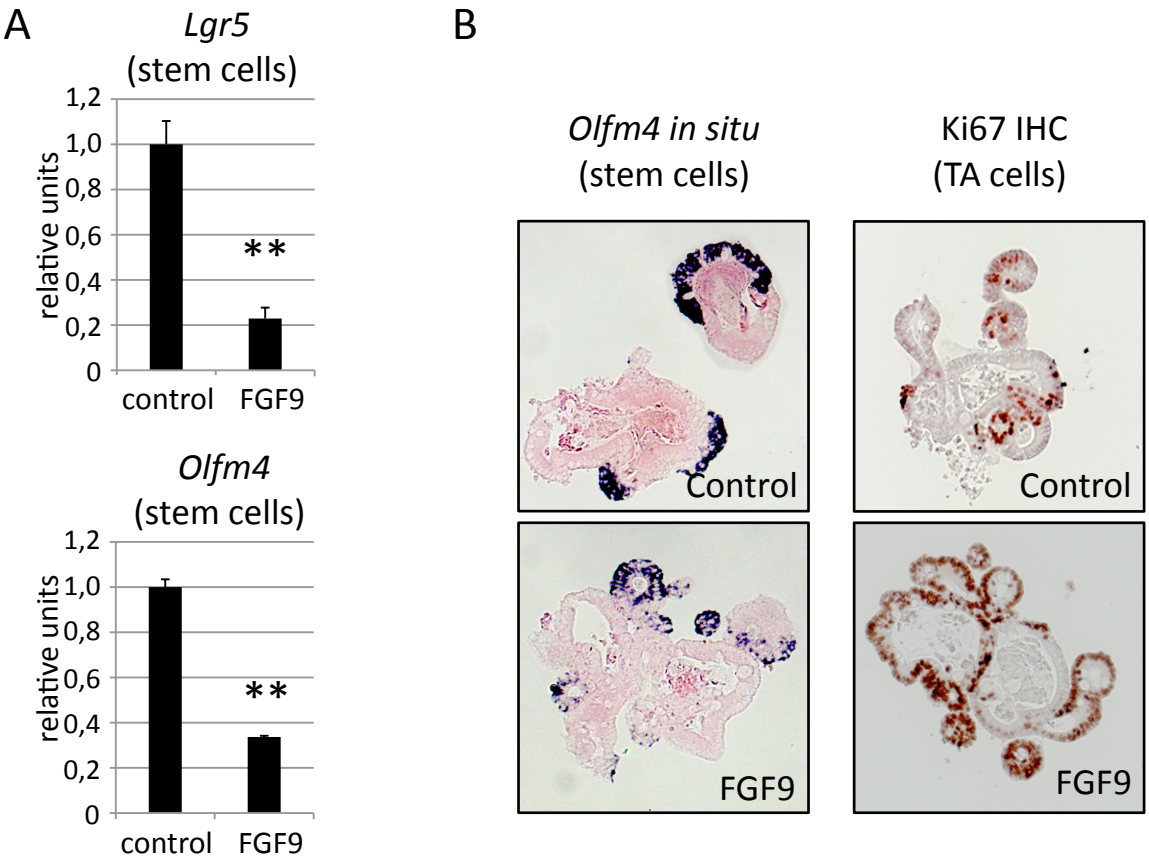

Fig 28: The level of intestinal stem cell markers is decreased in FGF9-supplemented organoids. (A) Analysis of the intestinal stem cell markers *Lgr5* and *Olfm4* in organoids upon 3d FGF9 stimulation, using qRT-PCR (mean of 3 biological replicates, ±SEM). Expression was normalized against *Pmm2.* Asterisks indicate significance (**=p<0.01, t-test). (B) Visualization of stem cells (*in situ* hybridization for *Olfm4* (blue)*;* counterstained with eosin (pink)) and TA cells (IHC for KI67 (brown)) in representative sections of control and FGF9-treated organoids.

To investigate changes in the stem cell population and the mechanism of organoid growth following FGF9 supplementation, the proliferation kinetics of intestinal stem cells were quantified. This experiment was initiated by me, but analyzed by Antje Brouwer-Lehmitz and Markus Morkel. I isolated mouse small intestinal crypts of the jejunum and cultured them in the presence of exogenous FGF9 for three days. To determine actively proliferating cells, FGF9-treated and control organoids were exposed for 45 minutes to the synthetic nucleoside Bromodeoxyuridine (BrdU). These organoids were harvested, paraffin sectioned, and immunostained for BrdU, which labels all proliferating cells due to the incorporation of BrdU into S-phase nuclei (Fig. 28A). Stem cells in these organoid sections were simultaneously visualized by *Olfm4 in-situ* hybridization (Fig.28A). By immunofluorescence microscopy, we found 17.3 and 17.5 *Olfm4*-positive stem cells per crypt section in control

and FGF9-treated organoids, respectively (n=116 crypts; no significant difference) (Fig. 28B). Next, proliferation of *Olfm4*-positive stem cells was assessed. Here, we found a significantly higher percentage of BrdU-positive stem cells in crypt bases of FGF9-treated organoids as compared to control counterparts (n=116 crypts; 60.2% *versus* 51.0%, $p<0.006$) (Fig. 28C). These findings indicate that, while the number of *Olfm4*-positive stem cells per crypt is not affected by exogenous FGF9 treatment, the cell cycle of intestinal stem cells is accelerated. These data also imply that the increase in crypt numbers in FGF9-treated organoids (Fig. 26) reflects an equally substantial increase in the total number of stem cells. The higher percentage of stem cell proliferation may indirectly affect the pool of transiently amplifying progenitor cells, which could therefore also contribute to the enlarged organoid size.

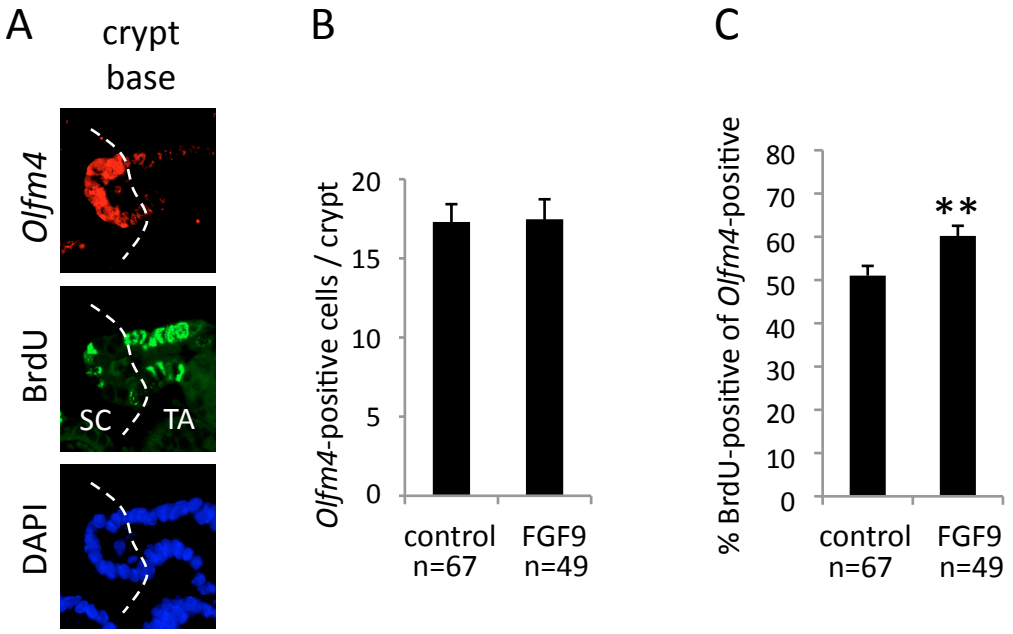

Fig. 29: FGF9 induces stem cell proliferation. Quantification of stem cell proliferation in FGF9-supplemented (3d) and control organoid crypt bases. (A) Representative images of the *Olfm4*, BrdU and DAPI channels of one organoid crypt. Dashed line indicates the border between crypt bases that contain stem cells (SC, *Olfm4*-positive) and transiently amplifying zone (TA, *Olfm4*-negative). Crypt bases were defined as regions with at least five *Olfm4*-positive cells. (B) Quantification *Olfm4* positive stem cells per crypt domain (n=116 crypts). (C) Quantification of stem cell proliferation in crypt bases (n=116 crypts; $p<0.006$, t-test).

3.6.3 Endogenous FGF Signals are Essential for Crypt and Stem Cell Maintenance

To define the roles for endogenous FGF signals in the intestinal epithelium, FGF signals was inhibited in cultured intestinal organoids. First, I employed the chemical FGF receptor inhibitor SU5402 to target the entire FGF signaling spectrum. For this experiment, small intestinal crypts of the jejunum were isolated and cultured in the presence of the FGF receptor inhibitor. Morphologically, FGF receptor-inhibited organoids initially showed no difference from untreated counterparts and grew at an approximately equivalent rate (Fig. 30). Within 4-6 days, however, treated organoids developed irregular crypts that contained only a few cells with visible granules (Fig. 30), which indicates a loss of Paneth cells (Sato et al., 2009). Finally, proliferation ceased in the majority of organoids, which disintegrated approximately 7-10 days after inhibition of FGF receptors. These results show that FGF signals are essential for intestinal crypt maintenance.

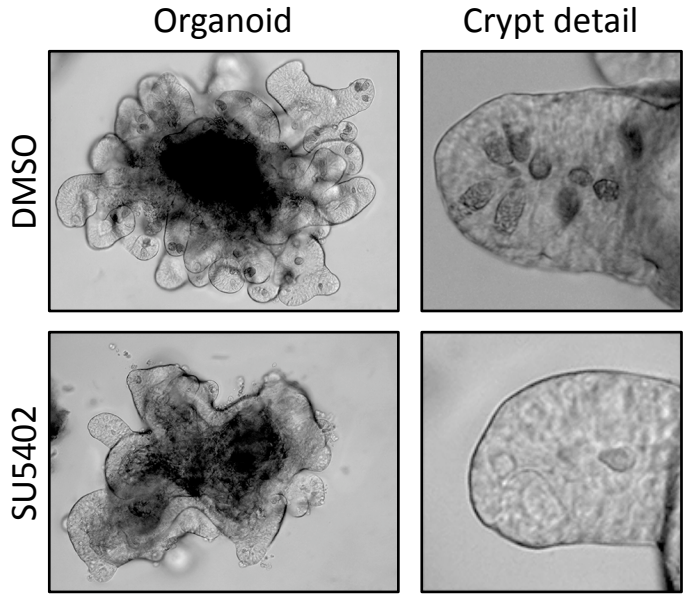

Fig. 30: FGF receptor inhibited organoids develop malformed crypt domains. Morphology of representative solvent control (DMSO) and SU5402-treated organoids after 5 days of treatment. Dark granules in crypt areas are indicative of Paneth cells.

To investigate the cellular composition of crypt domains in FGF receptor inhibited organoids the expression levels of crypt marker genes was analyzed by qRT-PCR. To this end, I examined crypt organoids after culture for six days in the presence of the FGF receptor inhibitor. In line with the morphological appearance (Fig. 30), I could show that the expression of marker genes for all crypt lineages and regions, including stem cells, transiently amplifying cells, and Paneth cells, was strongly and significantly reduced after six days of SU5402 treatment, as compared to control organoids (Fig. 31). The differential

expression pattern upon FGF receptor inhibition confirms that FGF signals affect intestinal tissue homeostasis.

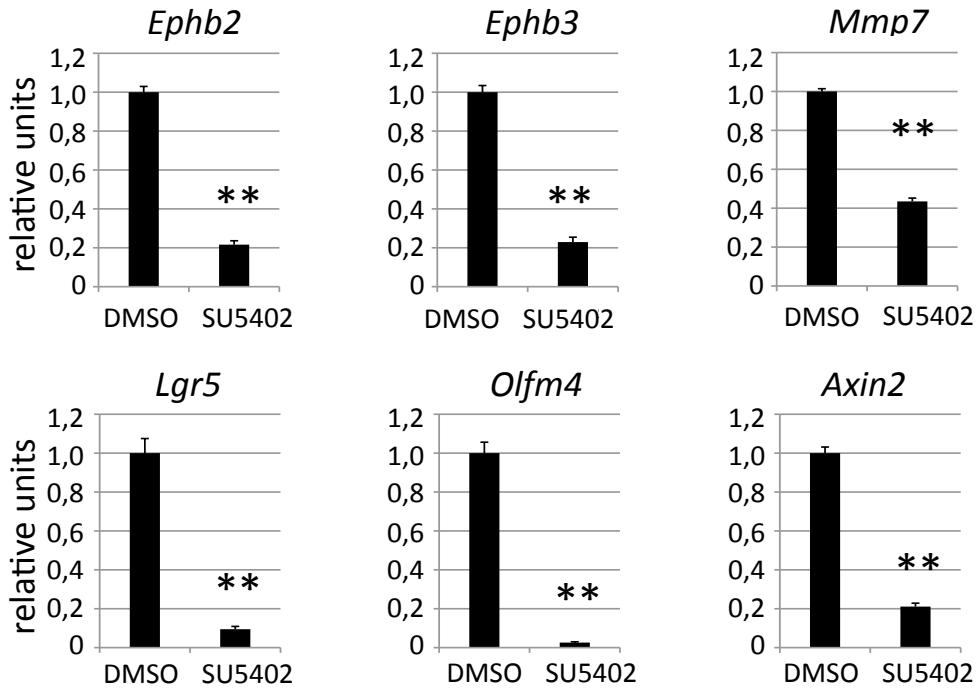

Fig. 31: Crypt lineage markers are diminished in FGF receptor inhibited organoids. Analysis of crypt lineage markers in control and SU5402-treated organoids 6 days after the start of treatment (as in Fig. 30), using qRT-PCR: *Ephb2*, *Ephb3*, *Mmp7* (crypts/Paneth cells); *Lgr5*, *Olfm4* (stem cells); *Axin2* (Wnt signal in crypt base and TA cells). Expression was normalized against *Pmm2.* Asterisks indicate significance (mean of 3 biological replicates, ±SEM; **=p<0.01, t-test).

This cellular alteration of intestinal crypt organoids upon FGF receptor inhibition was also confirmed by histological analysis. Again, small intestinal crypts of the jejunum were cultured for six days in the presence of the FGF receptor inhibitor and subsequently histologically analyzed for Lysozyme, *Olfm4* and KI67, in comparison to solvent controls. These studies confirmed that Paneth cells, stem cells and TA cells were mostly absent in FGF receptor inhibited organoids at this time point (Fig. 32A). In addition, it was observed that subcultured SU5402-treated crypts did not effectively initiate new organoids (Fig. 32B). Consequently, these findings infer that the stem cell pool in SU5402-treated organoids was largely exhausted.

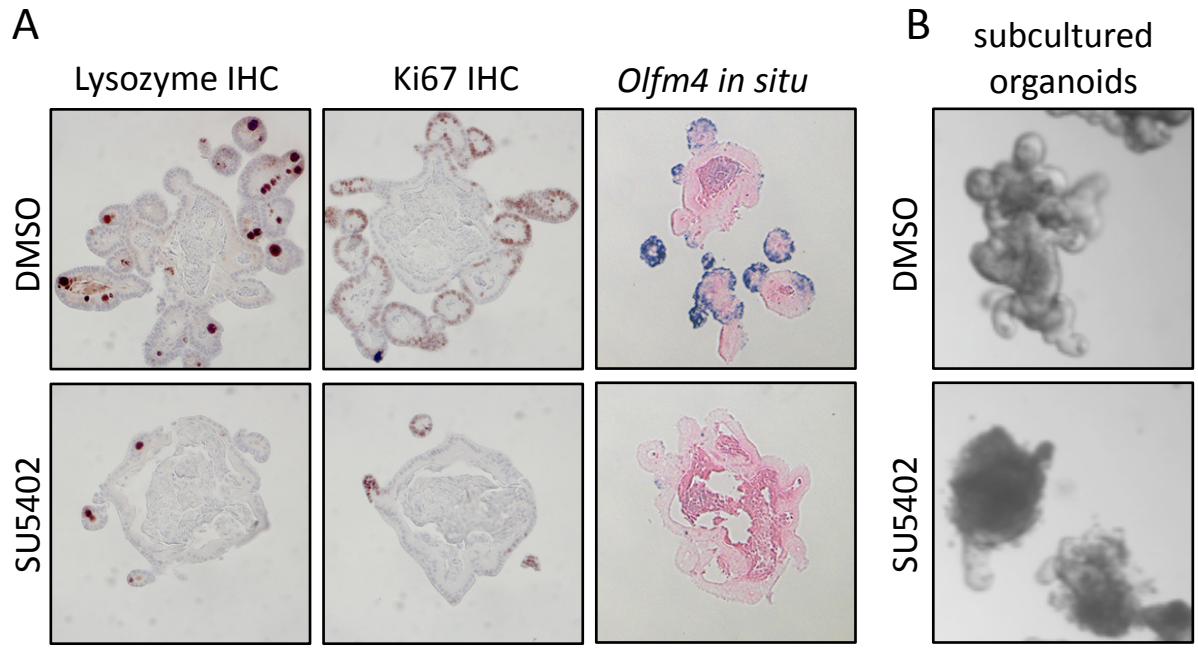

Fig. 32: Intestinal stem cells are not maintained in FGF receptor inhibited organoids. (A) Visualization of Paneth cells (IHC for Lysozyme), proliferative TA cells (IHC for KI67) and stem cells (*in-situ* hybridization for *Olfm4*; counterstain with eosin) in representative sections of organoids after six days of FGF receptor inhibition using SU5402. (B) Subcultured SU5402-treated crypts did not effectively initiate new organoids and disintegrate in 7-10 days.

Different FGF ligands and FGF receptors are expressed in the intestinal crypt as shown in Fig. 22A and (Vidrich et al., 2004). The chemical compound SU5402, however, inhibits all FGF receptor variants. To address the individual roles of the FGF9 ligand and the highly expressed *Fgfr3* receptor in the intestinal epithelium, the endogenous mRNAs of *Fgf9* and *Fgfr3* in organoids were targeted using siRNAs from Dharmacon, which are specifically modified for use without a transfection reagent. I initiated siRNA treatment in mature organoids. These organoids were passaged after three days. Subcultured organoids were continuously siRNA-treated for an additional five days before harvesting for further analysis. Using qRT-PCR analysis, I initially determine an approximately 50% knockdown efficacy for the *Fgf9* and *Fgfr3* siRNAs (Fig. 33A). Next, the expression of the stem cell marker *Lgr5* was assessed. Importantly, I found that the 50% reduction in *Fgf9* expression significantly reduced the expression of the intestinal stem cell marker *Lgr5* (Fig. 33B). In contrast, the reduction of *Fgfr3* had no significant effect on *Lgr5* expression (Fig. 33B). The observed downregulation in *Lgr5* expression upon *Fgf9* knockdown implies that FGF9 signals act on intestinal stem cell properties.

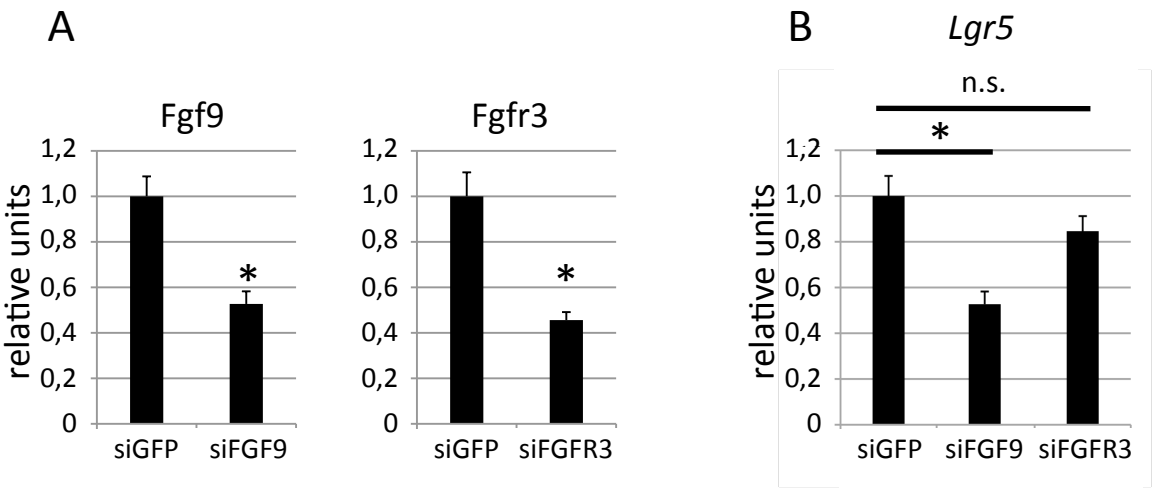

Fig. 33: FGF9 signals are essential for stem cell maintenance. (A) Knockdown efficacy for the *Fgf9* and *Fgfr3* siRNAs in mouse primary intestinal organoids of the jejunum. (B) Expression of stem cell marker *Lgr5* after experimental RNA interference with *Fgf9*, *Fgfr3* or *GFP* (control). Bars indicate mean of 3 biological replicates, ±SEM. Asterisks indicate significance (*=p<0.05, t-test; n.s. = not significant).

The ability of individual *Fgf9* and *Fgfr3*-silenced crypt bases to re-constitute organoids in the absence of differentiated villus cells, which may produce growth factors that affect neighboring crypt cells was then assessed. To this end, I initiated siRNA treatment (as above) in mature organoids and passaged them after three days. Before re-embedding, however, passaged organoid pieces were size filtered (70µm) and therefore enriched for crypt bases. Subcultures were continuously siRNA-treated for another four days. In this experiment, I observed that control crypt bases quickly closed the disruption edges at the upper crypt border to form spherical structures, and rapidly proliferated to reconstitute complete organoids within the four day time window (Fig. 34). In contrast, *Fgf9* siRNA-treated crypt bases closed at the disruption edges, but were mostly blocked at this stage, and did not further proliferate (Fig. 34). Crypt bases that were treated with *Fgfr3* siRNA initiated organoids that were often malformed, and proliferated slower than controls (Fig. 34). These observations suggest a role for FGF9 as a growth factor that is essential for intestinal stem cell function in the crypt base. FGFR3 may, in concert with other FGF receptors, play a role in transmitting the FGF9 and other FGF signals within this structure.

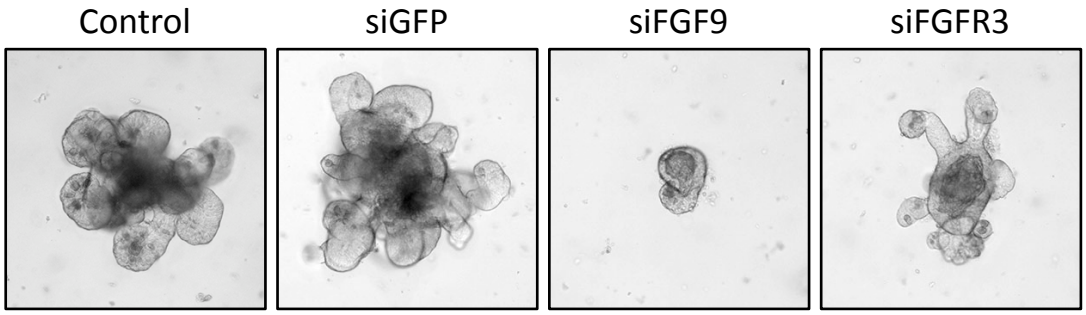

Fig. 34: FGF9 signals are essential for crypt outgrowth. Phenotypes of organoids initiated from individual crypt bases after experimental RNA interference with *Fgf9*, *Fgfr3,* or *GFP* (control). Representative images are shown.

3.6.4 FGF Signals Affect the Villus Lineage Specification

Next, the impact of endogenous FGF signals on the specification of intestinal villus lineages was examined. For this, I initially again blocked FGF signals in organoids by SU5402 treatment. Small intestinal crypt organoids were cultured for six days in the presence of the FGF receptor inhibitor and compared to solvent controls. By using qRT-PCR analysis, I observed an approximately three-fold up-regulation of *Ifabp*, marking enterocytes, while *Ngn3* and *Muc2*, marking secretory enteroendocrine and goblet cells (Gambus et al., 1993; Lee et al., 2002), respectively, were significantly decreased (Fig. 35A). This indicates that the ratio between absorptive and secretory lineages was altered upon FGF receptor inhibition. Consequently, FGF signals impinge on cell lineage specification within the intestinal epithelium. Histological analysis for ChromograninA confirmed a strong reduction of enteroendocrine cells by FGF receptor inhibition (Fig. 35B).

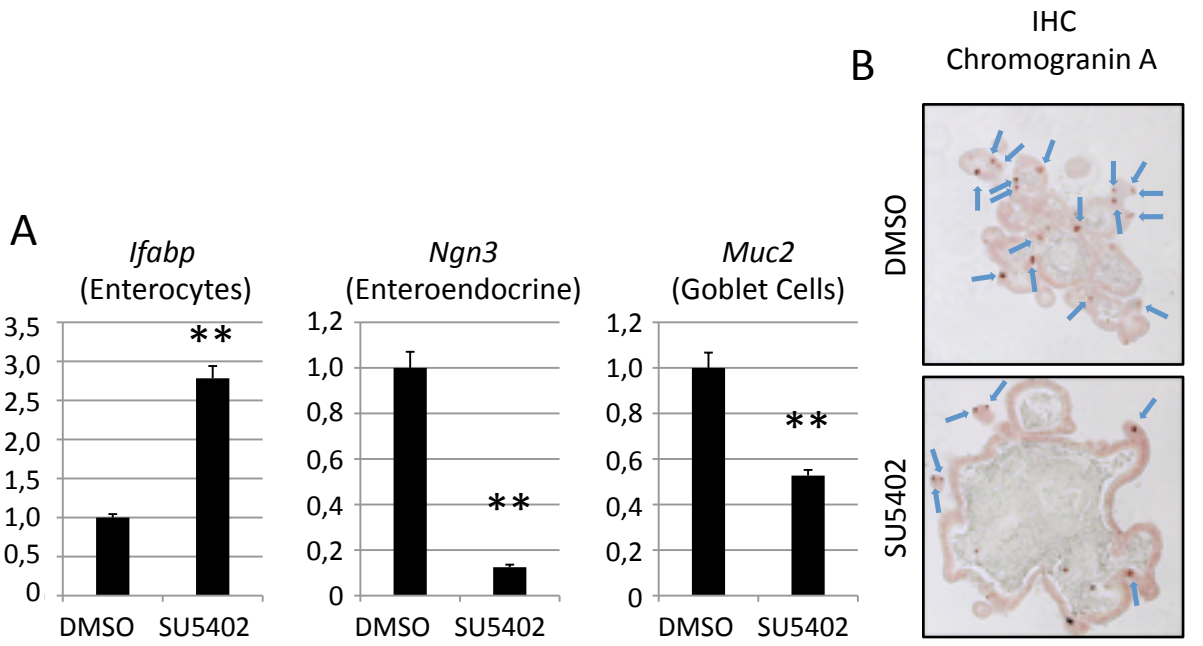

Fig. 35: FGF signaling modulates intestinal cell lineage specification. (A) Analysis of villus markers in solvent control (DMSO) and SU5402-treated organoids 6 days after start of the treatment, using qRT-PCR. Expression of *Ifabp* (enterocytes), *Ngn3* (enteroendocrine cells) and *Muc2* (goblet cells) was assessed. (B) Immunohistochemical analysis of ChromograninA, marking enteroendocrine cells in control and SU5402-treated organoids. Positive cells are marked by arrows.

The biased lineage specification in SU5402-treated organoids leading to the loss of all secretory lineages (goblet cells, enteroendocrine, and Paneth cells) resembles the *Math1* loss-of-function phenotype (van der Flier and Clevers, 2009; van Es et al., 2010). The basic helix-loop-helix transcription factor *Math1* controls cell fate decisions of various tissues including cell fate determination within the intestinal epithelium (van Es et al., 2010). To assess the impact of FGF signals on intestinal cell fate determination, I additionally investigated early imbalances between the lineages one or two days after FGF receptor inhibition in subcultured and size-filtered (70µm) organoid crypt bases. Importantly, size controlled crypt bases are depleted for cells that previously had differentiated into either the absorptive or secretory lineage of the villus. These studies demonstrated that the expression of markers for secretory lineages, including *Math1*, which is already expressed in secretory precursor cells (VanDussen and Samuelson), was immediately decreased (Fig. 36). This observation infers that FGF signals likely influence early lineage specification and not later events during cell differentiation. Furthermore, markers for stem cells and Paneth cells – which are both long-lived (Ireland et al., 2005) – were also diminished already two days

after FGF receptor blockade (Fig. 36). These cell lineages may therefore have a mutual dependence for survival. Alternatively, both cell types could require FGF signals.

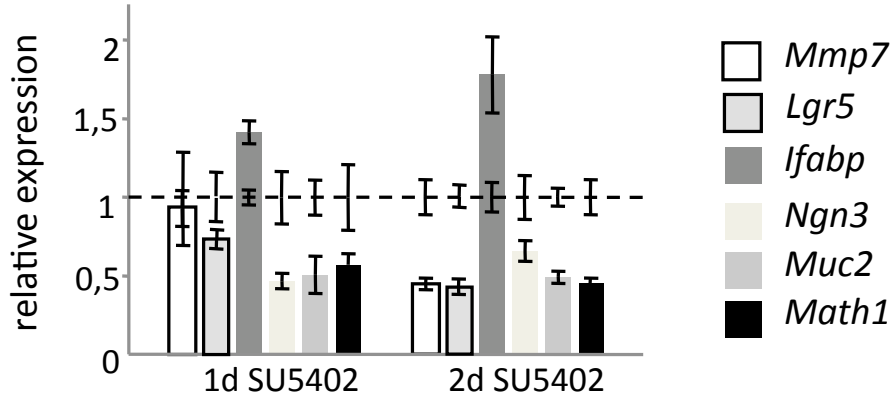

Fig. 36: FGF signals control early lineage specification. Relative expression of lineage markers in re-seeded crypt bases, one and two days after the start of SU5402 treatment. Expression of *Lgr5* (stem cells), *Mmp7* (Paneth cells), *Ifabp* (enterocytes), *Ngn3* (enteroendocrine cells), *Muc2* (goblet cells), and *Math1* (enteroendocrine and goblet cells and precursors) was assessed, and normalized to control organoids. Bars indicate mean of 3 biological replicates, ±SEM. (SEM of controls is given on the dashed control line).

To address the individual roles of the FGF9 ligand and FGFR3 on intestinal lineage specification, *Fgf9* or *Fgfr3* mRNAs were targeted in crypt organoids by siRNA as described above. RNA interference with either *Fgf9* or *Fgfr3* siRNA led to an imbalanced specification towards the absorptive lineage. By qRT-PCR I ascertained that *Fgfr3* knockdown results in lower expression of secretory lineage markers such as *Ngn3* and *Muc2*, marking secretory enteroendocrine and goblet cells, respectively (Fig. 37A). In the case of *Fgf9* interference, the lineage bias became apparent by higher expression of the enterocyte marker Ifabp (Fig. 37A). In contrast, the relative expression level of *Ngn3* and *Muc2* was unaltered after *Fgf9* interference, likely due to lower proportions of crypt domains in these organoids (see Fig. 37B for a model of crypt and villus phenotypes observed after interference with FGF signaling). These results indicate that FGF9 has roles in intestinal stem cell maintenance and lineage specification, and that FGFR3 plays an essential role in the transmission of the FGF9 signal.

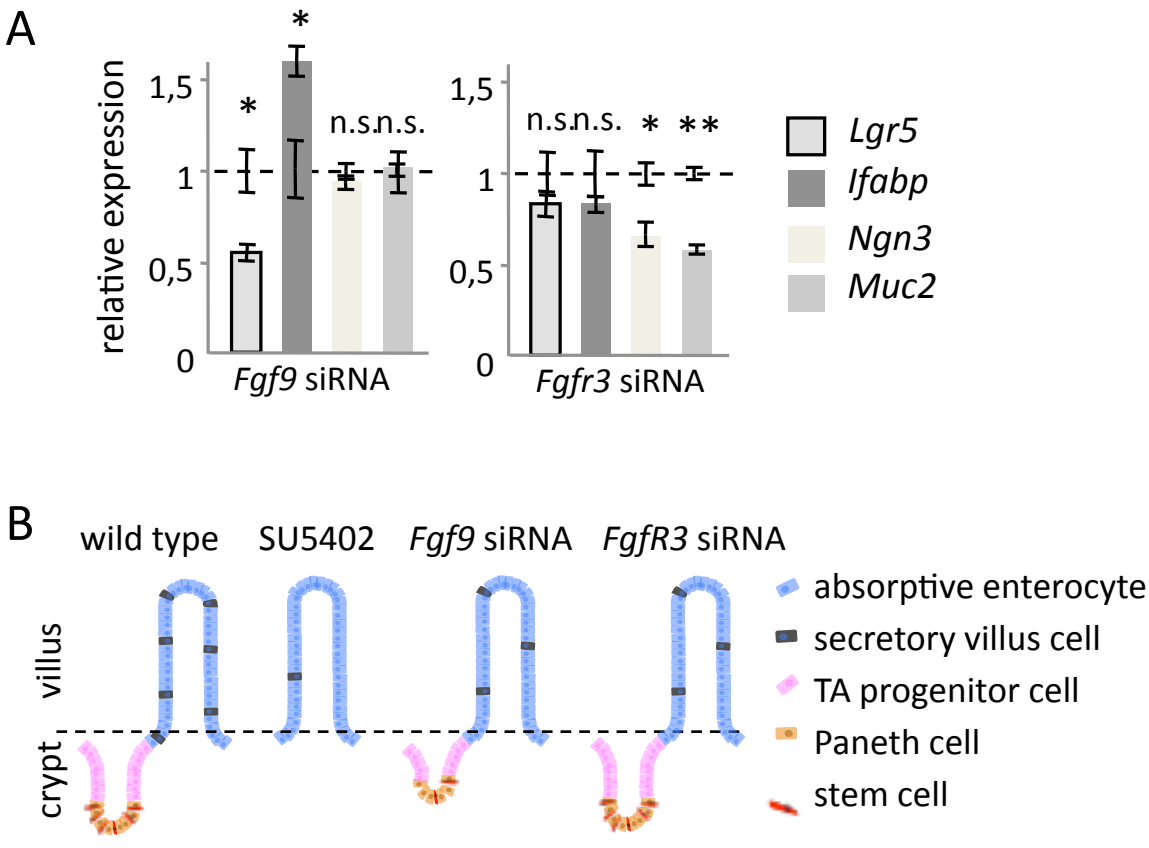

Fig. 37: FGF9 signals control lineage specification. (A) Expression of the villus lineage markers *Ifabp* (absorptive enterocytes) *Ngn3* and *Muc2* (secretory lineages) after RNA interference with *Fgf9* or *Fgfr3* was assessed, and normalized to control organoids. *Lgr5* expression (see Fig. 33B) is given as a reference. Bars indicate mean of 3 biological replicates, ±SEM. Asterisks indicate significance (*=p<0.05; **=p<0.01, t-test). (B) Models of crypt and villus tissue compositions after general inhibition of FGF receptor signals, or after interference with *Fgf9* or *Fgfr3*: in the absence of all FGF receptor signals (SU5402), crypt lineages are lost, and secretory lineages are strongly diminished. Upon interference with *Fgf9,* stem cells and secretory lineages are reduced. Upon interference with *Fgfr3,* secretory lineages are reduced, while the stem cell pool appears unchanged.

3.6.5 FGF and Wnt Signals Interact in the Intestinal Epithelium

The crypt and villus phenotypes after inhibition of FGF signaling were reminiscent of intestinal models with impaired Wnt signaling (Pinto et al., 2003; Ireland et al., 2004). In agreement, the direct Wnt target gene *Axin2* (Lustig et al., 2002) was significantly downregulated already one day after FGF receptor inhibition, as judged by qRT-PCR (Fig. 38), demonstrating that the intestinal Wnt signal is immediately downregulated after inhibition of endogenous FGF signals. I also tested a potential interaction between FGF signals and Notch signals, which are also important in intestinal homeostasis. The Notch pathway plays an essential role in maintaining the balance between the secretory and absorptive lineages

in the intestinal epithelium. However, the key Notch target *Hes1* (Suzuki et al., 2005) was not deregulated after one day, and only mildly affected after two days of inhibitor treatment, possibly due to the general reduction of the crypt cell lineages upon FGF receptor inhibition (Fig. 38). Collectively, the above results suggest that FGF signals co-operate with Wnt signals, but not with Notch signals to control intestinal tissue homeostasis.

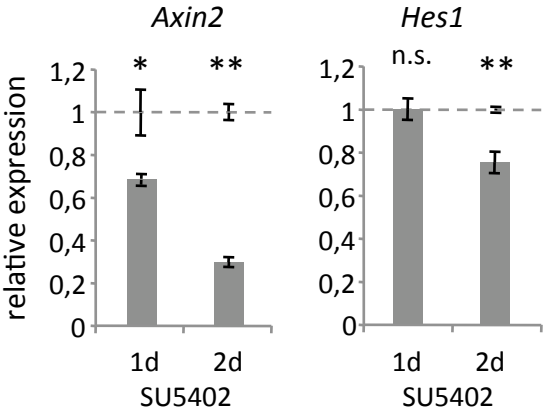

Fig. 38: FGF signals co-operate with Wnt signals to control intestinal tissue homeostasis. Expression of the Wnt target gene *Axin2* and the Notch target gene *Hes1* after one and two days of SU5402 treatment. Bars indicate mean of 3 biological replicates, ±SEM. Asterisks indicate significance (*=p<0.05; **=p<0.01, t-test).

3.7 Impact of FGF signaling on intestinal tumor progression

3.7.1 Expression of FGF9 is Generalized in Human Colon Carcinoma

My previous analyses suggested that FGF9 signaling affects intestinal stem cell proliferation and tissue homeostasis. A hallmark of tumor initiation and progression is the deregulation of tissue homeostasis. Therefore, to substantiate a potential role for FGF9 signals in intestinal tumor progression, it was important to examine the expression pattern of *FGF9* in human colon cancer. These analyses were conducted in cooperation with Antje Brouwer-Lehmitz and Markus Morkel. Here, we found generalized expression of *FGF9* mRNA (Fig. 39A) and protein (Fig. 39 B) in the tumor epithelium of primary tumors and metastases by *in situ* hybridization and immunohistochemistry, respectively. In addition, we detected interspersed FGF9 positive cells in the tumor stroma, which were enriched at the interface between the tumor epithelium and stroma (Fig. 39B, magnification). Such mesenchymal FGF9 positive cells could be either tumor- or stromal derived, as tumor cells at the invasion front preferentially undergo EMT and disseminate from the primary tumor as spindle shaped cells (Fodde and Brabletz, 2007). These expression analyses, in combination with the functional data, provide evidence for a role for FGF9 signaling in the progression of human

colon carcinoma, either by an autocrine (within the tumor epithelium) and/or a paracrine manner (from stromal to tumor cells).

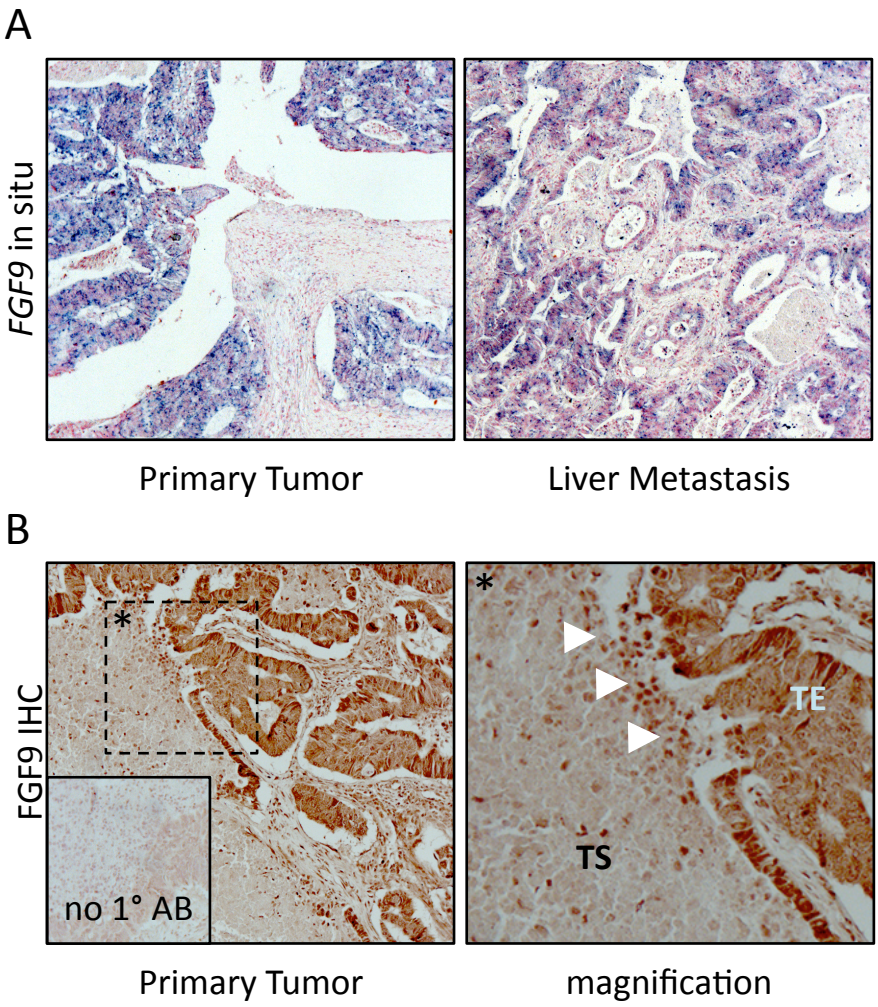

Fig. 39: FGF9 is expressed in human colon cancer. Staining for FGF9 mRNA (A) and protein (B) in sections from human colon tumors, as indicated. Insert (no 1° AB) in the immunohistochemical staining (IHC) shows a negative control without primary antibody. The dashed box represents the magnified area to the right. The magnification demonstrates the tumor-stromal interface, which harbors the invasive front, as indicated by white arrowheads. TE: tumor epithelium; TS: tumor stroma.

3.7.2 FGF9 Inversely Correlates with Patients' Survival

Our analyses of untransformed small intestinal crypt organoids suggested that FGF9 augments intestinal stem cell proliferation. Expansion of the stem cell pool is found in colon cancer, and the proportion of stem cells in the tumor correlates with patient survival (Ricci-Vitiani et al., 2007; O'Brien et al., 2007). We therefore examined the expression of *FGF9* and

the *FGF receptors* in a set of expression profiles of human colon cancer. These data were generated at the Max-Delbrück-Center for Molecular Medicine, Berlin, in the group of Walter Birchmeier by Markus Morkel and Johannes Fritzmann (Fritzmann et al., 2009). The analyzed set of 95 expression profiles comprised normal colon (4 profiles), locally advanced non-metastatic colon carcinoma (staged T3/4N0M0 by International Union Against Cancer (UICC) criteria; 17 profiles), metastatic colon carcinoma (staged T3/T4 by UICC criteria; 24 profiles) and metastases to lymph nodes, liver, and lung (50 profiles). We used this data set to determine the expression patterns of *FGF9* and *FGFR3*. The majority of tumor profiles displayed basal expression levels of *FGF9* and *FGFR3* comparable to the expression level of the normal colon tissue profiles (Fig. 40). Intriguingly however, we observed high expression of *FGF9* or *FGFR3* in distinct subgroups of colon tumors (*FGF9*: 2/17 non-metastatic tumors, 5/24 metastatic tumors, and 7/50 metastases; *FGFR3*: 0/17, 3/24, 7/50, respectively; cut-off >2-fold compared to normal tissue) (Fig. 40). In contrast, none of the profiles exhibited elevated expression of the FGF receptors 1, 2 and 4 (data not shown). High expression of *FGF9* was maintained between pairs of primary tumors and metastases derived from three patients (Fig. 40). This expression pattern indicates that *FGF9* activation in the colon tumors can persist over prolonged periods of time.

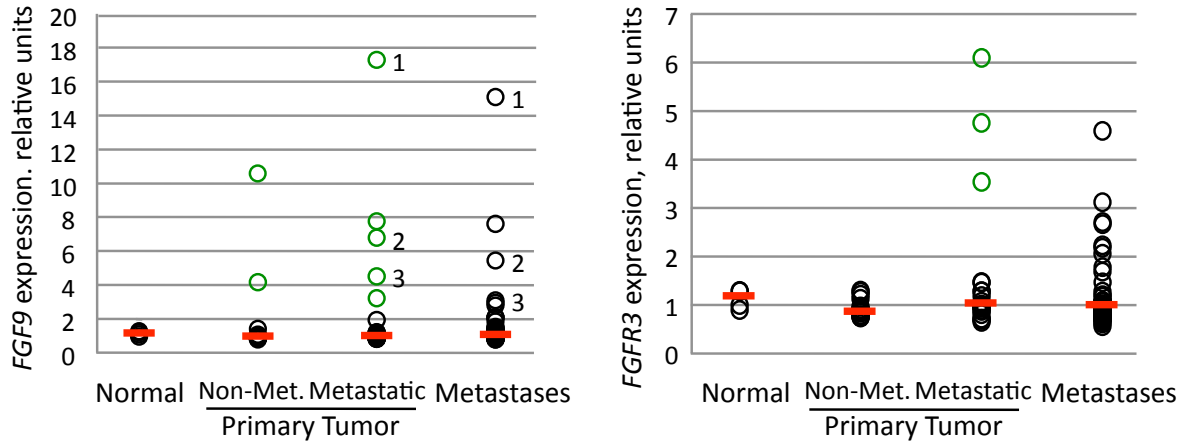

Fig. 40: *FGF9* is overexpressed in a subgroup of colon carcinomas. Expression of *FGF9* or *FGFR3* in invasive and metastatic colon carcinoma, as assessed by microarray analysis (n=95). Expression in each sample is indicated by a circle, median expression in each group is given by red bar. Numbers in *FGF9* graph indicate primary tumor/metastasis pairs derived from the same patient.

Finally, we correlated the expression of *FGF9* and *FGFR3* in the primary tumors (n=39) with patient survival using a Kaplan-Meier analysis. This analysis revealed that the subgroup of

patients with high expression of *FGF9* had a significantly shorter survival rate when compared to patients with low *FGF9* expression (Fig. 41, *p*=0.008). A similar patients' survival correlation was obtained when patients with high expression of *FGFR3* were included in the group (Fig. 41, *p*=0.006). These data suggest that enhanced levels of FGF9 or other FGF signaling components could augment the tumor phenotype, and imply *FGF9* expression as a candidate prognostic marker for colon cancer.

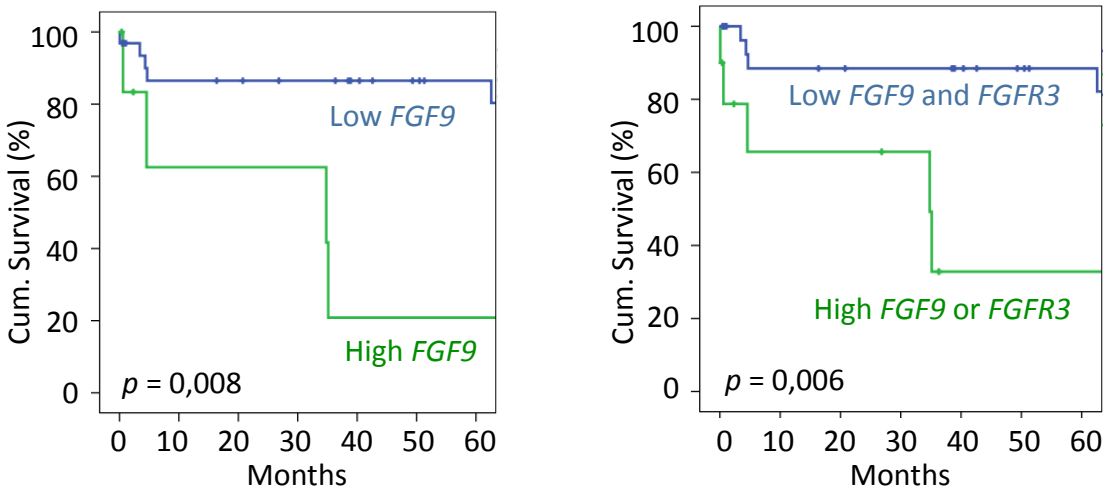

Fig. 41: FGF9 inversely correlates with patient survival. Kaplan-Meier survival analysis of patients examined in Fig. 40 (primary tumors with follow-up data only, n=39). Patients were grouped according to high (>2-fold of median, indicated by green circle in Fig. 40) and low *FGF9* and *FGFR3* expression.

4 Discussion

The aim of this thesis was to identify novel genes involved in intestinal tumor progression. To this end, I assessed the impact of a shortlist of EMT candidate genes, selected by their embryonic expression pattern, on colon cancer cells. In a loss-of-function screen I identified, among other genes, *FGF9*. Silencing of *FGF9* induced an epithelial cell morphology. In order to determine the significance of FGF signals in the intestine I then characterized the expression of FGF signaling components in the untransformed mouse intestinal epithelium and human intestinal tumors. In addition, I assessed the impact of FGF signals on intestinal stemness and tissue homeostasis. Taken together, I report here novel roles for FGF signaling in both gut physiology and colon cancer. These results provide evidence that intestinal FGF signals are key factors in the control of intestinal tissue homeostasis and may, when deregulated, contribute to the progression of colon cancer.

4.1 Identification of Several Genes that Modulate Morphology of SW480 Tumor Cells

In an RNAi based phenotypic screen I assessed the impact of 364 genes on the phenotype of SW480 colon cancer cells. This shortlist of candidate genes was selected by their restricted expression patterns at the caudal end of a mid-gestation mouse embryo hosting the remaining primitive streak. Affected by WNT, FGF, and other signaling pathways epithelial cells at the streak undergo an Epithelial to Mesenchymal Transition (EMT) leading to a phenotypic switch to a mesenchymal state of low cell adhesion and high cell motility (as reviewed by Arnold and Robertson, 2009). The adenoma to carcinoma progression of epithelial tumors resembles this EMT process. Accordingly, multiple studies have provided evidence that key pathways orchestrating the EMT process are conserved between developmental and tumor-associated EMT (Thiery and Sleeman, 2006; Yang and Weinberg, 2008).

The loss-of-function screen ultimately identified 18 genes whose silencing induced an epithelial morphology in SW480 human colon cancer cells. It is therefore probable that these genes support a mesenchymal, potentially motile and invasive, phenotype of human colon cancer cells and therefore may promote intestinal tumor progression. A large proportion of

the identified genes were found represent either transcription factors or signaling molecules. For instance, TCF7L1 represents a member of the LEF/TCF transcription factor family. Members of this transcription factor family interact with nuclear β-catenin to regulate the transcription of WNT target genes. While TCF7L2 has been proposed to transduce intestinal WNT signals (Korinek et al., 1998), our result therefore suggests additional roles of the TCF7 family member TCF7L1.

PTCH, GLI2, and GLI3 are members of the Hedgehog pathway. Hedgehog signaling is essential during morphogenesis of the gut. Accordingly, Hedgehog pathway mutations are associated with multiple malformations along the intestinal tract. For instance, *Gli2*-deficient mice exhibit an imperforate anus and a recto-urethral fistula, while *Gli3*-knockout mice have anal stenoisis and ectopic anus (Kimmel et al., 2000; Mo et al., 2001). Interestingly, Hedgehog signaling was shown to restrict the expression of WNT target genes to the crypt base in the intestinal epithelium (van den Brink et al., 2004). Consequently, WNT and Hedgehog signals may interact to control intestinal crypt physiology. My results indicate additional roles of Hedgehog signaling in intestinal tumor progression.

Six1 is a member of the Homeobox gene family. This transcription factor has been implicated in multiple processes, including cell differentiation and tumor progression. *Six1* has been shown to activate several genes that promote cell proliferation and motility such as *Cyclin-D1* and *c-myc* in a mouse model of the pediatric skeletal muscle cancer rhabdomyosarcoma (Yu et al., 2006). My findings indicate that increased Six1 expression might also support intestinal tumor progression.

TAX1BP3 represents a PDZ domain containing protein. Most PDZ domain proteins act as protein scaffolds that interact with multiple proteins. PDZ domain proteins often contain multiple PDZ domains as well as other protein domains. TAX1BP3, however, is composed almost entirely of just one PDZ domain. Consequently, TAX1BP3 might acts as an inhibitor (Alewine et al., 2006). Interestingly, TAX1BP3 was shown to form a complex with β-catenin and to negatively regulate WNT signaling in colon cancer cells (Kanamori et al., 2003).

The extracellular ligand FGF9 has been shown to regulate the process of intestinal development during mouse embryogenesis. Further roles of FGF9 in the process of intestinal development and tumorigenesis are described below (see section 4.2 – 4.4).

Taken together, many of the genes identified by the loss-of-function screen can be linked, directly or indirectly, to processes known to affect tumor progression. My results indicate that these genes may have specific roles in molecular pathways promoting intestinal tumor progression. To establish the significance of these genes it would be important to characterize their expression pattern along the crypt-villus axis in the untransformed intestinal epithelium, as well as their expression in the different stages of intestinal tumors from benign adenomas, to metastatic carcinoma. Finally, loss- and gain-of-function studies using the intestinal organotypic culture system as well as conditional mouse models would provide essential information about the function of these genes in intestinal tumor progression.

4.2 FGF Signaling in Tumorigenesis

The identification of FGF9 in the screen provided evidence for an important role of FGF signals in the control of intestinal cell morphology and motility. I therefore initiated in-depth studies of FGF signaling in intestinal biology. Here, I first give an overview on previously identified functions for FGF signals in tumorigenesis.

It is well established that FGF signals control cell proliferation, survival, and migration of cells in the developing embryo. Due to their ability to induce cell motility and proliferation, which are also important in the context of tumorigenesis, cancer cells often engage FGF signals in a non-physiological manner. Several studies have identified different types of genetic mutations in genes of the FGF family, supporting an oncogenic role for FGF signaling molecules. Among these alterations are gene amplifications, activating mutations, chromosomal translocations, single nucleotide polymorphisms and aberrant splicing at the post-transcriptional level (as reviewed by Turner and Grose, 2010). Importantly, components of the FGF signaling pathway have been determined to be the most frequently mutated coding regions in a screen for non-synonymous somatic mutations in the human kinome (representing 518 protein kinases) of 210 diverse human cancers (Greenman et al., 2007).

In particular, bladder cancer has been strongly associated with FGF receptor mutations. Approximately 50% of bladder carcinomas carry mostly activating somatic mutations in the *FGFR3* coding region (Cappellen et al., 1999). In addition, *FGFR3* activating mutations are also found in other cancer types such as cervical cancers, multiple myeloma, prostate

cancer, and spermatocytic seminomas. *FGFR2* activating-mutations have been identified in a significant proportion of endometrial carcinomas. Intriguingly, *FGFR3* and *HRAS* mutations in bladder cancer as well as *FGFR2* and *KRAS* mutations in endometrial cancer are mutually exclusive (Jebar et al., 2005; Byron et al., 2008). These observations substantiate an epistatic relationship between FGF receptor and RAS-MAP kinase signaling in these tumor entities. Furthermore, gene amplifications of individual FGF receptors have been detected in several cancer types including gastric, breast and ovarian carcinoma.

Several mouse models have demonstrated that ectopic overexpression of FGF ligands also contributes to cancer. Such tumor models include ectopic FGF ligand expression in both epithelial cells and stromal fibroblast, generating either an autocrine or paracrine stimulation of cancer cells (as reviewed by Turner and Grose, 2010). Moreover, several human cancer types display ligand dependent activation of the FGF pathway. For instance, the expression of *FGF1*, *FGF2,* and *FGF7* is typically upregulated in the stroma of breast and prostate cancer patients as compared to the stroma of untransformed tissue samples (Finak et al., 2008).

Deregulation of FGF receptor isoforms and other FGF pathway components can lead to oncogenic signals that promote intestinal tumorigenesis. For instance, the FGF signal co-activator FGF-BP1 (FGF Binding Protein) was shown to be upregulated in human colorectal adenoma samples and in adenomas from Apc^{Min} mice (Tassi et al., 2006). Moreover, it has been demonstrated that the distinct splice variant *FGFR3-IIIc* mediates colorectal cancer growth and migration. In particular, *FGFR3-IIIc* interference in colon carcinoma cells was shown to inhibit cell growth and migration, and to attenuate tumor growth in SCID mouse xenograft models (Sonvilla et al., 2010). Deregulation of FGF ligands has also previously been found in colon cancer. FGF18 for instance, has been identified to promote intestinal tumor progression by stimulating both tumor cell proliferation, as well as migration of fibroblasts localized in the associated tumor stroma (Sonvilla et al., 2008). In addition, overexpression of *FGF7* has been detected in intestinal tumor cells (Watanabe et al., 2000).

The data presented in this thesis corroborates roles for FGF signals in colon tumor cells, and adds FGF9 to the shortlist of FGF ligands that may have oncogenic roles in colon cancer. I have shown that inhibition of FGF receptor signals abrogated cell motility and induced E-cadherin mediated cell adhesion in colon tumor cells, resulting in an epithelialized

phenotype. A similar, albeit not as complete, phenotype was induced by the knockdown of FGF9 in the same cells. Loss of epithelial characteristics and acquisition of a migratory phenotype is strongly associated with invasive tumor progression and metastasis (as reviewed by Yang and Weinberg, 2008). Consequently, my findings indicate that FGF signals may contribute to colon cancer progression, and that FGF9 is among the FGFs involved in the process. In agreement, I observed upregulated and delocalized expression of *FGF9* in human colon cancer, which may, in combination with other signals, influence intestinal cell morphology and motility. Furthermore, high expression of *FGF9* or *FGFR3* was present in distinct subgroups of human colon carcinomas (Fritzmann et al., 2009). In this cohort of human colon cancer patients we indentified a significantly shorter survival rate for patients with high *FGF9* expression as compared to patients with low expression of *FGF9*. Taken together, these data suggests an important and as yet unknown function for FGF9 induced signals in the contribution of intestinal tumor progression.

Previously, a genomic region on chromosome 13 encompassing the *FGF9* gene has been shown to be a common area of loss-of-heterozygosity (LOH) in colon carcinoma (Sivarajasingham et al., 2003). My data are not in agreement with this model, in which loss of *FGF9* would lead to a selective advantage in intestinal tumor cells. I therefore propose that the frequent loss of this part of chromosome 13 in colon carcinoma is due to genes other than FGF9. Importantly, the chromosomal region identified in the study also contains the tumor suppressor LATS2, whose loss may be oncogenic, and provide the tumor cells with the observed growth advantage.

4.2.1 The Relationship Between FGF and MAP Kinase Signaling

Intestinal tumorigenesis involves a well-defined sequence of histological stages, ranging from aberrant crypt proliferation or hyperplasia to benign adenomas, to locally circumscribed carcinoma, and finally to metastatic carcinoma; corresponding to the stepwise progression of this disease (Fearon and Vogelstein, 1990). This multi-step process may take several years to decades to progress, while the sequential stages of the malignancy are characterized by the occurrence of distinct somatic mutations in oncogenes and tumor suppressor genes (Fearon and Vogelstein 1990). Activation of the Wnt pathway is an early event in this cascade. Accordingly, activating mutations in the Wnt pathway are generally found in colorectal tumors, and are essential for tumor initiation. Importantly, there is

evidence that other colon cancer-associated oncogenes do not transform the intestinal epithelium in the absence of mutations in the Wnt pathway. Consequently, mutations in the Wnt pathway are considered as the "gatekeeper" mutations for oncogenic transformation of the intestine (as reviewed by Kinzler and Vogelstein, 1996). WNT hyperactivation is often followed by mutational activation of *KRAS or BRAF*, which typically stimulates the MAP kinase signaling pathway. Hyperactive MAP kinase signals in colon cancer can also be induced by oncogenic mutations in genes coding for RTKs including *EGFR* or *c-MET*, which funnel into the RAS signaling cascade (Birchmeier et al., 2003). Depending on the cellular context, FGF signals can stimulate the RAS-MAPK signaling pathway (Turner and Grose, 2010). My analysis of signaling events downstream of FGF receptor, using phosphorylation studies and expression profiling, identified an epistatic relationship between FGF and MAP kinase signals in colon cancer cells. These data suggest that FGF signals may promote colon cancer progression through MAP kinase activation.

Interestingly, I found that changes to FGF signaling can modulate the activity of the MAPK pathway in SW480 colon tumor cells, which contain an oncogenic *KRAS* mutation. This suggests that FGF receptor signals can modulate the MAP kinase signaling even in the presence of oncogenic mutations in the downstream pathway. My experiments showed that in SW480 cells, inactivation of FGF receptors leads to a reduction of ERK1/2 activity by approximately 30%. In this context, the remaining 70% activity of the MAP kinase pathway may be due to the ligand-dependent activity of other receptor tyrosine kinases, or may be due to the oncogenic KRAS mutation in the absence of upstream stimuli. Further experiments using colon cancer cell lines that do not contain mutations in the KRAS/BRAF functional cluster would be required to investigate the exact functional relationship between FGF receptors, KRAS/BRAF mutations and MAP kinase activity.

4.2.2 Interaction of FGF Signaling with other Pathways

FGF signals activate various downstream signal transduction pathways, depending on the specific cellular context (Turner and Grose, 2010). In human colon cancer cells, I verified an epistatic relationship between FGF and MAP kinase signals. Several studies have demonstrated that the MAP kinase-signaling cascade activates the transcription factors SNAI1 and SNAI2 as reviewed in (Thiery, 2002). These transcriptional repressors emerged as key factors that downregulate the cell adhesion molecule E-cadherin and thereby promote

EMT during multiple processes during embryonic development and malignant tumor progression (as reviewed by Peinado et al., 2007). Via gene expression analysis of treated SW480 cells I found that FGF signaling weakly upregulates the expression of the E-cadherin transcriptional repressor SNAI2 (data not shown). SNAI2 could thus bridge the functional cascade downstream of FGF-MAPK and upstream of the observed regulation of E-cadherin. Since I observed only a weak regulation of SNAI2, I suggest that other mechanisms likely contribute to the overall regulation of E-cadherin observed.

FGF signals have previously been shown to molecularly interact with the WNT signaling pathway in the control of cell morphology and migration of cells in the primitive streak during mouse gastrulation (Ciruna and Rossant, 2001). The authors demonstrated that FGF induced downregulation of E-cadherin modulates the cytosolic level of β-catenin. This course of events generates a molecular link between FGF and WNT signals at the primitive streak. In contrast, I did not detect an FGF signal-induced modulation of WNT pathway activity in SW480 cells as determined in a TOPFlash reporter assay of FGF receptor inhibited compared to control SW480 cells (data not shown). Of note, SW480 cells carry a loss-of-function APC mutation, which leads to accumulation of β-catenin. Consequently, the WNT signaling pathway in SW480 cells is constitutively active and might, therefore, operate independently of additional interference such as FGF signals. In untransformed mouse intestinal epithelium, however, I established the FGF pathway as an essential signaling component in the intestine for the maintenance of canonical Wnt signals. Specifically, I observed immediate downregulation of direct Wnt target genes including Axin2 and Lgr5 upon FGF receptor inhibition. The molecular bridge between FGF and WNT signals in this context, however, remains to be determined. Further analysis using dominant active or inactive components of the WNT and MAP kinase pathways would be required to investigate the impact of FGF-induced MAP kinase signaling on WNT signaling in the intestinal epithelium.

4.2.3 FGF9 Signals might Promote Tumor Associated EMT

During intestinal tumor progression from adenoma to carcinoma, there is an increase in nuclear accumulation of β-catenin. While low-grade adenomas display small quantities of nuclear β-catenin in a few areas, nuclear β-catenin reaches a maximum in EMT-associated tumor cells located at the tumor stroma interface of invasive carcinomas (Fodde and

Brabletz, 2007). The invasive front of malignant colon cancer forms a distinct microenvironment. At the front, myofibroblasts interact with tumor cells by secreting growth factors and extracellular signaling molecules that locally promote cell proliferation and migration. For instance, TGF-β, Hepatocyte Growth Factor (HGF), and EGF have all been identified as secreted microenvironmental factors that can promote EMT at the tumor/host interface of invasive colon tumors (Brabletz et al., 2005). In the loss-of-function phenotypic screen I identified FGF9 to promote a mesenchymal morphology in human colon cancer cells, likely by stimulating MAP kinase signals. In agreement, RAS-dependent MAP kinase hyperactivation has been determined of crucial importance for EMT in tumor cells by both *in vitro* and *in vivo* studies (as reviewed by Thiery, 2003). Moreover, I observed interspersed FGF9-positive cells within the tumor stroma, and FGF9-positive cells were enriched at the interface between the tumor epithelium and stroma. Mesenchymal FGF9-positive cells within the tumor stroma could be either tumor- or stromal derived, as tumor cells at the invasion front preferentially undergo EMT and disseminate from the primary tumor as spindle shaped cells (Fodde and Brabletz, 2007). Further analysis of intestinal epithelial and stromal markers would be essential to define the origin of FGF9-positive cells at the invasion front. Taken together, the expression analyses in colon cancer sections, in combination with my functional data, suggest that FGF9 signals exert autocrine (within the tumor epithelium) and/or paracrine (from stromal to tumor cells) functions in the progression of colon cancer.

4.3 FGF Signals as Intestinal Stem Cell Promoting Signals

My study revealed novel important physiological roles for FGF9 signaling in the untransformed mouse intestinal epithelium. Previously, a number of studies already reported roles for FGF receptor signaling in the intestine. For example, a knockout study of the *Fgfr3* receptor has shown reduced numbers of intestinal crypts and stem cells, while Paneth cell specification and/or differentiation was perturbed (Vidrich et al., 2009). Several FGF ligands have also been identified as able to control intestinal tissue homeostasis in the mouse. For instance, *Fgf7*, which is expressed by mesenchymal cells juxtaposed to the intestinal epithelium, promotes proliferation of intestinal epithelial cells (Housley et al., 1994). In addition, expression of *Fgf1*, *Fgf2,* and *Fgf9* has been detected in the mouse intestinal epithelium (Vidrich et al., 2004). Furthermore, FGF9 was demonstrated to control

small intestinal elongation and proliferation of mesenchymal cells associated with the intestinal epithelium (Geske et al., 2008).

4.3.1 FGF9 as Pro-Proliferative Factor for Intestinal Stem Cells

I initially observed that stimulation of intestinal organoids with exogenous FGF9 dramatically increased the organoid sizes and multiplied the amount of crypt domains per intestinal organoid. Importantly, I found equal numbers of intestinal stem cells per crypt domain in FGF9 treated as compared to control organoids. Consequently, exogenous FGF9 treatment increased the absolute number of intestinal stem cells per organoid (as judged by the increase in numbers of crypts per organoid). The FGF9-induced expansion of the intestinal stem cell pool suggested an accelerated cell cycle division time for intestinal stem cells in such treated organoids. To determine this possibility, I monitored actively cycling intestinal stem cells by BrdU incorporation into *Olfm4* positive cell nuclei of intestinal organoids. Indeed, this investigation revealed a significantly increased amount of BrdU positive stem cell nuclei in exogenous FGF9 treated organoids as compared to controls. Taken together, these observations indicate that FGF9 signaling promotes the rate of intestinal stem cell proliferation and thereby regulates the number of stem cells in the intestinal epithelium.

Histological analysis of the untransformed mouse small intestinal epithelium identified Paneth cells as the source for endogenous FGF9 signals in the intestine. This cell type typically intermingles with intestinal stem cells at the crypt bottom in the untransformed small intestinal epithelium. Multiple extracellular factors generated by Paneth cells, including secreted WNT proteins and the Notch ligand Dll4 have been identified as essential niche signals for maintaining intestinal stem cells (Sato et al., 2010). Paneth cells are therefore considered to constitute important niche signals for stem cells in the small intestinal epithelium. The expression analyses of the untransformed intestinal tissue in combination with my functional data collectively indicate that FGF9 represents another important component of the intestinal stem cell niche supplied by Paneth cells. Additional experiments however would be necessary to substantiate the function of FGF9 as a *bona fide* niche component for intestinal stem cells. It has been demonstrated that stem cell/Paneth cell doublets exhibit a significantly increased efficiency in forming intestinal crypt organoids *in vitro* as compared to single sorted intestinal stem cells (Sato et al., 2010). Assuming that FGF9 signals provided by Paneth cells support the intestinal stem cell

function, exogenous FGF9 stimulation of single sorted intestinal stem cells should increase the efficiency of organotypic outgrowth. Additional niche signals, however might be fundamentally essential for the *in vitro* culture of intestinal stem cells. Consequently, combinatorial stimulation experiments of individual intestinal stem cells with FGF9, in the absence or presence of additional niche factors, might be necessary to determine the impact of exogenous FGF9 on the ability to culture intestinal stem cells.

As the above findings demonstrate, exogenous FGF9 stimulation of intestinal organoids results in rapid growth and acceleration of the intestinal stem cell cycling time. Surprisingly, however, the intestinal stem cell markers *Lgr5* and *Olfm4* were significantly decreased in FGF9 treated crypt organoids as compared to controls as judged by qRT-PCR. Histologically, I determined equal absolute numbers of *Olfm4* positive stem cells per crypt domain in FGF9 treated and control intestinal crypt organoids. In addition, I verified that FGF9-stimulated organoids are maintained even after long-term treatment and multiple passages. Accordingly, the stem cell pool in FGF9 treated organoids is preserved and functional. These observations suggest that the decrease of *Lgr5* and *Olfm4* gene expression is based on transcriptional alterations that occur in FGF9-stimulated intestinal stem cells. Indeed, when staining for *Olfm4* mRNA in sections of FGF9-treated and control organoids, the staining was weaker on the FGF-treated organoids. This again corroborates that the observed loss of stem cell markers is due to their downregulation on a transcriptional level. FGF signals regulate multiple pathways that affect the transcriptional regulation of several downstream target genes (as reviewed by Turner and Grose, 2010). Importantly, stem cell markers are known to be regulated by complex mechanisms that involve multiple pathways initiated by WNT and other signals (Vermeulen et al., 2010). Since the *Lgr5* and *Olfm4* markers have been isolated as marker genes only, and have not been assigned functions in stem cell maintenance, the functional significance of the downregulation of *Lgr5* and *Olfm4* is not known. Importantly, $Lgr5^{-/-}$ animals die before they reach adulthood (Morita et al., 2004), whereas *Olfm4* has not yet been genetically inactivated. Conditional mutagenesis could be used to inactivate these genes specifically in intestinal stem cells to study their functional significance.

4.3.2 FGF9 as an Endogenous Regulator of Stem Cell Function

The results regarding the effect of FGF9 stimulation in intestinal cells prompted the question for roles of the endogenous FGF9. This issue was addressed by two lines of experiments, using intestinal crypt organoids treated either with an FGF receptor inhibitor to target general FGF signals or using specific siRNAs against *Fgf9* and a candidate receptor, *Fgfr3*. FGF receptor inhibited organoids developed irregular crypt domains and disintegrated within days. In agreement, I detected that crypt lineages and regions, including stem cells, transiently amplifying cells, and Paneth cells, were strongly and significantly reduced in organoids blocked for FGF signals as compared to control organoids. These observations substantiated an important role for endogenous FGF signaling in maintaining intestinal stem cell function and tissue homeostasis. Consistent with the proposed function of FGF9 as an intestinal stem cell niche signal, I found that interference with *Fgf9* in intestinal crypt organoids significantly reduced expression of the intestinal stem cell marker *Lgr5.* In line, reseeded crypt bases were not able to reconstitute properly formed intestinal crypt organoids. These observations indicate that endogenous FGF9 signals are required for intestinal stem cell maintenance and/or proliferation. Further experiments would be necessary to distinguish between these two functions. In contrast to interfering with *Fgf9* gene expression, silencing of the high affinity FGF9 receptor *Fgfr3* in organoids had no significant effect on the *Lgr5* gene expression level. However, additional FGF receptors in the intestinal epithelium may act redundantly and thereby compensate for effects induced by *Fgfr3* knockdown. Alternatively, residual FGFR3 signals due to incomplete *Fgfr3* interference might be sufficient to promote stem cell maintenance in intestinal crypt organoids.

4.3.3 Role of FGF Signaling in Lineage Specification

In addition to the impact of FGF signals on intestinal stem cell maintenance, I found that FGF receptor inhibition as well as interference with either *Fgf9* or *Fgfr3* gene expression in organotypic culture of the mouse small intestinal epithelium resulted in a biased ratio between absorptive and secretory villus lineages. The imbalance in lineage specification towards the absorptive cell fate already became apparent one day after FGF receptor inhibition in organotypic subcultures of filtered (70µm) crypt bases. Importantly, size-controlled crypt bases are depleted for cells that previously had differentiated into either the absorptive or secretory lineage of the villus. The biased lineage specification in FGF

receptor-inhibited crypt bases, which leads to a depletion of all secretory lineages (goblet cells, enteroendocrine, and Paneth cells) resembles the *Math1* loss-of-function phenotype (van der Flier and Clevers, 2009; van Es et al., 2010). The basic helix-loop-helix transcription factor *Math1* is expressed in all intestinal secretory cell types as well as in their undifferentiated secretory progenitors (Gregorieff and Clevers, 2005). The intestine of *Math*$^{-/-}$ mutant mice is lined only by absorptive enterocytes (Shroyer et al., 2007). Consequently, expression of *Math1* promotes cellular differentiation of intestinal progenitors into the secretory lineage. I found *Math1*, immediately downregulated in filtered (70µm) crypt bases upon FGF receptor inhibition. These observations suggest that FGF signals impinge on intestinal lineage specification by transcriptionally regulating the cell fate determinant transcription factor *Math1.*

4.3.4 Interaction Between FGF and other Signaling Pathways in the Intestine

It is well established that both Wnt/β-catenin and Notch signals are essential for intestinal tissue homeostasis, while they have opposing roles in intestinal lineage specification via the transcription factor MATH1 (Pinto et al., 2003; Fre et al., 2005; van Es et al., 2005b; Shroyer et al., 2007). The direct Notch target gene *Hes-1* negatively regulates the transcription of *Math1* (Jensen et al., 2000). Notch activation therefore promotes the absorptive lineage in the intestinal epithelium. Activated WNT signaling, in contrast, was shown to promote *Math1*-positive precursors in the intestinal epithelium (Pinto et al., 2003). Accordingly, Wnt signals stimulate intestinal precursor cells to differentiate into the secretory lineage.

Thus, the lineage bias observed after inhibition of FGF signaling could result from both Notch pathway stimulation and/or WNT signaling inhibition. I therefore investigated a potential interaction between FGF and Notch signals in the intestinal epithelium. Here, I found that the key Notch target gene *Hes1* (Suzuki et al., 2005) was not deregulated after one day, and only mildly affected after two days, possibly due to the general reduction of the crypt domain upon FGF receptor inhibition. This indicates that the Notch pathway is not affected by FGF signals in the intestinal epithelium. In contrast, I observed an immediate downregulation of the direct Wnt target gene *Axin2* (Lustig et al., 2002) and *Lgr5* upon FGF receptor inhibition, suggesting that FGF signals are required for the maintenance of Wnt signals in the intestinal epithelium. Consistent with an interaction of FGF and WNT signals in the intestine it has been demonstrated that exogenous FGF9 stimulation of intestinal Caco-2

cells significantly increased the TOPFlash reporter activity, indicating enhanced activity of the WNT signaling pathway after FGF9 stimulation (Vidrich et al., 2009). Importantly, multiple studies highlight the significance of active WNT signals in the control of intestinal tissue homeostasis as reviewed in (van der Flier and Clevers, 2009). Taken together, these observations in combination with my functional data, suggest an interaction between FGF and Wnt signaling pathways that is able to affect intestinal tissue homeostasis and lineage specification.

4.4 An Integrated View of FGF Signals in the Intestine

Intestinal tissue homeostasis is ensured by multiple molecular pathways, which functionally interact. Signaling pathways that control intestinal tissue homeostasis are known to also be among the key players in intestinal tumor formation and progression. For instance, active Wnt signaling is essential for maintaining cell proliferation, stem cell function, and tissue homeostasis in the intestinal crypt. On the other hand, oncogenic activation of Wnt/β-catenin signals in intestinal stem cells initiates hyperproliferation and rapid formation of intestinal adenoma (Barker et al., 2009). Furthermore, active RAS-MAP kinase signaling controls proliferation of intestinal cells and thereby regulates intestinal tissue homeostasis (Aliaga et al., 1999). Physiological MAP kinase signals are confined to undifferentiated progenitors within the intestinal crypt (Aliaga et al., 1999). Oncogenic mutations of KRAS stimulate MAP kinase signals and markedly accelerate intestinal tumor growth (Fearon and Vogelstein, 1990; Birchmeier et al., 2003). It is well know that multiple RTKs funnel into the MAP kinase pathway. My observations suggest that FGF signals modulate the activity of WNT signals and the MAP kinase pathway in intestinal cells. In this regard, I found FGF9 to be a novel player that regulate intestinal tissue homeostasis by impinging on the proliferation rate of intestinal stem cells. On the other hand, I observed FGF9 treatment to promote phenotypic alterations towards a mesenchymal state in colon cancer cells, suggesting a role in intestinal tumor progression. Collectively, these findings imply that FGF9 can affect signaling axes that regulate both intestinal homeostasis and tumor progression. The question remains whether there is a molecular link between these functions.

How does the effect of FGF signaling on cell morphology and migration act together to impact intestinal stemness and tissue homeostasis in order to promote intestinal tumor progression? Recent models for cancer progression imply that uncontrolled activation of

developmental signaling pathways and embryonic gene expression programs results in a coordinated loss of cell adhesion, gain of cell motility, and the acquisition of stem cell traits – finally leading to metastatic tumor cells (Mani et al., 2008). My results provide evidence that activated FGF9 signaling in colon tumors can promote all of these pro-metastatic traits. Based on my functional analysis of the role of FGF9 signals in the untransformed intestine it seems plausible that FGF signals could regulate the tumor stem cell pool in colon carcinoma, and, at the same time, impinge on the phenotype of tumor cells by inducing mesenchymal traits, such as low cell adhesion and motility. Importantly, the number of tumor initiating cells correlates with the disease progression and clinical outcome of colon cancer (Ricci-Vitiani et al., 2007), and the grade of tumor cell differentiation at the invasive front likewise correlates with patient survival (Brabletz et al., 2002).

FGF signals, therefore, represent a prime candidate signaling pathway that, when overexpressed, could result in the formation of migrating tumor stem cells (Brabletz et al., 2005). Moreover these effects may be generated by FGF-mediated regulation of the WNT and the MAP kinase pathways.

4.5 FGFR inhibitors as potential drugs

In order to improve the medical treatment of colon cancer patients, various therapeutical reagents that block key cellular signal transducers of the malignancy have been developed. Typically, monoclonal antibodies (mAB) as well as small molecule inhibitors are used to interfere with factors that are over-represented in tumor cells and/or within the tumor microenvironment. Transmembrane receptors constitute promising therapeutic targets due to their accessibility at the cell surface. For instance, the epidermal growth factor receptor (EGFR) and vascular endothelial growth factor (VEGF), which have both been shown to promote colon cancer progression are currently used in individual cases of CRC as therapeutic targets (as reviewed by Winder and Lenz, 2010). My results indicate that FGF9-induced signaling may function as another signaling axis to promote intestinal tumor progression. At present, several pharmaceutical companies are developing highly potent reagents that interfere with FGF signaling components. Most agents are small molecule inhibitors, but neutralizing antibodies are also under investigation (Turner and Grose, 2010). Therapeutic targeting of FGF signaling components might support future colon cancer treatment for selected patients with elevated levels of FGF signaling.

5 Abbreviations and Definitions

5.1 Abbreviations

aa	amino acid
AP	alkaline phospatase
APC	adenomatous polyposis coli
B6	C57BL/6J
°C	degree Celsius
CBC	crypt base columnar
cDNA	complementary DNA
Co	colon
CRC	colorectal cancer
d	day
DEPC	diethylpyrocarbonate
DIG	digoxigenin
DNA	deoxyribonucleic acid
dNTP	deoxyribonucleotide-triphosphate
DTT	dithiothreitol
EMT	epithelial to mesenchymal transition
FAP	familial adenomatous polyposis
Fig.	figure
GDP	guanosine diphosphost
GFP	green fluorescent protein
GTP	guanosine triphosphost
h	hour
H&E	Hematoxylin and Eosin
HNPCC	hereditary non-polyposis colorectal cancer
ID	identification
IVT	in-vitro transcription
l	liter
LOH	loss of heterozygosity
M	molarity
m	meter
Min	C57BL/6J $Apc^{Min/+}$
min	minute
MPIMG	Max Planck Institute for Molecular Genetics
mRNA	messenger RNA
PBS	Phosphate buffered saline
pH	the logarithm of the reciprocal of hydrogen-ion concentration in
rcf	relative centrifuge force
RNA	ribonucleic acid
RT	room temperature
SE	standard error
sec	second

SEM	standard error of the mean
SI	small intestine
ssDNA	salmon sperm DNA
Tab.	table
Taq	thermus aquaticus
Tris	tris(hydroxymethyl)aminomethane
tRNA	transfer RNA
UTP	uridine-triphosphate
WNT	Wg (wingless) and Int

5.2 Units

A	ampere
Bp	basepair
cm	centimeter
Da	Dalton
g	gram(s)
h	hour(s)
l	liter(s)
µ	micro
M	molar, (mol/l)
min	minute(s)
mm	millimeter(s)
Mol	ca. 6,023 x 1023 molecules
rpm	rounds pro Minute
sec	second(s)
U	units of enzyme activity
V	volt

5.3 Prefix

k	kilo 10^{3}
m	milli 10^{-3}
µ	micro 10^{-6}
n	nano 10^{-9}
p	pico 10^{-12}
f	femto 10^{-15}

5.4 Nucleotide

A	adenosine
C	cytosine
G	guanosine
T	thymidine

6 Material

6.1 Animals

CD-1 Charles River (http://www.criver.com)

6.2 Antibodies

6.2.1 For Western Blot

Antibody	Source	Dilution	Company
α-E-cadherin	mouse	1:5000	BD Biosciences
α-β-catenin	mouse	1:5000	BD Biosciences
α-phospho FGFR	rabbit	1:1000	Cell Signaling
α-Phospho ERK1/2	rabbit	1:1000	Cell Signaling
α-Phospho P85PI3K	rabbit	1:1000	Cell Signaling
α-Phospho-Akt (Thr308)	rabbit	1:1000	Cell Signaling
α-Phospho-Akt (Ser473)	rabbit	1:1000	Cell Signaling
α-Histone H3	rabbit	1:10000	Abcam
α-Rho (-A, -B, -C), clone 55	mouse	1:1000	Upstate
α-mouse-HRP		1:2000	Cell Signaling
α-rabbit-HRP		1:2000	Cell Signaling

6.2.1 For Immunostaining

Antibody	Source	Dilution	Company
α-E-cadherin	mouse	1:200	BD Biosciences
α-β-catenin	mouse	1:200	BD Biosciences
α-RhoA	mouse	1:100	Santa Cruz

α-γ-Tubulin	mouse	1:100	Santa Cruz
α-Phospho-Histone H3	mouse	1:100	Upstate
α-Lysozyme	rabbit	1:100	Invitrogen
α-ChromograninA	rabbit	1:100	Invitrogen
α-KI67	rabbit	1:100	Abcam
α-FGF9	rabbit	1:100	Abcam

6.3 Buffers and Solutions

If not specially listed below, buffers and solutions were prepared according to Sambrook et al., 2001; Molecular Cloning: A Laboratory Manual.

6.3.1 Amidoblack Staining to Measure the Protein Concentration

Solution	**Composition**
6 BSA standards: 0.0; 0.25; 0.5; 1.0; 2.0; 4.0 (mg/ml)	
Elution buffer (100ml)	50ml ethanol 10µl 0.5M EDTA 5ml 0.5M NaOH 45ml ddH_2O
Destain solution	90% methanol 2% acetic Acid ddH_2O
Staining solution	0.1% Amidoblack 45% methanol 10% acetic acid ddH_2O

6.3.2 Western Blot

Solution	Composition
Cell Lysis Buffer	1% SDS 10 mM Tris pH7,5 2mM EDTA Protease Inhibitor (Complete, Roche) Phosphatase Inhibitor (Phosphostop, Roche)
TBST	50 mM Tris-HCL pH 7,5 (with 37% HCL solution) 150 mM NaCl 0,1% Tween20
(for 10x stock: 60.57g/l Tris to pH7.5 with up to 1000g H2O)	37% HCl solution, 87.65g/l NaCl, 10g/l Tween20,
Transfer Buffer (semi-dry blot)	5,82 g/l Tris 2,9 g/l Glycine 3,75 ml/l 10% SDS 20% MetOH

6.3.3 *In situ* Hybridization

Solution	Composition
Blocking solution	1% Blocking Reagent 10% inactivated lamb-serum in TBSX
BCIP	50µg/µl BCIP in dimethylformamide
DEPC-H_2O	0.1% diethylpyrocarbonat in ddH_2O
Hybridization solution	25% 20x SSC pH 5.0 50% formamide 1% SDS 100µg/ml heparine 100µg/ml tRNA 100µg/ml ssDNA
NBT	75µg/µl NBT 70% dimethylformamide ddH_2O

NTMT	50mM MgCl2 100mM NaCl 100mM Tris pH 9,5 0,1% Tween 20
Staining solution	0,35% BCIP 0,45% NBT NTMT
TBS	81,1g NaCl 2g KCl 30,3g Tris-base add to 900 ml and dissolve use 37% HCl to adjust pH7,5 (approx. 30ml) add water to 1L
TBST	0,1% Tween-20 in TBS
TBSX	0,1% Triton X 100 in TBS
20x SSC	3M NaCl 0,3M Na-Citrat ddH_2O adjust with HCL/NaOH to pH5,0

6.3.4 Immunohistochemistry/fluorescence

Solution	Composition
1% H_2O_2 in H_2O	16,6 ml 30% H_2O_2 to 500 ml ddH_2O
0,01M Sodium Citrate Buffer pH6	2,94 g/l NaCitrate adjust pH with 1M citric acid

6.4 Enzymes

Enzymes were obtained from Promega, Roche, New England Biolabs, Invitrogen and Qiagen.

6.5 Kits

Kit	Company
Go taq qPCR Master Mix	Promega

ECL Western Blotting Detection reagents	GE Healthcare
Illumina TotalPrep RNA Amplification Kit	Ambion
ImmPress Reagent Anti Mouse Ig/ Anti Rabbit Ig	Vector Laboratories
RNeasy Mini Kit	Qiagen
RNeasy Micro Kit	Qiagen
Superscript II First Strand	Invitrogen

6.6 Nucleic Acid

6.6.1 qRT-PCR Primer

Primer	species	Sequence
Lgr5 fwd	mouse	CCACAGCAACAACATCAGGT
Lgr5 rev	mouse	AACAAATTGGATGGGGTTGT
Lgr5 fwd	human	ACCTGAAAGCCCTTCATTCA
Lgr5 rev	human	TGCTATGGTCCACACTCCAA
Olfm4 fwd	mouse	GCTGGAAGTGAAGGAGATGC
Olfm4 rev	mouse	AGGCACAAGGTCACTTTTGG
Olfm4 fwd	human	GATCAAAACACCCCTGTCGT
Olfm4 rev	human	CACAGACGGTTTGCTGATGT
Axin2 fwd	mouse	AGGAGCAGCTCAGCAAAAAG
Axin2 rev	mouse	GCTCAGTCGATCCTCTCCAC
Axin2 fwd	human	AGAGCAGCTCAGCAAAAAGG
Axin2 rev	human	CATCCTCCCAGATCTCCTCA
Ephb2 fwd	mouse	CCGCATCACCTGGATACTGT
Ephb2 rev	mouse	CCGGCTTTACCTCTTTCGAC
Ephb3 fwd	mouse	GGTTTGCATCCTTTGACCTG
Ephb3 rev	mouse	TGTCCTGGATACTGCAGAGG
Mmp7 fwd	mouse	CCCGGTACTGTGATGTACCC
Mmp7 rev	mouse	AATGGAGGACCCAGTGAGTG
Hes1 fwd	mouse	GAAGCACCTCCGGAACCT
Hes1 rev	mouse	GTCACCTCGTTCATGCACTC

Math1 fwd	mouse	CCAAGTGTGTCCAGCAGTGT
Math1 rev	mouse	TGCATTGGCAGTTGAGTTTC
Ifabp fwd	mouse	TTGCTGTCCGAGAGGTTTCT
Ifabp rev	mouse	GCTTTGACAAGGCTGGAGAC
Muc2 fwd	mouse	TACATGGCAAAAGTCCCACA
Muc2 rev	mouse	CAGACCAGAGTCCCTTGCTC
Ngn3 fwd	mouse	CCCCAGAGACACAACAACCT
Ngn3 rev	mouse	AGTCACCCACTTCTGCTTCG
Fgf9 fwd	mouse	TCACCTCAGCTCCACTGTTG
Fgf9 rev	mouse	CCTCTCTCCCCTGCTTTTGT
Fgf9 fwd	human	GGGGAGCTGTATGGATCAGA
Fgf9 rev	human	GTGAATTTCTGGTGCCGTTT
Fgfr1 fwd	mouse	CAGTGCCCTCTCAGAGACCT
Fgfr1 rev	mouse	GTACTGGTCCAGCGGTATGG
Fgfr2 fwd	mouse	GCATGCTGTACCCTCACAGA
Fgfr2 rev	mouse	GGCTGGGTGAGATCCAAGTA
Fgfr3 fwd	mouse	GGCTGAAGAATGGCAAAGAA
Fgfr3 rev	mouse	TCGGAGGGTACCACACTTTC
Fgfr4 fwd	mouse	TGGAAGCTCTGGACAAGGTC
Fgfr4 rev	mouse	AAAACCGAGTCACTGGAGGA
GFP fwd	jellyfish	CAAAGACCCCAACGAGAAGCGC
GFP rev	jellyfish	CGGCGGCGGTCACGAACT
Pmm2 fwd	mouse	AGGGAAAGGCCTCACGTTCT
Pmm2 rev	mouse	AATACCGCTTATCCCATCCTTCA
GAPDH fwd	mouse/human	TCAAGAAGGTGGTGAAGCAG
GAPDH rev	mouse/human	ACCACCCTGTTGCTGTAGCC

6.6.2 siRNAs

6.6.2.1 Human esiRNAs for Gene Knock-down in SW480 Cells

The esiRNAs for the loss of function screen in SW480 cells were generated and provided from the laboratory of Frank Buchholz, Max Planck Institute of Molecular Cell Biology and Genetics, Dresden. A list of ensembl IDs of genes targeted by esiRNAs is attached in the appendix (section 8.1).

6.6.2.2 Accell siRNAs for Gene Knock-down in Intestinal Crypt Organoids

siRNA	Target Gene	Species	Company
Accell siRNA Smartpools	Gapdh	mouse	Dharmacon
Accell siRNA Smartpools	Gfp	jellyfish	Dharmacon
Accell siRNA Smartpools	Fgf9	mouse	Dharmacon
Accell siRNA Smartpools	Fgfr3	mouse	Dharmacon

6.7 Tissue/Organoid Culture

6.7.1 Cell Lines

Cell line	Tissue Source	Tumor Site	Reference
CACO-2	Colon	Primary	Fogh et al., 1977
HT29	Colon	Primary	Fogh & Trempe et al., 1975
SW480	Colon	Primary	Leibovitz et al., 1976
SW620	Colon	Lymph node	Leibovitz et al., 1976

6.7.2 Media

Medium	Composition (Company)
Cell Culture Medium	DMEM (Lonza) 10% FCS (Gibco) 1% glutamine (Lonza) 50U/ml penicillin (Lonza) 50U/ml streptomycin (Lonza)
Crypt Culture Medium	Advanced DMEM (AdD; Invitrogen) (¾:1) F12 (Invitrogen)(¼:1) GlutaMax (Invitrogen) 1:100 Hepes (Sigma, final 10 mM) 1:100 Penicillin/Streptomycin (Invitrogen) 1:100 N2 supplement (Invitrogen) 1:100 B27 supplement, retinoic acid free (Invitrogen) 1:50 Mouse recombinant EGF (Invitrogen, final 50 ng/ml) 1000x Mouse recombinant noggin (Peprotech, final 100 ng/ml) 1000x Human recombinant R-spondin1 (R&D, final 500ng/ml) 1000x N-Acetylcysteine (Sigma, final 1uM) 1000x

Freezing Medium	DMEM (Lonza) 10% FCS (Gibco) 10% DMSO (Sigma)
Trypsin-EDTA	0,5g/l Trypsin (Lonza) 0,2g/l EDTA (Lonza)

6.7.3 Growth Factors

6.7.1 For Western Blot

Growth Factor	Species	Solvent	Final conc.	Company
EGF	mouse	H_2O	50ng/ml	Peprotec
FGF9	human	PBS	100ng/ml	R&D systems
Noggin	mouse	H_2O	100ng/ml	Peprotec
R-Spondin	mouse	PBS	500ng/ml	R&D systems

6.7.2 Inhibitor

Small Chemical Compound	Inhibitor of	Solvent	Final conc.	Company
AKT Inhibitor	AKT	DMSO	30µM	Calbiochem
LY294002	PI3K	DMSO	20µM	Calbiochem
PD173074	FGFR	DMSO	65µM	Calbiochem
SP600125	JNK	DMSO	20µM	Calbiochem
SU5402	FGFR	DMSO	42µM	Calbiochem
U0126	MAPK	DMSO	10µM	Calbiochem

6.7.3 Transfection Reagents

Reagent	Company
Lipofectamine 2000	Invitrogen
Oligofectamine	Invitrogen

6.7.4 Consumables and Materials

Reagent/Material	Company
Calibrated Pipets 50µl	Drummond Scientific Company
Cell Strainer (40µm)	BD Biosciences
Cell Strainer (70µm)	BD Biosciences
DMSO	Sigma
PBS	Lonza

7 Methods

7.1 Molecular Biology

All standard DNA manipulation techniques were performed as described in Sambrook et al., 2001; Molecular Cloning: A Laboratory Manual.

7.1.1 Nucleic Acid

7.1.1.1 RNA Isolation (Trizol Combined with Mini/Micro RNeasy Columns; Invitrogen)

- Disintegrate cells/tissue/organoids in an appropriate volume of Trizol (typically 0,5-1 ml).
- Add 0.2 ml of chloroform per 1.0 ml of Trizol Reagent and vortex tube for 15 seconds.
- Centrifuge at 12000g, 4°C for 10 minutes.
- Transfer upper aqueous phase to a new tube and measure the volume (typically 2-3x of the chloroform volume).
- Add 1 volume of 70% EtOH to the aqueous phase and mix by pipetting. Do not centrifuge.
- Pipette whole volume into an RNeasy mini column (Qiagen) and centrifuge for 15 seconds at 8000g. Discard the flow- through.
- Pipet 350 µl buffer RW1 into the RNeasy mini column, and centrifuge for 15 seconds at 8000g. Discard the flow-through.
- Prepare DNase I by adding 10 µl DNase I stock solution to 70 µl RDD buffer. Mix by gently inverting the tube.
- DNase I is especially sensitive to physical denaturation. Mixing should only be carried out by gently inverting the tube. Do not vortex.
- Pipet the DNase I mix (80 µl) onto the RNeasy silica-gel membrane. Incubate at room temperature for 15 minutes.
- Pipet 350 µl buffer RW1 into the RNeasy mini column, and centrifuge for 15 seconds at 8000g. Discard the flow-through.

- Transfer the RNeasy column into a new 2 ml collection tube. Pipet 500 µl buffer RPE (supplemented with EtOH) onto the RNeasy column. Close the tube gently, and centrifuge for 15 seconds at 8000g. Discard the flow-through.
- Add another 500 µl buffer RPE (supplemented with EtOH) (500 µl 80% EtOH for micro column) to the RNeasy column. Close the tube gently, and centrifuge for 2 minutes at 8000g. Discard the flow-through.
- Place the RNeasy column in a new 2 ml collection tube. Centrifuge in a microcentrifuge at full speed for 1 minutes (5 minutes for micro column).
- Transfer the RNeasy column to a new 1.5 ml collection tube. Pipet 30 µl nuclease free water (15 µl for micro column; pre-warm water to 50-65°C to increase yield) onto the RNeasy silica-gel membrane. Close the tube gently, and incubate 1minute at RT.
- Centrifuge for 2 minutes at full speed to elute.

7.1.1.2 First-Strand complementary DNA Synthesis

The first-strand complementary DNA (cDNA) is synthesized from a mature mRNA template in a reaction catalyzed by the Reverse Transcriptase enzyme. All first-strand cDNA syntheses were performed using the SuperScript II Reverse Transcriptase (Invitrogen) and random-hexamer primer according to manufacture's instructions.

7.1.1.3 Gene Expression Analysis (qRT-PCR)

To detect and quantify the expression level of individual genes of interest the qRT-PCR approach was employed using the Step One Plus detection system and SYBR green. For all qRT-PCR analyses independent biological triplicates were applied. Data was analyzed with Step One Software v2.1 (Applied Biosystems) using the CT (ΔΔCT) method. The gene of interest expression level was normalized to *Pmm2* (for crypt organoids) or *GAPDH* (for human cell lines) as a (housekeeping) reference gene.

Reaction	**Composition**	
qRT-PCR (20 µl)	10 µl	Go taq qPCR Master Mix (Promega)
	2 µl	Primer Mix (5µM each)
	x µl	cDNA (template DNA)
	x µl	H_20 (fill up to 20 µl)

7.1.1.4 Gene Expression Profiling (Illumina Microarrays)

To analysis the transcriptome of specifically treated SW480 cells, Illumina whole-genome expression arrays were employed. For gene expression profiling, three independent replicate profiles of SW480 cells of each treatment were prepared. RNA isolation from SW480 cells was performed using Mini RNeasy columns (Qiagen) as described above. RNA was labeled using the Illumina TotalPrep RNA Amplification Kit (Ambion) and probes were hybridized to Illumina "Sentrix BeadChip Array for gene Expression HumanRef-8 V2" microarrays, according to manufacturer's instructions. Expression data was processed using Bead Studio GX software (Illumina), using the quantile normalization method, and background subtraction. Absent and marginally expressed genes were removed for analysis. Deregulated genes were selected by more than 1,3-fold change in expression with a P-value <0.05 in an unpaired Welch t-test, without multiple testing correction.

7.1.2 Protein Biochemistry

7.1.2.1 Quantification of the Protein Concentration (Amidoblack Staining)

Amidoblack dye is used to stain and quantify for total protein on transferred membrane blots. The staining protocol is specified stepwise in the following:

- Spot 2ul of the standard solutions on a nitrocellulose membrane.
- Spot 2ul of sample protein solution on the same nitrocellulose membrane.
- Rinse membrane 2min in staining solution (solution can be reused several times).
- Rinse membrane 2-5x in destain solution, till membrane is white again.
- Cut out the black protein spots from the membrane as close as possible to the spot.
- Transfer the spots with forceps to 1.5ml tube containing 200ul elution buffer.
- Transfer tubes to a thermal shaker at 1000rpm for 10 minutes at 50C.
- Measure Absorption at 630nm (600nm works as well).
- Recommendation: use Excel to calculate standard curve from BSA standards, let Excel calculate formula, use the formula to determine the protein content of your samples.

7.1.2.2 Western Blot

Proteins were separated by SDS-PAGE using prefabricated Minigels from Invitrogen. For Western blotting, proteins were transferred to a nitrocellulose membrane after SDS-PAGE

using the I-Blot system from Invitrogen. ECL staining (Amersham) was used to detect and quantify secondary antibody signals. For the assessment of FGF signaling in SW480, cells were transfected with a plasmid coding for a FGFR1 eukaryotic expression construct, since the pFGFR antibody employed cannot detect endogenous receptor activity, according to the manufacture. The Western blot protocol is specified stepwise below:

Cell Lysis

- Wash cells 1x cold PBS.
- Lyse immediately in cold Lysis buffer.
- Pass protein lysates 3-4 times trough a syringe to shear DNA.
- Heat lysates immediately to 95°C, 5minutes.
- Vortex 5 sec. and centrifuge at full speed for 30 sec.
- Quantify (using Amidoblack staining).
- Optional: freeze at -80°C for storage.
- Load 10µg Protein per lane (protein lyses containing loading buffer (4X) and Reducing Agent (10x))on a Minigel (Invitrogen).

Transfer

Protein transfer to a nitrocellulose membrane was performed using the I-blot system (Invitrogen) according to manufactures instructions.

Alternative: Protein transfer to a membrane was performed using a semi dry blotter as described in the following:

- Equilibrate gel 15min. in Transfer Buffer (5.82g/l Tris, 2.9g/l Glycine, 3.75ml/l 10%SDS, 20% MetOH).
- Equilibrate 12 x Whatman, membrane (Pre-wet Nitrocellulose in H2O, PVDF in MetOH) in Transfer Buffer for some sec.
- Use semi-dry blotter: (Bottom-up: Electrode/6 x Whatman/Membrane/Gel/6x Whatman).
- Transfer at 2.5mA/cm2, 1.5h.

Detection

- Rinse membrane in 1 x TBST (50mM Tris-HCl pH 7,5; 150mM NaCl; 0,1% Tween20).
- Block 1h 5% milk in TBST.
- Wash 3x 5min TBST.
- 1st AB in 5%BSA in TBST at 4°C O/N (1:500-1000, if no other concentration was established for the AB).
- Wash 3x 10min TBST.
- 2nd AB in 5%milk in TBST RT 1h (cell signal α-rabbit 1:2000, others 1:5000).
- Wash 3x 10min TBST.
- Rinse 2x with TBS (=TBST without Tween20); (alternatively with H_2O).
- For detection, use standard Amersham ECL kit first; if no signal appears with 10min exposure, use ECL advanced kit.

Quantification

- Western blot signals were quantified using the ImageJ software (http://rsbweb.nih.gov/ij).

7.1.2.3 Rho Activity Assay

Rho GTPases operate by alternating between an active, GTP-bound state and an inactive, GDP-bound state. The Rho activation assay uses the Rho binding domain (RBD) of the Rho effector protein, Rhotekin, which specifically binds to the active GTP-bound form. The Rhotekin-RBD protein is linked to a GST fusion protein, which allows to "pull-down" the Rhotekin-RBD/Rho-GTP complex. The assay therefore quantifies Rho activation in cells. The amount of activated Rho is determined by a western blot using a Rho specific antibody. For the Rho activity assay, SW480 cells were seeded at $5x10^4$ cells /cm^2. 24h after seeding cells were serum-starved for 24h in the presence of the individual inhibitors or solvent-control (DMSO) respectively. Rho activity was assessed 5 minutes after re-stimulation with 10% serum, using the Rho activation assay kit (Millipore/Upstate; anti-RhoA,B,C antibody) according to manufacturer's instructions.

7.2 Cell Culture

Within the scope of this thesis SW480, SW620, HT29 and Caco2 colon cancer cells have been used for eukaryotic cell culture experiments. These cell lines grow as adherent monolayers on the bottom of the plastic cell culture dishes and were cultured at 37°C in a 7,5% CO2 humidified atmosphere with complete medium. Complete medium consisted of Dulbecco's Modified Eagle Medium (DMEM), containing 1% Penicillin (250 U/ml) and Streptomycin (250 U/ml), and 10% fetal bovine serum (FBS). At > 80% confluence cells were typically passaged at a dilution of 1:5 using Trypsin-EDTA. Before seeding the cell number was determined by a hemocytometer (Neubauer-Zählkammer; dilution factor 10^4).

7.2.1 Loss of function Study in SW480 Cells

For the loss of function screen in SW480 cells candidate genes were down regulated using the esiRNA technology in co-operation with the laboratory of Frank Buchholz, Max Planck Institute of Molecular Cell Biology and Genetics, Dresden. This RNA interference approach is based on the generation of siRNAs by digestion of long dsRNAs with recombinant Escherichia coli RNase III. The resulting endoribonuclease-prepared siRNAs (esiRNAs) were shown efficiently and specifically mediate RNAi in mammalian cells (Buchholz et al., 2006). SW480 cells were pre-plated at a density of 3 x 10^4 cells/cm2 on coverslips the day before transfection, and individual esiRNAs were transfected in 48-well plates using Oligofectamine (Invitrogen), according to manufacture's instructions and as described previously. Bright field and E-cadherin immunofluorescence images were recorded 72h after transfection, and judged independently of each other.

7.2.2 Small Molecule Inhibitor Treatment in Colon Cancer Cells

Distinct signaling pathways were blocked in colon cancer cells using small molecule inhibitors. The following inhibitors and final concentrations were employed: SU5402 (42µM), PD173074 (65µM), U0126 (10µM), SP600125 (20µM), Ly294002 (20µM) and AKT inhibitor (30µM). In all cases inhibitors were solved in DMSO. The inhibitors were exchanged daily at their individual final concentrations.

7.2.3 Immunofluorescence on Cells

Immunofluorescence uses the specificity of antibodies to their antigen to target a fluorescent dyes to specific proteins within a cell. This technique therefore allows visualizing the distribution of the target molecule through the sample. Cells were grown on coverslips and subsequently treated as specified in the following:

- Wash 2x with PBS.
- Fix with 4% paraformaldehyde (in PBS) for 15 minutes.
- Permeabalize with 0.5% Triton X100 (in PBS) for 5 minutes.
- Wash 2x with PBS.
- Block with 10% FBS (in DMEM) for 30 minutes.
- Apply 1. Antibody (dilution in 10% FBS in DMEM) for 1 hour.
- Wash 2x with PBS.
- Apply fluorescent dye conjugated 2. Antibody (dilution in 10% FBS in DMEM) for 1 hour.
- Wash 2x with PBS.
- Add DAPI (dilution in PBS) for 2 minutes.
- Stick the cover slip upside down in Immumount on a slide.

7.2.4 Scratch Wound Healing Assay in SW480 Cells

SW480 cells were plated at a density of 3 x 10^5 cells/cm2 onto glass slides. 24h after seeding cells were exposed to small molecule inhibitors and incubated for another 24h. The scratch was performed with a p200 pipette tip (48h after seeding). After scratch wounding the confluent monolayer, cells were further cultured in the presence of the inhibitor. Wound healing was evaluated 24h, 48h and 72h upon scratching the cell monolayer.

7.3 Histology on Tissue Sections

7.3.1 Fixation and Sectioning

7.3.1.1 Paraffin Sections

- Fix specimens in 4% paraformaldehyde at 4°C overnight and embed in paraffin according to standard protocols.

- Mount 4µm sections on Super Frost Plus slides.
- Dry slides on 37°C heating plate for at least two hours or over night, then put on 4°C.

7.3.1.2 Cryo Sections

- Fix specimens in 4% paraformaldehyde at 4°C overnight.
- Wash in PBS, 4°C.
- 5% Sucrose/PBS, 4°C for 1h.
- 10% Sucrose/PBS, 4°C for 3h.
- 20% Sucrose/PBS, 4°C O/N.
- Snap freeze in OCT compound using Isopentan and dry ice.
- Mount 6µm sections on Super Frost Plus slides.

7.3.2 Haematoxylin and Eosin Staining

Haematoxylin and eosin staining is widely used in histology, especially for pathology and histological diagnosis. Haematoxylin stains nucleic acids, so that predominantly the nuclei become blue-purple. Eosin stains proteins, thereby coloring mainly cytoplasm but also extra cellular regions in a bright pink.

The staining protocol was performed as follows:

- Prewarming of slides at 60°C for 10min.
- Dewaxing in 2 changes of xylene, 8min each.
- Rehydration in 2 changes of 100%, 95%, 85%, 70% ethanol, H_2O, 5min each.
- Haematoxylin stain for 5min, followed by washing in warm H_2O.
- Differentiation in 0.25% HCl in ethanol for 3s, followed by washing in H_2O.
- Eosin stain for 30s-2min, followed by short washing in H_2O.
- Rehydration by dipping in 90% ethanol, 2 changes of 100% ethanol for 5min each.

7.3.3 *In situ* Hybridization

With *in situ* hybridization it is possible to localize mRNAs in histological sections and thereby identify regions were specific gene expression takes place. RNA probes labeled with digoxigenin are in a first step hybridized to the corresponding mRNA. Digoxigenin can then by detected by specific antibodies.

7.3.3.1 *In situ* Hybridization using a DIG-ab Conjugated with Alkaline Phosphatase

The alkaline phosphatase activity is visualized by a color reaction. The 3 days *in situ* hybridization protocol was performed as follows:

Day1

- All solutions used during the first day were prepared with DEPC-H_2O.
- Prewarming of slides at 60°C for 10min.
- Dewaxing in 3 changes of xylene, 5min each.
- Rehydration in 2 changes of 100% for 5min each, 95%, 85%, 70%, 30% ethanol for 2min each, PBS for 5min each.
- Refixing in 4% paraformaldehyde for 15min, 2 changes of PBS for 5min each.
- Bleaching in 6% H_2O_2 in PBS for 15min, 3 change of PBS for 2min each.
- Digesting in 10µg/ml Proteinase K in PBS for 10min, stop with 0.2% Glycin in PBS for 2min, 2 changes of PBS for 2min each.
- Refixing in 4% paraformaldehyde for 10min, 3 changes of PBS for 2min each.
- 100mM Tris pH 7,5 for 2min, acetylation in 0.25% acetic anhydride in 100mM Tris pH 7,5 for 10min, 2 changes of 2x SSC pH 5 for 2min each.
- Dehydration in 30%, 70%, 85%, 95%, 100% ethanol for 2min each.
- Air-drying for 30min
- Hybridization with 200-800 ng/ml probe in hybridization solution, 200µl per slide covered with a hybri-slip, 63°C overnight.

Day 2

- Floating off hybri-slips in 5x SSC, 50% formamide at 60°C.
- 5x SSC, 50% formamide at 60°C for 5min.
- Washing in 2 changes of 2x SSC, 50% formamide at 60°C for 10min each with gentle rocking.
- Washing in 2 changes of 1x SSC at 60°C for 15min each with gentle rocking and 0.2x SSC at 60°C for 30min with gentle rocking.
- 2x changes of TBS for 5 min each.
- Blocking in blocking solution for 2h at 4°C, meanwhile antibody blocking 1:1000 anti-DIG-AP Fab in blocking solution for 2h rocking at 4°C, 20800 rcf at 4°C for 10min.
- Antibody binding with supernatant from antibody solution at 4°C overnight.

Day 3

- Washing in 6 changes of TBSX for 15min each with gentle rocking.
- 2x changes of NTMT for 10min each.
- 1x changes of NTMT plus 1mMLevamisole for 10min.
- Staining with 0.45% Nitrobluetetrazolium, 0.35% 5-Bromo-4-Chloro-3-indolylphosphat in NTMT.
- After a signal developed the reaction was stopped in PBS, counterstained with fast nuclear red, dehydrated and mounted with Entellan.

In situ Hybridization Using a DIG-ab Conjugated with Horse-Radish Peroxidase

Cryo-sections were hybridized at 500ng/ml for 48h as in (Gregorieff et al., 2005). Next, sections were washed in 0.2 x SSC for 1h at 65°C, and blocked in a buffer containing 0.1M Tris, pH7.5, 0.1M NaCl, and 0.5% blocking reagent (Roche). Sections were incubated with a-digoxigenin-POD Fab fragments (1:100, Roche) in blocking buffer, washed in a buffer containing 0.1M Tris pH7.5, 0.1M NaCl, and 0.05% Tween20, incubated with Biotinyl Tyramide (Perkin Elmer) for 7 minutes, washed again, and signals were detected using extravidine-Cy3 (1:100 in blocking buffer).

7.3.4 Immunohistochemistry on Tissue Sections

Paraffin sections

Deparaffinize and rehydrate

- 3x 5 min Xylene
- 2x 5 min 100% EtOH
- 3 min 96% EtOH
- 3 min 80% EtOH
- 3 min 70% EtOH
- 3-5 min H_2O

Cryo sections

Postfixation

- Warm at RT for 15 minutes.
- Postfix 3 minutes in cold MetOH (-20°C) on ice.
- 3x 3 minutes wash in PBS.

Paraffin sections & Cryo sections

Bleaching with hydrogen peroxide treatment to quench endogenous peroxidase activity

- Incubate slides for 10 min in 1% H_2O_2 in H_2O.
- Wash at least 3 times for 5 min in PBS.

Antigen retrieval

- Boil slides in 0,01M Citrat Buffer pH6 for 20 min in a beaker.
- Cool slowly down at RT (~35-40°C)
- Wash at least 3 times for 3 min in PBS.

Blocking

- Cover section with 1ml 1,5% BSA in PBS (sterile filtered through 0.45µm) and place in a humidity chamber and incubate at RT for 30 minutes.

Primary antibody incubation

- One slide: no AB (neg. control).
- Shake the slide with a flick of the wrist to remove the blocking solution.
- Wipe back and edges of the slide with a square of Whatman paper.
- Aspirate excess liquid from slide.
- Place slide on a flat surface and draw around section(s) with a glycerol pen (PAP-pen, Kisker- Biotech); this prevents solutions from running off the edges of the slide.
- Cover section with 200µl pre-diluted primary antibody solution (diluted in 1,5% BSA in PBS (sterile filtered through 0.45µm)) and incubate in a humidity chamber at 4°C O/N.
- Wash slides 3 times for 5 min in PBS under slightly moving.

Secondary antibody incubation

- Wipe back and edges of the slide with a square of Whatman paper.
- Cover sections with ImmPRESS anti-rabbit/mouse secondary antibody solution (VECTOR) and incubate at RT in humidity chamber for 60 min.
- Wash slides 3 times for 3 min in PBS under slightly moving.
- Remove excess of liquid.

Staining (using VECTOR NovaRED Substrate Kit for peroxidase)

- Prepare substrate solution in distilled H_20:

dest. H_20	5 ml	2.5 ml	1 ml	0.5 ml
Reagent 1	60 µl	30 µl	12 µl	6 µl
Reagent 2	40 µl	20 µl	8 µl	4 µl
Reagent 3	40 µl	20 µl	8 µl	4 µl
H_2O_2 sol.	40 µl	20 µl	8 µl	4 µl

- Wipe back and edges of the slide with a square of Whatman paper.
- Cover sections with substrate at RT.
- Incubate sections until suitable staining develops, generally 1-10 minutes. Longer incubations may increase sensitivity. Examine under binocular.
- Wash sections for 5 min with tap water.

Counterstain with hematoxylin (optional)

- Incubate slides for 5 sec. in hematoxylin.
- Wash for 5 min in tap water.
- Incubate in HCl-70% Ethanol (200 ml 70% Ethanol + 1.4 ml 37% HCl).
- Wash for 5 min in tap water.

Dehydration and mounting

- Dehydrate quickly (10 sec./step) through ethanol: 70%, 80%, 90%, 100%, 100%.
- 2x xylene.
- Wipe off excess xylene from edges of slide.
- Immediately add mounting medium (Entellan, Merck) and cover with coverslip.

7.3.5 Immunofluorescence on Tissue Sections

Paraffin sections

Deparaffinize and rehydrate

- 3x 5 min Xylene
- 2x 5 min 100% EtOH
- 3 min 96% EtOH
- 3 min 80% EtOH
- 3 min 70% EtOH
- 3-5 min H_2O

Cryo sections

Postfixation

- Warm at RT for 15 minutes.
- Postfix 3 minutes in cold MetOH (-20°C) on ice.
- 3x 3 minutes wash in PBS.

Paraffin sections & Cryo sections

Antigen retrieval

- Boil slides in 0,01M Citrat Buffer pH6 for 20 min in a beaker.
- Cool slowly down at RT (~35-40°C).
- Wash at least 3 times for 3 min in PBS.

Blocking

- Cover section with 1ml 1,5% BSA in PBS (sterile filtered through 0.45µm) and place in a humidity chamber and incubate at RT for 30 minutes.

Primary antibody incubation

- One slide: no AB (neg. control).
- Shake the slide with a flick of the wrist to remove the blocking solution.
- Wipe back and edges of the slide with a square of Whatman paper.
- Aspirate excess liquid from slide.
- Place slide on a flat surface and draw around section(s) with a glycerol pen (PAP-pen Kisker- Biotech); this prevents solutions from running off the edges of the slide.
- Cover section with 200µl pre-diluted primary ABsolution (diluted in 1,5% BSA in PBS (sterile filtered through 0.45µm)) and incubate in a humidity chamber at 4°C O/N.
- Wash slides for 5 min in PBS/DAPI (1µl DAPI (5mg/ml) in 200ml PBS).
- Wash slides 3 times for 5 min in PBS under slightly moving.

Secondary antibody incubation

- Wipe back and edges of the slide with a square of Whatman paper.
- Cover sections with fluorochrome-labeled secondary antibody in PBS and incubate at RT in humidity chamber for 60 min (in the dark).
- Wash slides 3 times for 3 min in PBS under slightly moving.
- Remove excess of liquid

Mounting

- Mount with Vectashield Mounting Medium (optional with DAPI).
- Seal off with metallic nail polish.
- Store in the dark.
- Take images the next day.

7.3.6 Combined Immunohistochemistry and *in situ* Hybridization

- Normal in situ protocol until day 2 antibody incubation.
- Combined Antibody incubation: 1. Antibody for immunohistochemistry plus Dig-Antibody binding with supernatant from antibody solution at 4°C overnight.

Day 3

- Washing in 6 changes of TBS for 5min each with gentle rocking.
- Cover sections with ImmPRESS anti-rabbit/mouse secondary antibody solution (VECTOR) and incubate at RT in humidity chamber for 60 min.
- Wash slides 3 times for 3 min in PBS under slightly moving.
- Remove excess of liquid.

Staining (using VECTOR NovaRED Substrate Kit for peroxidase)

- Prepare substrate solution in distilled H_20:

dest. H_20	5 ml	2.5 ml	1 ml	0.5 ml
Reagent 1	60 µl	30 µl	12 µl	6 µl
Reagent 2	40 µl	20 µl	8 µl	4 µl
Reagent 3	40 µl	20 µl	8 µl	4 µl
H_2O_2 sol.	40 µl	20 µl	8 µl	4 µl

- Wipe back and edges of the slide with a square of Whatman paper.
- Cover sections with substrate at RT.
- Incubate sections until suitable staining develops, generally 1-10 minutes. Longer incubations may increase sensitivity. Examine under binocular.
- Washing in 3 changes of TBSX for 15min each with gentle rocking.
- 2x changes of NTMT for 10min each.
- 1x changes of NTMT plus 1mM Levamisole for 10min.
- Staining with 0.45% Nitrobluetetrazolium, 0.35% 5-Bromo-4-Chloro-3-indolylphosphat in NTMT.

- After a signal developed (3-5h) the reaction was stopped in PBS, counterstained with fast nuclear red, dehydrated and mounted with Entellan.

7.4 Organoid Culture

Intestinal crypt organoids grow as 3D long-term culture in Matrigel (Growth factor reduced, Phenol red free Matrigel (BD)) and were maintained at 37°C in a 7,5% CO2 humidified atmosphere with crypt culture complete medium. Growth factors were added every other day and the entire medium was exchanged every 4 days. Every 7-14 days intestinal organoid culture need to be passaged. For passage, organoid were removed from the Matrigel and mechanically disintegrated into single crypt domains and transferred into fresh Matrigel. Passage was performed with a 1:5 split ratio. For all organoids experiments within the scope of this thesis the jejunum part of the small intestine of CD1 mice (aged 8-12 weeks) was used. Organoids were generated as described below:

7.4.1 Isolation, Embedding and Culture of Intestinal Crypts

Preparation:

- Place PBS, PBS 2mM EDTA, advanced DMEM (AdD; Invitrogen) on ice
- Thaw Matrigel on ice
  (All steps at 4°C, if possible)

7.4.1.1 Isolation of Intestinal Crypts

- Isolate small intestine (10-15 cm of Jejunum) and put in cold PBS
- Remove the intestinal contents (squeeze out on coated paper with forceps)
- Transfer the intestinal tube to a 10 cm dish with cold PBS, remove the attached fat with small scissors
- Flush the intestinal tube with cold PBS using a syringe
- Cut longitudinally with small scissors
- Wash the opened small intestine with cold PBS.
- Scrape off the villi using a glass slide (2x with gentle pressure)
- Wash the small intestine again and transfer it to a 50ml falcon tube with 20 ml cold PBS
- Vortex for 5 sec. and discard the supernatant

- Repeat washing approx. 10 times.
- Transfer the intestinal piece to a fresh 50ml falcon tube containing 30 ml 2mM EDTA in PBS and set it at a rotator machine in the fridge for 30min.
- Transfer the intestinal piece to a fresh 50ml falcon tube containing 20 ml PBS. Invert the Falcon tube 5 times.
- Transfer the intestinal piece to a fresh 50ml falcon tube containing 10 ml PBS. Shake 5 times and transfer the intestinal piece to a fresh 50ml falcon tube containing 10 ml PBS. Keep the supernatant (= supernatant 1)
- Repeat three more times (increase each time the shaking force) (=supernatant 2-4)
- Check each supernatant for size and number of crypts under the microscope (use therefore 10µl of the supernatant).
- Pool the crypts containing supernatants in a 50 ml Falcon tube and fill it up with AdD.
- Spin the crypt suspension at 300g 5min.
- Remove the supernatant and re-suspend the pellet in 10ml AdD, pipette the crypt suspension onto a cell strainer 70µM filters (BD) in a 50 ml Falcon tube.
- Check crypt number under the microscope (10µl).

7.4.1.2 Embedding of Intestinal Crypts for Organoid Culture

- Spin the desired amount of crypts at 300g 5min in 1,5ml Eppendorf tubes. Remove most of the supernatant and put the pellet on ice (30sec).
- Re-suspend the pellet with cold Matrigel at around 2 crypts/µl. (For 1 well of a 24 well plate around 100 crypts need to be diluted in a 50µl Matrigel drop).
- Seed 50µl of the Matrigel-crypt suspension on a well of a 24-well plate, and incubate it for 5-10min at 37°C until the Matrigel is well solidified.
- Add 500µl of Crypt culture medium (AdD plus EGF, Noggin and R-Spondin) to each well, and incubate at 37°C.
- Typically, crypts start to bud after 2-3 days in culture.

7.4.1.3 Passage of Intestinal Crypt Organoids

- Pick organoids from the Matrigel (individual organoids with a fire-polished glass capillary mouthpipette under the binocular; all organoids with p1000) and transfer them into PBS.
- Transfer organoids in a PBS drop (50-500µl) with the mouthpipette.
- Mechanically dissociate organoids with the mouthpipette under the binocular.
- Optional: transfer organoid pieces through a 70µM strainer (BD). Flow-through is enriched for crypt bases.
- Transfer organoid pieces/crypt bases into a 1,5ml Eppi tubes and spin at 300g 5min.
- Remove most of the supernatant and put the pellet on ice (30sec).
- Re-suspend the pellet with Matrigel at around 2 crypt-domains/µl. (For 1 well of a 24 well plate around 100 crypt domains need to be diluted in a 50µl Matrigel drop).
- Seed 50µl of the Matrigel-crypt suspension on a well of a 24-well plate, and incubate it for 5-10min at 37°C until the Matrigel is well solidified.
- Add 500µl of Crypt culture medium to each well, and incubate at 37°C.

7.4.2 Small Molecule Inhibitor Treatment of Crypt Organoids

Pathway inhibition was induced by administration of the small molecule inhibitor to the culture. Inhibitor was added (every other day) at a final concentration (see section 6.7.2), and samples were compared against solvent (DMSO) control.

7.4.3 Expression Regulation and Analysis in Crypt Organoid

The impact of distinct FGF signaling components on intestinal tissue homeostasis was analyzed by loss of function studies in crypt organoids using Accell siRNA Smartpools (Dharmacon), which are specifically modified for use without a transfection reagent and work at a higher concentration compared to conventional siRNA with minimal off target effects. Accell siRNA treatment of organoids was performed following manufacturer's instructions. Complete crypt culture media with siRNA was exchanged every three days. Treatment start was performed on full-grown organoids. After three days of siRNA treatment organoids were passaged with or without filtering. Sub-cultured organoids were progressively incubated with siRNAs. Organoids were recorded and/or harvested four or five days after passaging.

7.4.4 Fgf9 Ligand Stimulation of Crypt Organoids

FGF9 stimulation of crypt organoids was performed by administration of human recombinant FGF9 protein (R&D systems) to the culture. FGF9 protein was daily added at a final concentration of 100ng/ml. Samples were compared against solvent (PBS) control.

7.4.5 BrdU Labeling

Proliferating cells in living organoids were detected by exposing the culture was to the synthetic nucleoside Bromodeoxyuridine (BrdU), which is an analogue of thymidine. BrdU is incorporated into synthesizing DNA of proliferating cells (during the S phase of the cell cycle), substituting for thymidine during DNA replication. Antibodies specific for BrdU detect the incorporated synthetic nucleoside, thus indicating those cells that were actively replicating their DNA during BrdU administration. BrdU labeling of organoids was performed for 45 minutes before harvesting, using the BrdU Labeling and Detection Kit (Roche), according to manufacturer's instructions.

7.4.6 Crypt Organoid Histology

For histological approaches, crypt organoids were removed from the Matrigel, fixed, dehydrated, embedded in paraffin and sectioned for further analysis.

7.4.6.1 Fixation of Intestinal Crypt Organoids

- Use a fire-polished glass capillary mouthpipette to pick organoids from the matrigel (under binocular) and transfer them into a cell strainer 70 or 30µM filters (BD) dipped in PBS in a 6cm dish.
- Cell strainer (containing organoids) will be transferred to 4% paraformaldehyde in PBS solution. After 30´, cell strainer (containing organoids) will be transferred for 5 minutes to PBS. Quickly proceed to the next step (see below).

7.4.6.2 Dehydration of Intestinal Crypt Organoids

- Transfer cell strainer with organoids through ethanol series:

Solvent	Time	Remarks
• 70% EtOH	10’	
• 70% EtOH	O/N	
• 80% EtOH	10’	
• 90% EtOH	10’	
• 100% EtOH	10’	(can be stored in 100% EtOH at -20C°)
• 100% EtOH	10’	
• 100% Xylene	20’	
• 100% Xylene	20’	
• 100% Paraffin O/N	at 60°C	

7.4.6.3 Paraffin Embedding of Crypt Organoids

- Pipette organoids (using the binocular) into metal form filled with liquid paraffin.
- Let Paraffin solidify for 30 minutes at room temperature and, put on ice for another 30 minutes.
- Carefully remove metal form.
- Crypts are now embedded in paraffin block (can be stored at 4C°).

7.4.6.4 Microtome Sectioning of Embedded Organoids

- Mount 4µm sections on Super Frost Plus slides.
- Dry slides on 37°C heating plate for at least two hours or over night, then put on 4°C.
- *In situ* hybridization and Immunohistochemistry/fluorescence as described above (Histology on Tissue sections).

7.5 Patient Data

Tumor specimen and follow-up data were selected from the tumor bank of the Robert-Rössle-Clinic, Berlin and has been described before (Fritzmann et al., 2009). Survival data was analyzed using SPSS software (IBM). Significance was assessed by Log Rank test.

8 Appendix

8.1 Ensemble IDs of Genes Silenced by esiRNA in SW480 Cells

ENSG00000003137	ENSG00000077092	ENSG00000105976	ENSG00000117448
ENSG00000004864	ENSG00000077274	ENSG00000105991	ENSG00000117707
ENSG00000004975	ENSG00000077943	ENSG00000105997	ENSG00000118257
ENSG00000005020	ENSG00000078399	ENSG00000106003	ENSG00000118271
ENSG00000005102	ENSG00000079459	ENSG00000106004	ENSG00000118495
ENSG00000005513	ENSG00000080823	ENSG00000106078	ENSG00000118520
ENSG00000009413	ENSG00000081059	ENSG00000106484	ENSG00000119630
ENSG00000019549	ENSG00000085741	ENSG00000106571	ENSG00000119772
ENSG00000019991	ENSG00000087303	ENSG00000106617	ENSG00000119888
ENSG00000030110	ENSG00000088305	ENSG00000106829	ENSG00000120075
ENSG00000030419	ENSG00000089225	ENSG00000107262	ENSG00000120149
ENSG00000037965	ENSG00000090776	ENSG00000107404	ENSG00000120833
ENSG00000038427	ENSG00000092445	ENSG00000107562	ENSG00000121966
ENSG00000039068	ENSG00000092969	ENSG00000107719	ENSG00000122176
ENSG00000041982	ENSG00000095539	ENSG00000107731	ENSG00000122592
ENSG00000043355	ENSG00000095585	ENSG00000107984	ENSG00000122870
ENSG00000048828	ENSG00000095596	ENSG00000108001	ENSG00000124212
ENSG00000049130	ENSG00000099849	ENSG00000108392	ENSG00000124216
ENSG00000051620	ENSG00000100503	ENSG00000108604	ENSG00000125378
ENSG00000052758	ENSG00000100968	ENSG00000110092	ENSG00000125798
ENSG00000053438	ENSG00000101115	ENSG00000110693	ENSG00000125818
ENSG00000054118	ENSG00000101144	ENSG00000111087	ENSG00000125931
ENSG00000056661	ENSG00000101266	ENSG00000111145	ENSG00000126016
ENSG00000058085	ENSG00000101417	ENSG00000111432	ENSG00000126217
ENSG00000059804	ENSG00000102081	ENSG00000112658	ENSG00000126749
ENSG00000060656	ENSG00000102145	ENSG00000112837	ENSG00000126756
ENSG00000061273	ENSG00000102316	ENSG00000112972	ENSG00000126778
ENSG00000064042	ENSG00000102678	ENSG00000113196	ENSG00000127418
ENSG00000064218	ENSG00000102882	ENSG00000113492	ENSG00000127616
ENSG00000064490	ENSG00000103222	ENSG00000113658	ENSG00000127863
ENSG00000066379	ENSG00000103449	ENSG00000113722	ENSG00000128052
ENSG00000067064	ENSG00000103742	ENSG00000114115	ENSG00000128645
ENSG00000068697	ENSG00000104267	ENSG00000114251	ENSG00000128683
ENSG00000070031	ENSG00000104290	ENSG00000114315	ENSG00000128710
ENSG00000071575	ENSG00000104313	ENSG00000114541	ENSG00000128714
ENSG00000072110	ENSG00000104332	ENSG00000114867	ENSG00000130158
ENSG00000073282	ENSG00000104341	ENSG00000115053	ENSG00000130396
ENSG00000074047	ENSG00000104722	ENSG00000115414	ENSG00000130545
ENSG00000074527	ENSG00000104964	ENSG00000115461	ENSG00000130635
ENSG00000075213	ENSG00000105220	ENSG00000116106	ENSG00000130988
ENSG00000075275	ENSG00000105699	ENSG00000117114	ENSG00000131264
ENSG00000075388	ENSG00000105880	ENSG00000117318	ENSG00000131914

ENSG00000132341	ENSG00000141582	ENSG00000162407	ENSG00000172893
ENSG00000132670	ENSG00000141753	ENSG00000162415	ENSG00000173020
ENSG00000132688	ENSG00000142102	ENSG00000162434	ENSG00000173253
ENSG00000132718	ENSG00000142188	ENSG00000162734	ENSG00000173638
ENSG00000133858	ENSG00000142627	ENSG00000162761	ENSG00000173673
ENSG00000134025	ENSG00000142798	ENSG00000162944	ENSG00000174238
ENSG00000134184	ENSG00000143320	ENSG00000162980	ENSG00000175832
ENSG00000134245	ENSG00000143867	ENSG00000162998	ENSG00000176720
ENSG00000134247	ENSG00000144485	ENSG00000163029	ENSG00000177283
ENSG00000134250	ENSG00000144724	ENSG00000163430	ENSG00000177426
ENSG00000134363	ENSG00000144730	ENSG00000163909	ENSG00000177508
ENSG00000134369	ENSG00000145147	ENSG00000164056	ENSG00000178053
ENSG00000134811	ENSG00000145423	ENSG00000164442	ENSG00000178951
ENSG00000134853	ENSG00000146374	ENSG00000164458	ENSG00000180011
ENSG00000134986	ENSG00000147065	ENSG00000164619	ENSG00000180447
ENSG00000135074	ENSG00000147257	ENSG00000164619	ENSG00000180818
ENSG00000135111	ENSG00000148516	ENSG00000164683	ENSG00000181234
ENSG00000135404	ENSG00000148700	ENSG00000164930	ENSG00000181826
ENSG00000135414	ENSG00000149089	ENSG00000165029	ENSG00000181965
ENSG00000135447	ENSG00000149922	ENSG00000165092	ENSG00000182985
ENSG00000135503	ENSG00000150630	ENSG00000165495	ENSG00000183837
ENSG00000135547	ENSG00000151276	ENSG00000165556	ENSG00000183963
ENSG00000135903	ENSG00000152284	ENSG00000166106	ENSG00000184012
ENSG00000135914	ENSG00000152785	ENSG00000166482	ENSG00000184304
ENSG00000135916	ENSG00000153179	ENSG00000166949	ENSG00000184323
ENSG00000135919	ENSG00000154342	ENSG00000167034	ENSG00000184347
ENSG00000136997	ENSG00000154639	ENSG00000167173	ENSG00000184363
ENSG00000137269	ENSG00000154764	ENSG00000167434	ENSG00000184697
ENSG00000137936	ENSG00000155760	ENSG00000168268	ENSG00000184697
ENSG00000138166	ENSG00000156374	ENSG00000168505	ENSG00000184937
ENSG00000138771	ENSG00000156427	ENSG00000168646	ENSG00000185082
ENSG00000138795	ENSG00000156925	ENSG00000169071	ENSG00000185155
ENSG00000139219	ENSG00000157216	ENSG00000169242	ENSG00000185201
ENSG00000139263	ENSG00000157240	ENSG00000169554	ENSG00000185386
ENSG00000139318	ENSG00000157557	ENSG00000169604	ENSG00000185669
ENSG00000139515	ENSG00000157933	ENSG00000170166	ENSG00000185885
ENSG00000139737	ENSG00000158258	ENSG00000170421	ENSG00000185920
ENSG00000139800	ENSG00000158747	ENSG00000170561	ENSG00000186174
ENSG00000139921	ENSG00000159166	ENSG00000170571	ENSG00000186895
ENSG00000139946	ENSG00000159307	ENSG00000170802	ENSG00000196208
ENSG00000139998	ENSG00000159618	ENSG00000170921	ENSG00000196329
ENSG00000140416	ENSG00000159840	ENSG00000170961	ENSG00000196358
ENSG00000140450	ENSG00000159842	ENSG00000171425	ENSG00000196498
ENSG00000140807	ENSG00000160145	ENSG00000171488	ENSG00000196562
ENSG00000140937	ENSG00000160191	ENSG00000171617	ENSG00000196781
ENSG00000141068	ENSG00000160285	ENSG00000171812	ENSG00000197102
ENSG00000141232	ENSG00000161202	ENSG00000171843	ENSG00000197757
ENSG00000141314	ENSG00000162129	ENSG00000171914	ENSG00000198300
ENSG00000141449	ENSG00000162344	ENSG00000172819	ENSG00000198554

9 References

Alewine, C., Olsen, O., Wade, J.B., and Welling, P.A. (2006). TIP-1 has PDZ scaffold antagonist activity. Mol Biol Cell *17*, 4200-4211.

Aliaga, J.C., Deschênes, C., Beaulieu, J.F., Calvo, E.L., and Rivard, N. (1999). Requirement of the MAP kinase cascade for cell cycle progression and differentiation of human intestinal cells. Am J Physiol *277*, G631-641.

Arnold, S.J., and Robertson, E.J. (2009). Making a commitment: cell lineage allocation and axis patterning in the early mouse embryo. Nat Rev Mol Cell Biol *10*, 91-103.

Barker, N., Ridgway, R.A., van Es, J.H., van de Wetering, M., Begthel, H., van den Born, M., Danenberg, E., Clarke, A.R., Sansom, O.J., and Clevers, H. (2009). Crypt stem cells as the cells-of-origin of intestinal cancer. Nature *457*, 608-611.

Barker, N., van de Wetering, M., and Clevers, H. (2008). The intestinal stem cell. Genes & Development *22*, 1856-1864.

Barker, N., van Es, J.H., Kuipers, J., Kujala, P., van den Born, M., Cozijnsen, M., Haegebarth, A., Korving, J., Begthel, H., Peters, P.J.*, et al.* (2007). Identification of stem cells in small intestine and colon by marker gene Lgr5. Nature *449*, 1003-1007.

Batlle, E., Bacani, J., Begthel, H., Jonkheer, S., Jonkeer, S., Gregorieff, A., van de Born, M., Malats, N., Sancho, E., Boon, E.*, et al.* (2005). EphB receptor activity suppresses colorectal cancer progression. Nature *435*, 1126-1130.

Batlle, E., Henderson, J.T., Beghtel, H., van den Born, M.M., Sancho, E., Huls, G., Meeldijk, J., Robertson, J., van de Wetering, M., Pawson, T.*, et al.* (2002a). Beta-catenin and TCF mediate cell positioning in the intestinal epithelium by controlling the expression of EphB/ephrinB. cell *111*, 251-263.

Batlle, E., Henderson, J.T., Beghtel, H., van den Born, M.M.W., Sancho, E., Huls, G., Meeldijk, J., Robertson, J., van de Wetering, M., Pawson, T.*, et al.* (2002b). Beta-catenin and TCF mediate cell positioning in the intestinal epithelium by controlling the expression of EphB/ephrinB. cell *111*, 251-263.

Birchmeier, C., Birchmeier, W., Gherardi, E., and Vande Woude, G.F. (2003). Met, metastasis, motility and more. Nat Rev Mol Cell Biol *4*, 915-925.

Birchmeier, W. (2005). Cell adhesion and signal transduction in cancer. Conference on cadherins, catenins and cancer. EMBO Rep *6*, 413-417.

Bisson, N., Poitras, L., Mikryukov, A., Tremblay, M., and Moss, T. (2007). EphA4 signaling regulates blastomere adhesion in the Xenopus embryo by recruiting Pak1 to suppress Cdc42 function. Mol Biol Cell *18*, 1030-1043.

Bjerknes, M., and Cheng, H. (1999). Clonal analysis of mouse intestinal epithelial progenitors. Gastroenterology *116*, 7-14.

Blanpain, C., Horslay, V., and Fuchs, E. (2007). Epithelial Stem Cells:

Turning over New Leaves. Cell.

Brabletz, T., Jung, A., and Kirchner, T. (2002). Beta-catenin and the morphogenesis of colorectal cancer. Virchows Arch *441*, 1-11.

Brabletz, T., Jung, A., Spaderna, S., Hlubek, F., and Kirchner, T. (2005). Opinion: migrating cancer stem cells - an integrated concept of malignant tumour progression. Nat Rev Cancer *5*, 744-749.

Brembeck, F.H., Schwarz-Romond, T., Bakkers, J., Wilhelm, S., Hammerschmidt, M., and Birchmeier, W. (2004). Essential role of BCL9-2 in the switch between beta-catenin's adhesive and transcriptional functions. Genes Dev *18*, 2225-2230.

Buchholz, F., Kittler, R., Slabicki, M., and Theis, M. (2006). Enzymatically prepared RNAi libraries. Nat Methods *3*, 696-700.

Byron, S.A., Gartside, M.G., Wellens, C.L., Mallon, M.A., Keenan, J.B., Powell, M.A., Goodfellow, P.J., and Pollock, P.M. (2008). Inhibition of activated fibroblast growth factor receptor 2 in endometrial cancer cells induces cell death despite PTEN abrogation. Cancer Res *68*, 6902-6907.

Cairns, J. (1975). Mutation selection and the natural history of cancer. Nature *255*, 197-200.

Cappellen, D., De Oliveira, C., Ricol, D., de Medina, S., Bourdin, J., Sastre-Garau, X., Chopin, D., Thiery, J.P., and Radvanyi, F. (1999). Frequent activating mutations of FGFR3 in human bladder and cervix carcinomas. Nat Genet *23*, 18-20.

Cheng, H., and Leblond, C.P. (1974a). Origin, differentiation and renewal of the four main epithelial cell types in the mouse small intestine. I. Columnar cell. Am J Anat *141*, 461-479.

Cheng, H., and Leblond, C.P. (1974b). Origin, differentiation and renewal of the four main epithelial cell types in the mouse small intestine. V. Unitarian Theory of the origin of the four epithelial cell types. Am J Anat *141*, 537-561.

Christensen, K.L., Patrick, A.N., McCoy, E.L., and Ford, H.L. (2008). The six family of homeobox genes in development and cancer. Adv Cancer Res *101*, 93-126.

Christofori, G., and Semb, H. (1999). The role of the cell-adhesion molecule E-cadherin as a tumour-suppressor gene. Trends Biochem Sci *24*, 73-76.

Ciruna, B., and Rossant, J. (2001). FGF signaling regulates mesoderm cell fate specification and morphogenetic movement at the primitive streak. Dev Cell *1*, 37-49.

Clevers, H., and Batlle, E. (2006). EphB/EphrinB receptors and Wnt signaling in colorectal cancer. Cancer Res *66*, 2-5.

Conacci-Sorrell, M., Simcha, I., Ben-Yedidia, T., Blechman, J., Savagner, P., and Ben-Ze'ev, A. (2003). Autoregulation of E-cadherin expression by cadherin-cadherin interactions: the roles of beta-catenin signaling, Slug, and MAPK. In J Cell Biol, pp. 847-857.

Cunningham, D., Atkin, W., Lenz, H.-J., Lynch, H.T., Minsky, B., Nordlinger, B., and Starling, N. (2010). Colorectal cancer. Lancet *375*, 1030-1047.

de la Chapelle, A. (2004). Genetic predisposition to colorectal cancer. Nat Rev Cancer *4*, 769-780.

DeSilva, D.R., Jones, E.A., Favata, M.F., Jaffee, B.D., Magolda, R.L., Trzaskos, J.M., and Scherle, P.A. (1998). Inhibition of mitogen-activated protein kinase kinase blocks T cell proliferation but does not induce or prevent anergy. Journal of immunology (Baltimore, Md : 1950) *160*, 4175-4181.

Eswarakumar, V.P., Lax, I., and Schlessinger, J. (2005). Cellular signaling by fibroblast growth factor receptors. Cytokine Growth Factor Rev *16*, 139-149.

Fearon, E.R., and Vogelstein, B. (1990). A genetic model for colorectal tumorigenesis. Cell *61*, 759-767.

Ferlay, J., Autier, P., Boniol, M., Heanue, M., Colombet, M., and Boyle, P. (2007). Estimates of the cancer incidence and mortality in Europe in 2006. Ann Oncol *18*, 581-592.

Finak, G., Bertos, N., Pepin, F., Sadekova, S., Souleimanova, M., Zhao, H., Chen, H., Omeroglu, G., Meterissian, S., Omeroglu, A.*, et al.* (2008). Stromal gene expression predicts clinical outcome in breast cancer. Nat Med *14*, 518-527.

Fodde, R., and Brabletz, T. (2007). Wnt/beta-catenin signaling in cancer stemness and malignant behavior. Curr Opin Cell Biol *19*, 150-158.

Fre, S., Huyghe, M., Mourikis, P., Robine, S., Louvard, D., and Artavanis-Tsakonas, S. (2005). Notch signals control the fate of immature progenitor cells in the intestine. Nature *435*, 964-968.

Friedl, P., and Wolf, K. (2003). Tumour-cell invasion and migration: diversity and escape mechanisms. Nat Rev Cancer *3*, 362-374.

Fritzmann, J., Morkel, M., Besser, D., Budczies, J., Kosel, F., Brembeck, F.H., Stein, U., Fichtner, I., Schlag, P.M., and Birchmeier, W. (2009). A colorectal cancer expression profile that includes transforming growth factor beta inhibitor BAMBI predicts metastatic potential. Gastroenterology *137*, 165-175.

Fu, Y., Kim, I., Lian, P., Li, A., Zhou, L., Li, C., Liang, D., Coffey, R.J., Ma, J., Zhao, P.*, et al.* (2010). Loss of Bicc1 impairs tubulomorphogenesis of cultured IMCD cells by disrupting E-cadherin-based cell-cell adhesion. Eur J Cell Biol *89*, 428-436.

Gambus, G., de Bolos, C., Andreu, D., Franci, C., Egea, G., and Real, F.X. (1993). Detection of the MUC2 apomucin tandem repeat with a mouse monoclonal antibody. Gastroenterology *104*, 93-102.

Geske, M.J., Zhang, X., Patel, K.K., Ornitz, D.M., and Stappenbeck, T.S. (2008). Fgf9 signaling regulates small intestinal elongation and mesenchymal development. Development *135*, 2959-2968.

Green, R.P., Cohn, S.M., Sacchettini, J.C., Jackson, K.E., and Gordon, J.I. (1992). The mouse intestinal fatty acid binding protein gene: nucleotide sequence, pattern of developmental and regional expression, and proposed structure of its protein product. DNA Cell Biol *11*, 31-41.

Greenman, C., Stephens, P., Smith, R., Dalgliesh, G.L., Hunter, C., Bignell, G., Davies, H., Teague, J., Butler, A., Stevens, C*., et al.* (2007). Patterns of somatic mutation in human cancer genomes. Nature *446*, 153-158.

Gregorieff, A., and Clevers, H. (2005). Wnt signaling in the intestinal epithelium: from endoderm to cancer. Genes Dev *19*, 877-890.

Gregorieff, A., Pinto, D., Begthel, H., Destrée, O., Kielman, M., and Clevers, H. (2005). Expression pattern of Wnt signaling components in the adult intestine. Gastroenterology *129*, 626-638.

Halberg, R.B., Katzung, D.S., Hoff, P.D., Moser, A.R., Cole, C.E., Lubet, R.A., Donehower, L.A., Jacoby, R.F., and Dove, W.F. (2000). Tumorigenesis in the multiple intestinal neoplasia mouse: redundancy of negative regulators and specificity of modifiers. Proc Natl Acad Sci USA *97*, 3461-3466.

Hall, A. (1998). Rho GTPases and the actin cytoskeleton. Science *279*, 509-514.

Hamamoto, T., Beppu, H., Okada, H., Kawabata, M., Kitamura, T., Miyazono, K., and Kato, M. (2002). Compound disruption of smad2 accelerates malignant progression of intestinal tumors in apc knockout mice. Cancer Res *62*, 5955-5961.

Hanahan, D., and Weinberg, R.A. (2000). The hallmarks of cancer. Cell *100*, 57-70.

Hancock, J.F. (2003). Ras proteins: different signals from different locations. Nat Rev Mol Cell Biol *4*, 373-384.

Harada, N., Tamai, Y., Ishikawa, T., Sauer, B., Takaku, K., Oshima, M., and Taketo, M.M. (1999). Intestinal polyposis in mice with a dominant stable mutation of the beta-catenin gene. EMBO J *18*, 5931-5942.

Haramis, A.-P.G., Begthel, H., van den Born, M., van Es, J., Jonkheer, S., Offerhaus, G.J.A., and Clevers, H. (2004). De novo crypt formation and juvenile polyposis on BMP inhibition in mouse intestine. Science *303*, 1684-1686.

Heath, J.P. (1996). Epithelial cell migration in the intestine. Cell Biol Int *20*, 139-146.

Hecht, D., Zimmerman, N., Bedford, M., Avivi, A., and Yayon, A. (1995). Identification of fibroblast growth factor 9 (FGF9) as a high affinity, heparin dependent ligand for FGF receptors 3 and 2 but not for FGF receptors 1 and 4. Growth Factors *12*, 223-233.

Herynk, M.H., Stoeltzing, O., Reinmuth, N., Parikh, N.U., Abounader, R., Laterra, J., Radinsky, R., Ellis, L.M., and Gallick, G.E. (2003). Down-regulation of c-Met inhibits growth in the liver of human colorectal carcinoma cells. Cancer Res *63*, 2990-2996.

Hooper, J.E., and Scott, M.P. (2005). Communicating with Hedgehogs. Nat Rev Mol Cell Biol *6*, 306-317.

Housley, R.M., Morris, C.F., Boyle, W., Ring, B., Biltz, R., Tarpley, J.E., Aukerman, S.L., Devine, P.L., Whitehead, R.H., and Pierce, G.F. (1994). Keratinocyte growth factor induces proliferation of hepatocytes and epithelial cells throughout the rat gastrointestinal tract. J Clin Invest *94*, 1764-1777.

Huelsken, J., and Behrens, J. (2002). The Wnt signalling pathway. J Cell Sci *115*, 3977-3978.

Iacopetta, B. (2003). TP53 mutation in colorectal cancer. Hum Mutat *21*, 271-276.

Ireland, H., Houghton, C., Howard, L., and Winton, D.J. (2005). Cellular inheritance of a Cre-activated reporter gene to determine Paneth cell longevity in the murine small intestine. Dev Dyn *233*, 1332-1336.

Ireland, H., Kemp, R., Houghton, C., Howard, L., Clarke, A.R., Sansom, O.J., and Winton, D.J. (2004). Inducible Cre-mediated control of gene expression in the murine gastrointestinal tract: effect of loss of beta-catenin. Gastroenterology *126*, 1236-1246.

Jaffe, A.B., and Hall, A. (2005). Rho GTPases: biochemistry and biology. Annu Rev Cell Dev Biol *21*, 247-269.

Jebar, A.H., Hurst, C.D., Tomlinson, D.C., Johnston, C., Taylor, C.F., and Knowles, M.A. (2005). FGFR3 and Ras gene mutations are mutually exclusive genetic events in urothelial cell carcinoma. Oncogene *24*, 5218-5225.

Jemal, A., Siegel, R., Ward, E., Hao, Y., Xu, J., Murray, T., and Thun, M. (2008). Cancer statistics, 2008. CA: a cancer journal for clinicians *58*, 71.

Jensen, J., Pedersen, E.E., Galante, P., Hald, J., Heller, R.S., Ishibashi, M., Kageyama, R., Guillemot, F., Serup, P., and Madsen, O.D. (2000). Control of endodermal endocrine development by Hes-1. Nat Genet *24*, 36-44.

Kanamori, M., Sandy, P., Marzinotto, S., Benetti, R., Kai, C., Hayashizaki, Y., Schneider, C., and Suzuki, H. (2003). The PDZ protein tax-interacting protein-1 inhibits beta-catenin transcriptional activity and growth of colorectal cancer cells. J Biol Chem *278*, 38758-38764.

Karam, S.M. (1999). Lineage commitment and maturation of epithelial cells in the gut. Front Biosci *4*, D286-298.

Kim, K.-A., Kakitani, M., Zhao, J., Oshima, T., Tang, T., Binnerts, M., Liu, Y., Boyle, B., Park, E., Emtage, P.*, et al.* (2005). Mitogenic influence of human R-spondin1 on the intestinal epithelium. Science *309*, 1256-1259.

Kimmel, S.G., Mo, R., Hui, C.C., and Kim, P.C. (2000). New mouse models of congenital anorectal malformations. J Pediatr Surg *35*, 227-230; discussion 230-221.

Kinzler, K.W., and Vogelstein, B. (1996). Lessons from hereditary colorectal cancer. Cell *87*, 159-170.

Knudson, A.G. (1996). Hereditary cancer: two hits revisited. J Cancer Res Clin Oncol *122*, 135-140.

Korinek, V., Barker, N., Moerer, P., van Donselaar, E., Huls, G., Peters, P.J., and Clevers, H. (1998). Depletion of epithelial stem-cell compartments in the small intestine of mice lacking Tcf-4. Nat Genet *19*, 379-383.

Kubens, B.S., and Zänker, K.S. (1998). Differences in the migration capacity of primary human colon carcinoma cells (SW480) and their lymph node metastatic derivatives (SW620). Cancer Lett *131*, 55-64.

Lee, C.S., Perreault, N., Brestelli, J.E., and Kaestner, K.H. (2002). Neurogenin 3 is essential for the proper specification of gastric enteroendocrine cells and the maintenance of gastric epithelial cell identity. Genes Dev *16*, 1488-1497.

Leibovitz, A., Stinson, J.C., McCombs, W.B., McCoy, C.E., Mazur, K.C., and Mabry, N.D. (1976). Classification of human colorectal adenocarcinoma cell lines. Cancer Res *36*, 4562-4569.

Li, L., and Xie, T. (2005). Stem cell niche: structure and function. Annu Rev Cell Dev Biol *21*, 605-631.

Loebke, C., Sueltmann, H., Schmidt, C., Henjes, F., Wiemann, S., Poustka, A., and Korf, U. (2007). Infrared-based protein detection arrays for quantitative proteomics. Proteomics *7*, 558-564.

Logan, C., and Nusse, R. (2004). The Wnt signaling pathway in development and disease.

Lustig, B., and Behrens, J. (2003). The Wnt signaling pathway and its role in tumor development. J Cancer Res Clin Oncol *129*, 199-221.

Lustig, B., Jerchow, B., Sachs, M., Weiler, S., Pietsch, T., Karsten, U., van de Wetering, M., Clevers, H., Schlag, P.M., Birchmeier, W*., et al.* (2002). Negative feedback loop of Wnt signaling through upregulation of conductin/axin2 in colorectal and liver tumors. Mol Cell Biol *22*, 1184-1193.

Lynch, H.T., and de la Chapelle, A. (2003). Hereditary colorectal cancer. N Engl J Med *348*, 919-932.

Mani, S., Guo, W., Liao, M., Eaton, E., Ayyanan, A., Zhou, A., Brooks, M., Reinhard, F., Zhang, C., and Shipitsin, M. (2008). The Epithelial-Mesenchymal Transition Generates Cells with Properties of Stem Cells. Cell *133*, 704-715.

Marshman, E., Booth, C., and Potten, C.S. (2002). The intestinal epithelial stem cell. Bioessays *24*, 91-98.

McCart, A.E., Vickaryous, N.K., and Silver, A. (2008). Apc mice: models, modifiers and mutants. Pathol Res Pract *204*, 479-490.

Micalizzi, D.S., Christensen, K.L., Jedlicka, P., Coletta, R.D., Barón, A.E., Harrell, J.C., Horwitz, K.B., Billheimer, D., Heichman, K.A., Welm, A.L.*, et al.* (2009). The Six1 homeoprotein induces human mammary carcinoma cells to undergo epithelial-mesenchymal transition and metastasis in mice through increasing TGF-beta signaling. J Clin Invest *119*, 2678-2690.

Milano, J., McKay, J., Dagenais, C., Foster-Brown, L., Pognan, F., Gadient, R., Jacobs, R.T., Zacco, A., Greenberg, B., and Ciaccio, P.J. (2004). Modulation of notch processing by gamma-secretase inhibitors causes intestinal goblet cell metaplasia and induction of genes known to specify gut secretory lineage differentiation. Toxicol Sci *82*, 341-358.

Mills, J.C., and Gordon, J.I. (2001). The intestinal stem cell niche: there grows the neighborhood. Proc Natl Acad Sci USA *98*, 12334-12336.

Mizuhara, E., Nakatani, T., Minaki, Y., Sakamoto, Y., Ono, Y., and Takai, Y. (2005). MAGI1 recruits Dll1 to cadherin-based adherens junctions and stabilizes it on the cell surface. J Biol Chem *280*, 26499-26507.

Mo, R., Kim, J.H., Zhang, J., Chiang, C., Hui, C.C., and Kim, P.C. (2001). Anorectal malformations caused by defects in sonic hedgehog signaling. Am J Pathol *159*, 765-774.

Mohammadi, M., Froum, S., Hamby, J.M., Schroeder, M.C., Panek, R.L., Lu, G.H., Eliseenkova, A.V., Green, D., Schlessinger, J., and Hubbard, S.R. (1998). Crystal structure of an angiogenesis inhibitor bound to the FGF receptor tyrosine kinase domain. EMBO J *17*, 5896-5904.

Mohammadi, M., McMahon, G., Sun, L., Tang, C., Hirth, P., Yeh, B.K., Hubbard, S.R., and Schlessinger, J. (1997). Structures of the tyrosine kinase domain of fibroblast growth factor receptor in complex with inhibitors. Science *276*, 955-960.

Morita, H., Mazerbourg, S., Bouley, D.M., Luo, C.-W., Kawamura, K., Kuwabara, Y., Baribault, H., Tian, H., and Hsueh, A.J.W. (2004). Neonatal lethality of LGR5 null mice is associated with ankyloglossia and gastrointestinal distension. Mol Cell Biol *24*, 9736-9743.

Moser, A.R., Pitot, H.C., and Dove, W.F. (1990). A dominant mutation that predisposes to multiple intestinal neoplasia in the mouse. Science *247*, 322-324.

Nucci, M.R., Robinson, C.R., Longo, P., Campbell, P., and Hamilton, S.R. (1997). Phenotypic and genotypic characteristics of aberrant crypt foci in human colorectal mucosa. Hum Pathol *28*, 1396-1407.

O'Brien, C.A., Pollett, A., Gallinger, S., and Dick, J.E. (2007). A human colon cancer cell capable of initiating tumour growth in immunodeficient mice. Nature *445*, 106-110.

Olson, E.N., and Nordheim, A. (2010). Linking actin dynamics and gene transcription to drive cellular motile functions. Nat Rev Mol Cell Biol *11*, 353-365.

Peinado, Olmeda, and Cano (2007). Snail, Zeb and bHLH factors in tumour progression: an alliance against the epithelial phenotype? Nat Rev Cancer.

Phelps, R.A., Chidester, S., Dehghanizadeh, S., Phelps, J., Sandoval, I.T., Rai, K., Broadbent, T., Sarkar, S., Burt, R.W., and Jones, D.A. (2009). A two-step model for colon adenoma initiation and progression caused by APC loss. Cell *137*, 623-634.

Pinto, D., Gregorieff, A., Begthel, H., and Clevers, H. (2003). Canonical Wnt signals are essential for homeostasis of the intestinal epithelium. Genes Dev *17*, 1709-1713.

Potten, C.S. (1977). Extreme sensitivity of some intestinal crypt cells to X and gamma irradiation. Nature *269*, 518-521.

Potten, C.S., Kovacs, L., and Hamilton, E. (1974). Continuous labelling studies on mouse skin and intestine. Cell Tissue Kinet *7*, 271-283.

Preston, S.L., Wong, W.-M., Chan, A.O.-O., Poulsom, R., Jeffery, R., Goodlad, R.A., Mandir, N., Elia, G., Novelli, M., Bodmer, W.F*., et al.* (2003). Bottom-up histogenesis of colorectal adenomas: origin in the monocryptal adenoma and initial expansion by crypt fission. Cancer Res *63*, 3819-3825.

Reya, T., and Clevers, H. (2005). Wnt signalling in stem cells and cancer. Nature *434*, 843-850.

Ricci-Vitiani, L., Lombardi, D.G., Pilozzi, E., Biffoni, M., Todaro, M., Peschle, C., and De Maria, R. (2007). Identification and expansion of human colon-cancer-initiating cells. Nature *445*, 111-115.

Sancho, E., Batlle, E., and Clevers, H. (2004). Signaling pathways in intestinal development and cancer. Annu Rev Cell Dev Biol *20*, 695-723.

Sangiorgi, E., and Capecchi, M.R. (2008). Bmi1 is expressed in vivo in intestinal stem cells. Nat Genet *40*, 915-920.

Sansom, O.J., Meniel, V., Wilkins, J.A., Cole, A.M., Oien, K.A., Marsh, V., Jamieson, T.J., Guerra, C., Ashton, G.H., Barbacid, M*., et al.* (2006). Loss of Apc allows phenotypic manifestation of the transforming properties of an endogenous K-ras oncogene in vivo. Proc Natl Acad Sci USA *103*, 14122-14127.

Sato, T., van Es, J.H., Snippert, H.J., Stange, D.E., Vries, R.G., van den Born, M., Barker, N., Shroyer, N.F., van de Wetering, M., and Clevers, H. (2010). Paneth cells constitute the niche for Lgr5 stem cells in intestinal crypts. Nature.

Sato, T., Vries, R., Snippert, H., van De Wetering, M., Barker, N., Stange, D., van Es, J., Abo, A., Kujala, P., Peters, P*., et al.* (2009). Single Lgr5 stem cells build crypt-villus structures in vitro without a mesenchymal niche. Nature.

Schmidt, G.H., Winton, D.J., and Ponder, B.A. (1988). Development of the pattern of cell renewal in the crypt-villus unit of chimaeric mouse small intestine. Development *103*, 785-790.

Shi, Y., and Massagué, J. (2003). Mechanisms of TGF-beta signaling from cell membrane to the nucleus. Cell *113*, 685-700.

Shroyer, N.F., Helmrath, M.A., Wang, V.Y.-C., Antalffy, B., Henning, S.J., and Zoghbi, H.Y. (2007). Intestine-specific ablation of mouse atonal homolog 1 (Math1) reveals a role in cellular homeostasis. Gastroenterology *132*, 2478-2488.

Sivarajasingham, N.S., Baker, R., Tilsed, J.V., Greenman, J., Monson, J.R.T., and Cawkwell, L. (2003). Identifying a region of interest in site- and stage-specific colon cancer on chromosome 13. Ann Surg Oncol *10*, 1095-1099.

Snippert, H.J., van der Flier, L.G., Sato, T., van Es, J.H., van den Born, M., Kroon-Veenboer, C., Barker, N., Klein, A.M., van Rheenen, J., Simons, B.D.*, et al.* (2010). Intestinal crypt homeostasis results from neutral competition between symmetrically dividing Lgr5 stem cells. Cell *143*, 134-144.

Sonvilla, G., Allerstorfer, S., Heinzle, C., Stättner, S., Karner, J., Klimpfinger, M., Wrba, F., Fischer, H., Gauglhofer, C., Spiegl-Kreinecker, S.*, et al.* (2010). Fibroblast growth factor receptor 3-IIIc mediates colorectal cancer growth and migration. Br J Cancer *102*, 1145-1156.

Sonvilla, G., Allerstorfer, S., Stattner, S., Karner, J., Klimpfinger, M., Fischer, H., Grasl-Kraupp, B., Holzmann, K., Berger, W., and Wrba, F. (2008). FGF18 in colorectal tumour cells: autocrine and paracrine effects. Carcinogenesis *29*, 15.

Soriano, P. (1999). Generalized lacZ expression with the ROSA26 Cre reporter strain. Nat Genet *21*, 70-71.

Stanger, B.Z., Datar, R., Murtaugh, L.C., and Melton, D.A. (2005). Direct regulation of intestinal fate by Notch. Proc Natl Acad Sci USA *102*, 12443-12448.

Su, L.K., Kinzler, K.W., Vogelstein, B., Preisinger, A.C., Moser, A.R., Luongo, C., Gould, K.A., and Dove, W.F. (1992). Multiple intestinal neoplasia caused by a mutation in the murine homolog of the APC gene. Science *256*, 668-670.

Suzuki, K., Fukui, H., Kayahara, T., Sawada, M., Seno, H., Hiai, H., Kageyama, R., Okano, H., and Chiba, T. (2005). Hes1-deficient mice show precocious differentiation of Paneth cells in the small intestine. Biochem Biophys Res Commun *328*, 348-352.

Takaku, K., Oshima, M., Miyoshi, H., Matsui, M., Seldin, M.F., and Taketo, M.M. (1998). Intestinal tumorigenesis in compound mutant mice of both Dpc4 (Smad4) and Apc genes. Cell *92*, 645-656.

Taketo, M.M., Trosko, J.E., Chang, C.-C., Upham, B.L., and Tai, M.-H. (2006). Mouse models of gastrointestinal tumors. Cancer Sci *97*, 355-361.

Tassi, E., Henke, R.T., Bowden, E.T., Swift, M.R., Kodack, D.P., Kuo, A.H., Maitra, A., and Wellstein, A. (2006). Expression of a fibroblast growth factor-binding protein during the development of adenocarcinoma of the pancreas and colon. Cancer Res *66*, 1191-1198.

Thiery, J.P. (2002). Epithelial-mesenchymal transitions in tumour progression. Nat Rev Cancer *2*, 442-454.

Thiery, J.P. (2003). Epithelial-mesenchymal transitions in development and pathologies. Curr Opin Cell Biol *15*, 740-746.

Thiery, J.P., and Sleeman, J.P. (2006). Complex networks orchestrate epithelial-mesenchymal transitions. Nat Rev Mol Cell Biol *7*, 131-142.

Trainer, D.L., Kline, T., McCabe, F.L., Faucette, L.F., Feild, J., Chaikin, M., Anzano, M., Rieman, D., Hoffstein, S., and Li, D.J. (1988). Biological characterization and oncogene expression in human colorectal carcinoma cell lines. Int J Cancer *41*, 287-296.

Turner, N., and Grose, R. (2010). Fibroblast growth factor signalling: from development to cancer. Nat Rev Cancer *10*, 116-129.

Uchida, H., Yamazaki, K., Fukuma, M., Yamada, T., Hayashida, T., Hasegawa, H., Kitajima, M., Kitagawa, Y., and Sakamoto, M. (2010). Overexpression of leucine-rich repeat-containing G protein-coupled receptor 5 in colorectal cancer. Cancer Sci *101*, 1731-1737.

Vallés, A.M., Boyer, B., Badet, J., Tucker, G.C., Barritault, D., and Thiery, J.P. (1990). Acidic fibroblast growth factor is a modulator of epithelial plasticity in a rat bladder carcinoma cell line. Proc Natl Acad Sci USA *87*, 1124-1128.

van de Wetering, M., Sancho, E., Verweij, C., de Lau, W., Oving, I., Hurlstone, A., van der Horn, K., Batlle, E., Coudreuse, D., Haramis, A.P*., et al.* (2002). The beta-catenin/TCF-4 complex imposes a crypt progenitor phenotype on colorectal cancer cells. Cell *111*, 241-250.

van den Brink, G.R., Bleuming, S.A., Hardwick, J.C.H., Schepman, B.L., Offerhaus, G.J., Keller, J.J., Nielsen, C., Gaffield, W., van Deventer, S.J.H., Roberts, D.J*., et al.* (2004). Indian Hedgehog is an antagonist of Wnt signaling in colonic epithelial cell differentiation. Nat Genet *36*, 277-282.

Van der Flier, L., Sabates–Bellver, J., and Oving, I. (2007a). The Intestinal Wnt/TCF Signature. Gastroenterology.

van der Flier, L.G., and Clevers, H. (2009). Stem cells, self-renewal, and differentiation in the intestinal epithelium. Annu Rev Physiol *71*, 241-260.

van der Flier, L.G., Haegebarth, A., Stange, D.E., van de Wetering, M., and Clevers, H. (2009a). OLFM4 is a robust marker for stem cells in human intestine and marks a subset of colorectal cancer cells. Gastroenterology *137*, 15-17.

Van der Flier, L.G., Sabates-Bellver, J., Oving, I., Haegebarth, A., De Palo, M., Anti, M., Van Gijn, M.E., Suijkerbuijk, S., Van de Wetering, M., Marra, G*., et al.* (2007b). The Intestinal Wnt/TCF Signature. Gastroenterology *132*, 628-632.

van der Flier, L.G., van Gijn, M.E., Hatzis, P., Kujala, P., Haegebarth, A., Stange, D.E., Begthel, H., van den Born, M., Guryev, V., Oving, I*., et al.* (2009b). Transcription factor achaete scute-like 2 controls intestinal stem cell fate. Cell *136*, 903-912.

van Es, J., de Geest, N., van de Born, M., Clevers, H., and Hassan, B. (2010). Intestinal stem cells lacking the Math1 tumour suppressor are refractory to Notch inhibitors. Nature Communications *1*, 1-5.

van Es, J.H., Jay, P., Gregorieff, A., van Gijn, M.E., Jonkheer, S., Hatzis, P., Thiele, A., van den Born, M., Begthel, H., Brabletz, T*., et al.* (2005a). Wnt signalling induces maturation of Paneth cells in intestinal crypts. Nat Cell Biol *7*, 381-386.

van Es, J.H., van Gijn, M.E., Riccio, O., van den Born, M., Vooijs, M., Begthel, H., Cozijnsen, M., Robine, S., Winton, D.J., Radtke, F*., et al.* (2005b). Notch/gamma-secretase inhibition turns proliferative cells in intestinal crypts and adenomas into goblet cells. Nature *435*, 959-963.

VanDussen, K.L., and Samuelson, L.C. Mouse atonal homolog 1 directs intestinal progenitors to secretory cell rather than absorptive cell fate. Dev Biol *346*, 215-223.

Vermeulen, L., De Sousa E Melo, F., van der Heijden, M., Cameron, K., de Jong, J.H., Borovski, T., Tuynman, J.B., Todaro, M., Merz, C., Rodermond, H*., et al.* (2010). Wnt activity defines colon cancer stem cells and is regulated by the microenvironment. Nat Cell Biol *12*, 468-476.

Vidrich, A., Buzan, J.M., Brodrick, B., Ilo, C., Bradley, L., Fendig, K.S., Sturgill, T., and Cohn, S.M. (2009). Fibroblast growth factor receptor-3 regulates Paneth cell lineage allocation and accrual of epithelial stem cells during murine intestinal development. AJP: Gastrointestinal and Liver Physiology *297*, G168-G178.

Vidrich, A., Buzan, J.M., Ilo, C., Bradley, L., Skaar, K., and Cohn, S.M. (2004). Fibroblast growth factor receptor-3 is expressed in undifferentiated intestinal epithelial cells during murine crypt morphogenesis. Dev Dyn *230*, 114-123.

Vooijs, M., Ong, C.-T., Hadland, B., Huppert, S., Liu, Z., Korving, J., van den Born, M., Stappenbeck, T., Wu, Y., Clevers, H*., et al.* (2007). Mapping the consequence of Notch1 proteolysis in vivo with NIP-CRE. Development *134*, 535-544.

Waerner, T., Alacakaptan, M., Tamir, I., Oberauer, R., Gal, A., Brabletz, T., Schreiber, M., Jechlinger, M., and Beug, H. (2006). ILEI: a cytokine essential for EMT, tumor formation, and late events in metastasis in epithelial cells. Cancer Cell *10*, 227-239.

Wagers, A.J., and Weissman, I.L. (2004). Plasticity of adult stem cells. Cell *116*, 639-648.

Watanabe, M., Ishiwata, T., Nishigai, K., Moriyama, Y., and Asano, G. (2000). Overexpression of keratinocyte growth factor in cancer cells and enterochromaffin cells in human colorectal cancer. Pathol Int *50*, 363-372.

Winder, T., and Lenz, H.-J. (2010). Vascular endothelial growth factor and epidermal growth factor signaling pathways as therapeutic targets for colorectal cancer. Gastroenterology *138*, 2163-2176.

Winton, D.J., Blount, M.A., and Ponder, B.A. (1988). A clonal marker induced by mutation in mouse intestinal epithelium. Nature *333*, 463-466.

Wong, G.T., Manfra, D., Poulet, F.M., Zhang, Q., Josien, H., Bara, T., Engstrom, L., Pinzon-Ortiz, M., Fine, J.S., Lee, H.-J.J*., et al.* (2004). Chronic treatment with the gamma-secretase inhibitor LY-411,575 inhibits beta-amyloid peptide production and alters lymphopoiesis and intestinal cell differentiation. J Biol Chem *279*, 12876-12882.

Yang, J., and Weinberg, R.A. (2008). Epithelial-mesenchymal transition: at the crossroads of development and tumor metastasis. Dev Cell *14*, 818-829.

Yang, L., Xie, G., Fan, Q., and Xie, J. (2010). Activation of the hedgehog-signaling pathway in human cancer and the clinical implications. Oncogene *29*, 469-481.

Yang, Q., Bermingham, N.A., Finegold, M.J., and Zoghbi, H.Y. (2001). Requirement of Math1 for secretory cell lineage commitment in the mouse intestine. Science *294*, 2155-2158.

Yen, T., and Wright, N. (2006). The gastrointestinal tract stem cell niche. Stem Cell Reviews and Reports *2*, 203-212.

Yu, Y., Davicioni, E., Triche, T.J., and Merlino, G. (2006). The homeoprotein six1 transcriptionally activates multiple protumorigenic genes but requires ezrin to promote metastasis. Cancer Res *66*, 1982-1989.

Zhu, L., Gibson, P., Currle, D.S., Tong, Y., Richardson, R.J., Bayazitov, I.T., Poppleton, H., Zakharenko, S., Ellison, D.W., and Gilbertson, R.J. (2009). Prominin 1 marks intestinal stem cells that are susceptible to neoplastic transformation. Nature *457*, 603-607.

Zwick, E., Bange, J., and Ullrich, A. (2001). Receptor tyrosine kinase signalling as a target for cancer intervention strategies. Endocr Relat Cancer *8*, 161-173.